# DEVELOPMENT OF A METRIC TO ASSESS COMPLETENESS OF LESIONS PRODUCED BY RADIOFREQUENCY ABLATION IN THE HEART

Herman D. Himel, IV

A dissertation submitted to the faculty of the University of North Carolina at Chapel Hill in partial fulfillment of the requirements for the degree of Doctor of Philosophy in the Department of Biomedical Engineering.

Chapel Hill
2006

Approved by:

Stephen B. Knisley

Albert J. Banes

Timothy A. Johnson

Andrew E. Pollard

James G. Whayne

## ABSTRACT

HERMAN D. HIMEL, IV: Development of a Metric to Assess Completeness of Lesions Produced by Radiofrequency Ablation in the Heart
(Under the direction of Professor Stephen B. Knisley)

For approximately 25 years, ablation of cardiac tissue by radiofrequency energy has been used to halt arrhythmic conduction in the heart. Efficacy of cardiac ablation for the treatment of atrial fibrillation and other arrhythmias depends on the completeness of lesions and their ability to block arrhythmic conduction without disturbing sinus rhythm. A rapid index of lesion quality measured during surgical ablation procedures may improve the probability of long-term success in patients. Trans-lesion stimulus-excitation time delay was evaluated as an intraoperative indicator of lesion completeness. Time delay was shown to be significantly different for complete vs. incomplete lesions. Further, it was shown that activation path length corresponds with time delay, providing an explanation for post-ablation increases in time delay.

Time delay of excitation measured on either side of a lesion having a small gap may increase after ablation, and then recover over time. This recovery would be important since the lesion may then be insufficient to suppress conduction. Although the Langendorff rabbit model used in this project is insufficient to observe long-term cardiac remodeling phenomena, short term recovery over tens of minutes post-ablation is practical with our apparatus. This would be useful for clinicians who may monitor time delay acutely in their patients before withdrawing the ablation probe. Complete recovery following initial trans-lesion block occurred within 5 minutes after ablation, while partial recovery occurred at 14.4

± 1.0 minutes after ablation. Recovery of the activation complex occurred at 23.7 ± 7.9 minutes after ablation.

Hyperthermia affects the myocardium in a wide variety of ways, including denaturation of myofilaments, disruption of the sarcolemmal membrane and/or denaturation of membrane ion channels, alterations in cellular metabolism, and alterations in intracellular and transmembrane calcium handling. Depending on the extent of the hyperthermic damage sustained during ablation, gaps within lesions may recover following a return to physiological temperature. Conduction recovery may occur following initially successful lesion formation, and it may allow arrhythmic conduction to resume or may result in the formation of one or more new arrhythmias. Further, the temperature of tissue within a small gap of an ablation lesion may correlate with the recovery of myocytes within these gaps. Thus temperature monitoring of ablated tissue may be a useful supplement for monitoring block by measuring time delay.

Temperatures within lesion gaps during complete recovery reached a maximum value of 63.44° C, while temperatures within lesions gaps during partial recovery reached a value of 52.7 ± 3.0° C. In lesions which did not show initial block, supernormal conduction was observed following ablation. Decreases in time delay of 17.8 ± 2.6% were observed, and minima of time delay occurred 28.0 ± 4.0 seconds after ablation. A relationship between temperature and time delay was observed in cases where supernormal conduction occurred, but a relationship was not observed in cases where post-ablation block occurred.

## DEDICATION

To my mother and father, who stood by me through difficult times, and never allowed me to stop believing in myself.

## ACKNOWLEDGEMENTS

I gratefully acknowledge the support, dedication, and honesty of my advisor, Dr. Stephen B. Knisley, who always told me what I needed to hear, rather than what I wanted to hear. I am also grateful to the members of my committee, who individually made valuable contributions and significantly improved the quality and completeness of this work. Dr. Albert J. Banes made contributions which greatly improved my understanding of the cellular aspects of radiofrequency ablation. Dr. Timothy A. Johnson gave valuable advice about the interpretation of both optical and electrical recordings, and helped me develop a critical eye with regard to data analysis. Dr. Andrew E. Pollard helped me to greatly improve my understanding of extracellular electrograms, which in turn improved my ability to analyze my own electrogram data. Mr. James G. Whayne was helpful with data analysis and experimental design, and his deep understanding of the clinical aspects of cardiac ablation helped me to appreciate the practical implications of this work. I would also like to acknowledge the help of John H. Dumas III, for all of his assistance with instrumentation, experimental preparation, analysis, and for the overall dedication he demonstrated toward the project. I would also like to acknowledge the encouragement and support of two of my undergraduate professors, Drs. Dennis Merino and David Norwood, who helped me to build the courage and confidence necessary to successfully pursue a graduate career.

**TABLE OF CONTENTS**

LIST OF TABLES ..... xi

LIST OF FIGURES ..... xii

ABBREVIATIONS AND SYMBOLS ..... xiv

I. INTRODUCTION AND BACKGROUND MATERIAL ..... 1

***A. CELLULAR EFFECTS OF HYPERTHERMIA AND RADIOFREQUENCY ENERGY*** ..... 4

***B. EFFECTS OF ABLATION UPON THE MICROVASCULATURE*** ..... 17

***C. HEAT TRANSFER IN PERFUSED LIVING TISSUE*** ..... 23

***D. OPTICAL MAPPING OF CARDIAC ABLATION LESIONS*** ..... 28

***E. ELECTROGRAM RECORDINGS OF ABLATION LESIONS*** ..... 29

***F. CONDUCTION VELOCITY AND CHANGES IN NORMAL PROPAGATION*** ..... 35

***G. CHANGES IN CONDUCTION VELOCITY DUE TO ISCHEMIA*** ..... 36

II. TRANSLESION STIMULUS-EXCITATION DELAY AS A METRIC FOR RADIOFREQUENCY ABLATION LESIONS IN HEARTS ..... 39

***A. INTRODUCTION*** ..... 39

***B. METHODS*** ..... 41

*Rabbit Heart Preparation* ..... 41

*Electrical Pacing and Recording* ..... 42

*Fluorescence Recording* ..... 43

*Ablation Procedures* ..... 44

*Analysis of Stimulus-Excitation Time Delay* ..... 45

*Viable Tissue Staining* ..... 45

*Statistical Analysis* ..... 46

***C. RESULTS*** ..... 47

*Examination of TTC-stained Hearts* ..... 47

*Electrograms* ..... 48

*Optical Maps* ..... 49

*Time Delay* ..... 53

***D. DISCUSSION*** ..... 56

*Epicardial Approach* ..... 56

*Time Delay* ..... 57

III. ABILITY OF MINIMUM ACTIVATION PATH LENGTH TO PREDICT TRANSLESION TIME DELAY ..... 60

***A. INTRODUCTION*** ..... 60

***B. METHODS*** ..... 61

*Rabbit Heart Preparation* ..... 61

*Electrical Pacing and Recording* ..... 61

*Ablation Procedures* ..... 62

*Analysis of Stimulus-Excitation Time Delay* ..... 62

*Viable Tissue Staining* ..... 63

*Minimum Activation Path Length Determination* ..... 63

***C. RESULTS*** ..... 65

***D. DISCUSSION*** ..... 67

IV. RECOVERY OF TISSUE WITHIN SMALL GAPS OF LINEAR RADIOFREQUENCY CARDIAC ABLATION LESIONS ..... 69

***A. INTRODUCTION*** ..... 69

***B. METHODS*** ..... 72

*Rabbit Heart Preparation* ..... 72

*Electrical Pacing and Recording* ..... 72

*Ablation Procedure* ..... 73

*Selection of Activations in Fractionated Electrograms* ..... 74

*Indication of Recovery* ..... 75

*Classification of Recovery* ..... 75

*Rate of Change in Time Delay* ..... 76

*Data Processing* ..... 76

*Statistical Analysis* ..... 76

***C. RESULTS*** ..... 78

*Control Recording* ..... 78

*Recovery of the Activation Complex* ..... 79

*Complete Recovery of Conduction* ..... 82

*Partial Recovery of Conduction* ..... 84

*Late Worsening of Conduction* ..... 86

*Probability of Observing Different Lesion Types* ..... 89

***D. DISCUSSION*** ..... 90

V. TIME COURSE OF TEMPERATURE WITHIN STUNNED MYOCARDIUM ADJACENT TO LINEAR RADIOFREQUENCY ABLATION LESIONS ..... 94

***A. INTRODUCTION*** ..... 94

***B. METHODS*** ..... 95

*Rabbit Heart Preparation* ..... 95

*Electrical Pacing and Recording* ..... 95

*Temperature Measurements* ..... 96

*Temperature Time Constant* ..... 97

*Time Response of Temperature Probe* ..... 98

*Classification of Recovery* ..... 99

*Supernormal Conduction* ..... 99

*Data Processing* ..... 100

*Statistical Analysis* ..... 100

***C. RESULTS*** ..... 101

*Summary of Temperature Results* ..... 101

*Temperature During Control Recordings* ..... 102

*Temperature During Complete Recovery* ..... 103

*Temperature During Partial Recovery* ..... 104

*Temperature During Changes in Activation Complex* ..... 105

*Temperature During Supernormal Conduction* ..... 106

*Correlation Between Time Delay and Temperature During Supernormal Conduction* ..... 108

*Summary of Temperature Dependence of Recovery* ..... 109

***D. DISCUSSION*** ..... 113

***APPENDIX: A GEOMETRIC MODEL FOR PREDICTING TIME DELAY AROUND A LINEAR ABLATION LESION IN A TWO-DIMENSIONAL SHEET OF MYOFIBERS*** ..... 117

**LIST OF TABLES**

Table 2.1 Time Delay Measured by Electrogram Recordings.....54

Table 2.2 Time Delay Measured by Optical Recordings.....54

Table 4.1 Summary of recovery times (50% and 90%) for all lesion types except those showing morphological changes post-ablation. .....87

Table 4.2 Times of activation complex recovery occurring post ablation.....88

Table 4.3 Averaged slopes of time delay for lesions showing partial recovery and late conduction worsening. .....88

Table 5.1 Summary of maximum temperatures ($T_{max}$), time constants ($\tau$), and times for 50% recovery ($t_{50}$) .....106

Table 5.2 Parameters describing supernormal conduction. $t_{min}$ indicates the time of the minimum time delay relative to the end of the ablation. .....108

**LIST OF FIGURES**


Figure 1.1 Myocardial model for cell damage following exposure to hyperthermia (first half) ..... 15

Figure 1.2 Myocardial model for cell damage following exposure to hyperthermia (second half) ..... 16

Figure 2.1 Diagram showing the arrangement of the ablation probe and electrogram recordings on the heart ..... 43

Figure 2.2 Photographs of incomplete and complete lesions ..... 47

Figure 2.3 Electrograms for incomplete and complete lesions ..... 48

Figure 2.4 Activation contour map and action potential recordings before RF ablation ..... 50

Figure 2.5 Activation contour map and action potential recordings after production of an incomplete lesion. ..... 51

Figure 2.6 Activation contour map and action potential recordings after production of a complete lesion. ..... 52

Figure 2.7 Electrical and optical time delays measured before lesion creation, and for incomplete and complete lesions ..... 55

Figure 3.1 Photograph showing the minimum activation path length ..... 64

Figure 3.2 Stimulus to excitation time delays as a function of minimum activation path length ..... 66

Figure 4.1 Five cm ablation probe with silicone gap ..... 73

Figure 4.2 Control recording of time delay over a 1-hour period ..... 79

Figure 4.3 Example of activation complex recovery following an RF ablation lesion ..... 81

Figure 4.4 Three-dimensional view of morphological changes following ablation indicating recovery of activation complex ..... 82

Figure 4.5 Complete recovery following an ablation lesion ..... 83

Figure 4.6 Electrograms taken during complete conduction recovery ..... 84

Figure 4.7 Partial conduction recovery in a complete lesion ..... 85

Figure 4.8 Electrograms for partial conduction recovery in an incomplete lesion. ..... 86

Figure 4.9 Late conduction worsening following RF ablation. Vertical dotted line indicates end of RF ablation. ..... 87

Figure 5.1 Photograph of ablation probe with temperature probe attached near gap region. ..... 97

Figure 5.2 Time response of temperature probe ..... 98

Figure 5.3 Gap temperature following RF ablation ..... 102

Figure 5.4 Control recording of time delay and temperature for a 60-minute period ..... 103

Figure 5.5 Graphs illustrating the relationship between time delay and temperature for a lesion showing complete recovery. ..... 104

Figure 5.6 Graphs illustrating the relationship between time delay and temperature for a lesion showing partial recovery. ..... 105

Figure 5.7 Supernormal conduction immediately following RF ablation ..... 107

Figure 5.8 Relationship between temperature and time delay during supernormal conduction ..... 109

Figure 5.9 Diagram for complete recovery ..... 110

Figure 5.10 Diagram for partial recovery ..... 111

Figure 5.11 Diagram for supernormal conduction ..... 112

**ABBREVIATIONS AND SYMBOLS**

AC – alternating current

AF – atrial fibrillation

AgCl – silver chloride

$A_i$ – area of the $i^{th}$ vessel

AERP – atrial effective refractory period

APA – action potential amplitude

APD – action potential duration

ATP – adenosine triphosphate

AV – atrioventricular

ATPase – adenosine triphosphatase

Ca-ATPase – Calcium$^{2+}$ transport adenosine triphosphatase

c – specific heat (heat capacity)

$c_b$ – specific heat of blood

Cys374 – cysteine residue present on F-actin

DNA – deoxyribonucleic acid

$(dV/dt)_{max}$ – maximum derivative of an electrogram peak

$(dV_m/dt)_{max}$ – maximum upstroke velocity of the transmembrane potential

**E** – electric field

F-actin – filamentous polymer form of actin

Hsps – heat shock proteins

$h_b$ – heating term due to blood circulation

$h_m$ – heating term due to metabolism

G-actin – globular monomer form of actin

GAG – glucosaminoglycan

**J** – current density

$\kappa$ – thermal conductivity

IVC – superior vena cava

NO – nitric oxide

$\rho$ – density

$\rho_b$ – density of blood

$P_i$ – circumference of the $i^{th}$ vessel

PV – pulmonary vein

**q** – heat flux vector

$Q_{el}$ – heat contribution due to conductive transfer between tissue and the ablation electrode

r – radius of lesion end

**r** - position vector

R – length of lesion minus twice the radius of the lesion end

RNA – ribonucleic acid

ROS – reactive oxygen species

RF – radiofrequency

SR – sarcoplasmic reticulum

SVC – superior vena cava

$\theta$ – angle between the direction of propagation and the fiber direction

$\theta_i$ – angle between vessel and exiting of entering surface of a tissue volume

$\theta_o$ – angle between the initial direction of propagation and the fiber direction (constant)

$\tau$ – time constant of temperature following ablation

$t_{50}$ – time of 50% recovery

$t_{90}$ – time of 90% recovery

$t_{min}$ – time of minimum time delay during supernormal conduction

$t_R$ – time of recovery of activation complex

T – temperature

$T_a$ – arterial temperature

$T_{bi}$ – flow-weighted average temperature of blood within the $i^{th}$ vessel

$\Delta TD_{decrease}$ – maximum percent decrease in time delay during supernormal conduction

$TD_{min}$ – minimum time delay during supernormal conduction

$TD_{pre}$ – pre-lesion time delay for the 2-D linear lesion model

$TD_{post}$ – post-lesion time delay for the 2-D linear lesion model

$T_{max}$ – maximum temperature

$T_s$ – temperature of solid tissue

$T_v$ – venous temperature

TUNEL – terminal deoxynucleotidyl transferase biotin-dUTP nick end labeling

$u_i$ – mean velocity within the $i^{th}$ vessel

$U_i$ – heat transfer coefficient of the $i^{th}$ vessel

UTP – Uridine 5'-triphosphate

$v_\theta$ – velocity of activation wave as a function of theta

$v_c$ – constant component of the velocity of the activation wave

$v_f$ – fiber dependent component of the velocity of the activation wave

$V_m$ – transmembrane potential

$x_{ei}$ – length over which temperature difference between blood and solid tissue will be reduced by a factor of 1/e

# CHAPTER 1

# INTRODUCTION AND BACKGROUND MATERIAL

Atrial fibrillation (AF) is the most common cardiac arrhythmia in the United States, currently affecting over 2.2 million of its citizens[1]. At the age of 40 years, the lifetime risk of developing AF is approximately 24.5%[2]. Once thought to be a benign consequence of aging, AF is now widely regarded as a dangerous arrhythmia which carries significant risks in addition to its direct effect upon cardiac output, where the atria account for approximately 25% of ventricular filling[3]. Some of the risks associated with AF include stroke[4] and other embolic phenomena, increases in morbidity and mortality, and increased risk of congestive heart failure. Data from the Framingham study shows that the incidence of stroke increases approximately five-fold for patients who have AF[5], and that the risk of death increases by a factor of 1.4-1.9 even after adjustment for preexisting cardiovascular conditions related to AF[6]. Atrial fibrillation has also been shown to be a progressive disease. If left untreated, AF leads to electrical and mechanical remodeling within the myocarium[7-12] which leads to greater inducibility and higher stability of AF. Following electrical remodeling during AF, subsequent episodes of AF are easier to induce, and occur for a longer time period[9].

Several different methods of treatment for AF have emerged, including anti-arrhythmic drug therapy, anti-arrhythmic pacing, and surgical ablation. Currently, surgical treatment of atrial fibrillation suffers from several weaknesses. The gold standard for surgical ablation, known as the Cox-Maze III lesion set, has a high success rate (~90%) but is highly

invasive and requires a thoracotomy and cardiopulmonary bypass. For the Maze III procedure, lesions are formed by making surgical incisions into the myocardium, electrically disconnecting adjacent tissue, and isolating certain regions of the atria. Also known as the "cut and sew" method, the Cox-Maze III lesion set eliminates AF by isolating ectopic foci which trigger fibrillatory activity, and by breaking up reentrant circuits which sustain this activity.

Alternatively, catheter ablation is minimally invasive but is associated with relatively poor success rates, particularly among those with structural heart disease. Also, catheter procedures require that hyperthermia be applied to the myocardium while the device is within a major vessel or within the atria, exposing blood to hyperthermic environments and increasing the risk of clotting and subsequent thromboembolic complications[13-15]. Another weakness of catheter ablation is its inability to consistently create continuous transmural lesions which emulate those of the Cox-Maze III lesion set. Specifically, it is technically challenging to create the linear transmural (i.e., complete) lesions which are prescribed by the Cox-Maze III procedure. Nonetheless, complete linear lesions are a key building block for the creation of the Maze lesion set, and the quality of these lesions directly impacts upon the success and recurrence rates of AF ablation surgery[16].

The objective of this work is to develop a metric which is capable of rapidly examining the efficacy of linear lesions, and to examine factors which may complicate or compromise the reliability of this metric. In the sections that follow, the effects of radiofrequency ablation upon the myocardium are reviewed. Since the metric which is the focus of this work is critically dependent upon tracking activation of myocytes, methods used to map activation are also examined in the context of radiofrequency ablation. Finally,

normal and abnormal conduction are examined, as well as changes in the myocardium due to ischemia, since radiofrequency ablation is known to decrease blood flow in the region of lesion creation[17].

### *A. Cellular Effects of Hyperthermia and Radiofrequency Energy*

Hyperthermia causes cellular damage by a number of different mechanisms, and has significant effects upon the sarcolemmal membrane, the cytoskeleton, cellular organelles, cellular metabolism, and specific types of protein production (heat shock proteins). This discussion will attempt to detail the effects of hyperthermia upon cardiac myocytes and indicate the relative importance of each effect.

Hyperthermia induced by radiofrequency ablation produces structural damage to sarcolemmal membranes which results in profound electrophysiological changes in cardiac myocytes. Nath et al reported that hyperthermia caused depolarization of the transmembrane potential ($V_m$), changes in $dV/dt_{max}$ (early increase followed by a late decrease), slight changes in action potential amplitude (APA), significant changes in action potential duration (APD), as well as reversible and irreversible losses of excitability[18]. Most electrophysiological effects are thought to be a consequence of damage to the plasma membrane, since the plasma membrane plays a critical role in ion transport and is the first cellular component to be affected by hyperthermia[19]. Hyperthermia is thought to affect the plasma membrane by increasing membrane fluidity, thereby increasing vulnerability to electric fields produced by the ablation electrode. Also, hyperthermia is thought to affect ion transport directly by impairment of receptor function and thermal inactivation of ion channels[19]. Also, inactivation of some voltage-dependent ion channels may be a consequence of a decrease in resting membrane potential due to extracellular increases in potassium and a subsequent inability of the transmembrane potential to return to normal resting values.

The effects of damage to mitochondria in myocytes due to hyperthermic conditions have recently been reported by Quian et al[20], who proposed a possible mechanism for cell

death by calcium overload. In addition to their role in ATP production, mitochondria also play an important role in the regulation of calcium. Damage to the mitochondria results in a reduction in Ca-ATPase activity within the mitochondria, which leads to an inability to remove calcium from the intracellular space. This condition may then lead to calcium overload and possibly death by irreversible contracture of the myocyte. Although the hyperthermia exposure time of Quian et al was of a longer duration (40 minutes) than what is typical during RF ablation (~1-5 minutes), similar types of mitochondrial damage were observed by both Quian[20] and Nath et al[21], who performed RF ablation. These effects include degradation of the mitochondrial membrane and cristae, as well as mitochondrial swelling. It is possible that this damage contributes to non-acute cell death (4-6 hours) that may account for late conduction block which has been reported after RF ablation surgery. The mitochondria have also been shown to play a key role in programmed cell death, as deactivation of certain anti-apoptotic molecules within the mitochondrial membrane may lead to apoptosis[22]. Mitochondrial membrane permeabilization has been shown to play a key role in apoptosis for both the extrinsic death receptor and the intrinsic mitochondrial pathways[23]. The mitochondria have also been implicated in the acidification of the intracellular environment[24,25]. Intracellular acidification leads to the mitochondrial release of caspase activators[24]. The caspases are a class of proteases central to perhaps all types of apoptosis[26,27].

The sarcoplasmic reticulum (SR) plays a critical role in intracellular calcium handling, which is important for normal excitation-contraction coupling in myocytes. Alterations to the SR that occur during hyperthermia may lead to imbalances in intracellular calcium concentrations which may cause reduced contractility or myocyte contracture.

Everett et al have proposed that irreversible contracture by intracellular calcium increase may be important in causing hyperthermia-induced injury to myocytes[28]. They reported that during moderately hyperthermic conditions (45-50 ºC), intracellular calcium concentrations were elevated but could be returned to normal levels by the calcium uptake into the SR. For temperatures above 50 ºC, however, myocytes were overwhelmed by increased calcium permeability due to hyperthermia-induced injury. It is possible that impaired function of the SR also contributes to cell death in the 50 ºC range, as studies suggest that hyperthermia exposure results in reductions in $Ca^{2+}$-ATPase activity in the SR[29].

Cytoskeletal damage in myocytes due to short-term hyperthermic exposure has not been investigated in depth. However some reports suggest that membrane bleb formation due to hyperthermia may be the result of cytoskeletal injury. It has been shown that bleb formation correlates well with cellular death[30]. Specifically, damage to microtubules, microfilaments, and intermediate filaments has been shown to occur during hyperthermia, although the specific mechanisms of such damage are unknown[31]. Although effects to the cytoskeleton are thought to play a minor role in post-ablation cell death in the region of acute necrosis, it is possible that cytoskeletal damage in the border zone may lead to cytoskeletal alterations which may affect activation patterns in the myocardium. The importance of actin cytoskeletal stability is illustrated in a report by Gabia et al, which showed that actin stability in tumor cells determined cellular resistance to both hyperthermia and certain forms of energy deprivation[32], and that membrane blebbing which precedes cell death occurred following increases in denatured actin. Changes in the conformation of actin have previously been measured using fluorescent labeling of actin molecules, which may be injected into living cells and subsequently monitored directly[33]. In another study by Schuler et al, the

authors use the fact that denatured (i.e. unfolded) actin molecules show a decrease in their DNase I-inhibiting activiy, and thus use the DNase I-inhibiting assay as a means of quantifying actin denaturation[34].

It is possible that diseases such as hypertrophy which result in damage to the cytoskeleton may play a role in predisposing cardiac myocytes to damage caused by heat or ischemia-reperfusion injury. Defects causing weaknesses in the myocyte cytoskeleton have been implicated in cardiomyopathy, a disease which results in ventricular dilation and typically causes valvular disorders[35].

Actin is the most abundant protein in myocytes, and comprises approximately 20% of total cell protein[36]. Actin exists as a globular monomer (G-actin) and as a filamentous polymer (F-actin) which is comprised of repeating units of G-actin. F-actin can form bundles of closely packed parallel filaments, and may also form loosely packed networks of filaments which may cross each other at any given angle[37]. Both bundles and networks are held together with actin cross-linking proteins, and may be attached to the cell membrane by membrane-microfilament binding proteins. Actin bundles are critical to the contractile function of the cardiac myocyte as well as its structural integrity. Actin has also been shown to play important roles in cell signaling[38,39] and ion channel regulation[40-44], which are critical to cardiac action potential conduction.

Effects of hyperthermia upon the actin cytoskeleton have been investigated by Huang et al, who reported that heat-induced disruption of the actin cytoskeleton occurred as a result of focal adhesion complex disassembly. In addition to actin binding to the cell membrane via focal adhesion complexes, it has also been suggested that actin may bind to the cell

membrane directly[45,46], thus hyperthermic conditions which affect membrane fluidity may affect the stability of the actin cytoskeleton.

In addition to causing cytoskeletal detachment from the cell membrane, hyperthermic conditions may also result in damage directly to actin filaments. While mild hyperthermia (41-43 ºC) typically does not induce damage to the actin filament network, higher temperatures (> 45 ºC) have been shown to destroy actin-containing contractile rings and cause damage to stress fibers[47].

Protein denaturation is strongly associated with hyperthermic damage, and cell survival rates and protein denaturation rates have been shown to obey similar kinetics (i.e., decaying exponentials in time)[48]. Since actin is the most abundant cellular protein, and is even more abundant in myocytes, it is likely that actin denaturation plays a significant role in cell death due to hyperthermia.

A recent report by Gicquaud et al provides evidence for a three-step mechanism for the thermal unfolding of F-actin. In this study, investigators determined the reversibility of each "calorimetric event" (i.e., step) during thermal denaturation, and determined that the first step is reversible, while each of the final two steps is irreversible. The third step is thought to correspond to the unfolding of F-actin, while the first and second events were shown not to correspond with the thermal unfolding of F-actin subdomains as previously thought[49], but rather an alteration to cys 374 (a cysteine residue) and a modification at the nucleotide binding site of actin[50]. Differential scanning calorimetry has shown that myosin also undergoes multiple steps in the denaturation process. However the number of steps observed depends on factors such as pH, scanning rate, and heating rate[51]. The thermal stability of myosin also varies widely by muscle types, as demonstrated by Vega-Warner et

al[51]. The degree to which cells recover will thus depend critically on the energy delivered to the actin and myosin fragments of the cytoskeleton, and whether or not sufficient energy is delivered to cause irreversible denaturation steps to occur.

The presence of ATP has been shown to have a protective effect upon F-actin[52] as well as myosin[53,54], while decreases in pH have sensitizing effects upon the thermal stability of actin[54] and myosin[55]. Thus ischemic conditions and low ATP levels which occur following damage to microvasculature may affect the stability of actin and myosin bundles, predisposing them to thermal denaturation.

The type of myosin (myosin II) which powers muscular contraction is a mechanochemical dimer which functions as an enzyme for ATP hydrolysis. Myosin molecules consist of head and tail regions, and myosin present in myocytes has head regions on both ends of the dimer molecule which may be used to bring together actin filaments from opposing ends of the cell membrane. In the presence of actin with exposed myosin binding sites (i.e., actin in the presence of calcium), the myosin head rapidly hydrolyzes ATP in order to generate mechanical forces which result in contraction. A single myosin molecule moves along an actin filament in discrete steps of 11-15 nm, and each step generates approximately 3-4 picoNewtons of force[37]. The myosin tail acts to regulate binding to cell membranes and assembly of thick filaments which are present in myocytes. Examination of head (S-1 subfragment) and tail (rod) regions of carp myofibrils following heating revealed that the tail portion of myocytes denatures more quickly than the head portion[56], suggesting that hyperthermia may be more likely to initially cause aggregation of myosin rather than an inability of the myosin head to hydrolyze ATP. However, there is evidence that the initial denaturation stage of the rod portion is readily reversible[57], and that the ATPase activity of

the myosin head is greatly reduced during hyperthermia[58-60]. Thus the contractility of cardiac myocytes near the border zone will likely be affected by hyperthermic exposure, and damage to the myosin head may result in permanent contractile dysfunction.

The extracellular matrix has been shown to undergo significant changes after even mild hyperthermia (~41 °C), such as that associated with the inflammatory response. Wagrowski et al have shown, in multiple cell lines, that the composition of the extracellular matrix is affected by hyperthermia[61]. Specifically, the production of the extracellular matrix component glucosaminoglycan (GAG) is inhibited, while the production of hyaluronan increases. Hyaluronan is typically present during inflammatory reactions, and acts to inhibit cell-to-cell adhesion and allow cell migration[37]. Proper myocardial conduction is dependent upon regular intercellular coupling, thus the restructuring of the extracellular matrix following hyperthermia may have significant effects upon cardiac excitation propagation, including wavebreak and slow conduction.

Although damage to the nuclear membrane has been reported for both endothelial cells in the microvasculature[17] as well as cardiac myocytes[21], the effects of this damage are thought to be of secondary importance in myocyte tissue death and recovery following RF ablation. While damage to DNA may be of critical importance in tumor cells where cell replication is accelerated, typically adult cardiac myocytes do not actively divide and thus DNA damage is thought to be of only minor importance. Also, damage to DNA and structured RNA are also thought to be unlikely to occur during RF ablation, since they typically do not undergo conformational changes below 85-90º C[62].

During RF ablation, coagulation necrosis typically takes place at the level of the microvasculature, resulting in eventual death to the surrounding tissue due to ischemia. In

addition, cells adjacent to the ischemic zone may die due to apoptosis[63], which may be indicated morphologically by cell shrinkage rather than cell swelling typically found following ischemic necrosis. Other indicators of apoptosis include fragmented DNA (which may be detected by terminal UTP nick end labeling, or TUNEL), condensation/clumping of nuclear chromatin, membrane blebbing, loss of cell-cell contact, phagocytosis of the apoptotic body by adjacent cells, little inflammatory reaction in the region of apoptotic cells, intracellular acidification, and the maintenance of organelle structure and function until late in the apoptotic process[22]. Although the appearance of a "ladder" pattern in gel electrophoresis assay has been regarded as the most characteristic feature of apoptotic cells, investigators have shown that DNA fragmentation is neither necessary nor sufficient for events leading to apoptosis[64]. And while the TUNEL assay provides evidence for apoptosis, the gold standard for apoptosis is still the identification of morphological indicators using light and electron microscopy[22].

Recently, apoptosis has been implicated as a possible cause of the progression of hypertensive heart disease into congestive heart failure[65], and increased apoptosis has been demonstrated in rats with hypertrophied left ventricles[66]. Cheng et al have demonstrated that increased apoptosis occurs due to mechanical stress on papillary muscles. Electron microscopy of RF ablation lesions has revealed significant mechanical damage to cardiac gap junctions, sarcomeres, and the plasma membrane. Also, adjacent myocytes were often found in to be in varying stages of contractility[21], suggesting the presence of significant mechanical stresses upon cardiac tissue adjacent to ablation lesions which may accelerate apoptosis.

Heat shock proteins (Hsps) serve to protect cellular proteins by aiding in the correct folding of partially denatured proteins and by degrading proteins which have been

irrevocably damaged, thus preventing aggregation. The Hsps probably play a minor role in regions of acute necrosis where cells are heated to temperatures above 60º C, however they may play a significant role in the recovery of tissue in the border region where heat exposure is less severe and ischemia plays a significant secondary role[67]. Heat shock proteins are synthesized in response not only to heat but also to ischemia and many other stresses, and therefore will be induced both by ablation-induced hyperthermia as well as late ischemia produced by damage to the microvasculature. Compelling evidence has been presented by Currie et al and others[68-72] which details the protective effects of Hsps in the myocardium following exposure to heat-shock, showing that both metabolic and contractile indicators of protection following secondary exposures to stress are correlated well with the presence of Hsps. Thus Hsps may be a possible cause of late recovery of myocardial tissue following thermal exposure during ablation surgery. Ilangovan et al[73] concluded one way in which Hsps increase survival rates of heat-treated cells is related to the regulation of nitric oxide. Specifically, some Hsps binding leads to the production of NO, which in turn reduces oxygen consumption in order to conserve energy during ischemic conditions. Actin depolymerization is thought to be inhibited by Hsp27, which may act as a cap-binding protein to stabilize actin filaments following hyperthermic exposure[74]. However a more recent report showed that while thermal denaturation of F-actin is not directly affected by Hsps, some Hsps (Hsp24 and Hsp27) will interact with denatured actin to prevent aggregation[75], indicating that Hsps may act on actin filaments at different stages of the denaturation process.

A number of interesting clinical uses for Hsps have been proposed, including their inhibition to enhance ablation of tumors[76] and drug-induced heat shock in order to improve post-ischemic ventricular recovery following cardiopulmonary bypass[77]. Drug-induced Hsps

inhibition may be useful in ablation therapy, as a means of achieving conduction block at lower temperature in order to prevent unwanted effects such as charring or popping which may result in thromboembolic complications (e.g., stroke).

Metabolic changes due to hyperthermia are thought to have profound effects upon the survival of the cardiac myocyte. Energy metabolism generally increases during hyperthermia, including glucose metabolism, ATP usage, and ATP synthesis[78]. Studies conducted in tumor cells reflect greatly increased demands for energy during heat exposure. Increases in energy metabolism may lead to a depletion of energy reservoirs, possibly contributing to late cell death following RF ablation. The synthesis of DNA, RNA, and proteins has been shown to be inhibited by hyperthermia in tumor cells. However adult myocytes do not actively replicate, thus the effects of DNA synthesis inhibition are not expected to play a large role in the physiology of post-ablation lesion healing. The degree to which protein synthesis affects the cell is highly dependent upon the type of synthesis that has been inhibited. An obvious class of proteins that may affect the survival of the cell are the heat shock proteins described above. Heat shock protein production is thought to be accelerated during mild hyperthermia, but may be inhibited during higher temperatures.

Hyperthermia also affects cells by sensitizing them to other stresses (by increasing cell membrane permeability, for example). In the case of RF ablation, this stress comes in the form of radiofrequency waves, and it is possible that electrical injury plays a significant role in lesion creation. Although it is generally agreed upon that the thermal effects account for the vast majority of tissue damage, the relative contributions of thermal and electrical injury are not precisely known, and it has been suggested that the combination of thermal and

electrical energy produce a synergistic effect greater than that produced by pure electrical or thermal energy alone[19,62].

Myocytes adjacent to acutely necrotic tissue are affected by a number of different mechanisms, some of which may act to increase lesion size while others may contribute to recovery of cardiac tissue. Radiofrequency ablation surgery in the clinical setting has shown that both cases occur frequently, with recovery of conduction leading to late failure of conduction block[79,80], while expansion of the lesion may result in complete atrioventricular block[81-83]. Improvements in success rates for the ablation of arrhythmias will depend upon our understanding of these factors and our ability to regulate the balance between those factors which lead to lesion expansion and those which lead to tissue recovery. A block model on the following two pages summarizes the aforementioned effects of hyperthermia upon cardiac myocytes. The rightmost block is acted upon by hyperthermia.

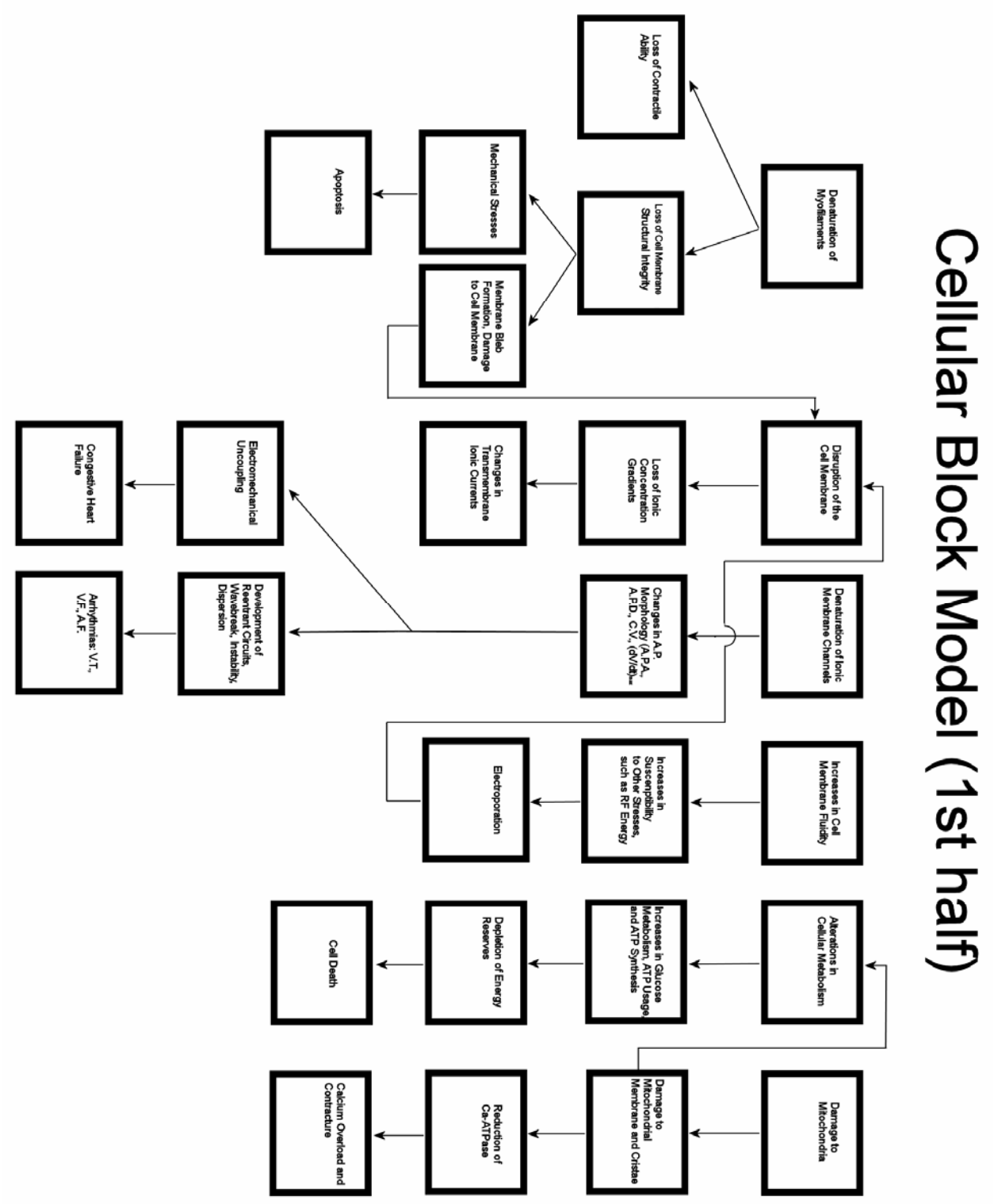


**Figure 1.1** Myocardial model for cell damage following exposure to hyperthermia (first half)

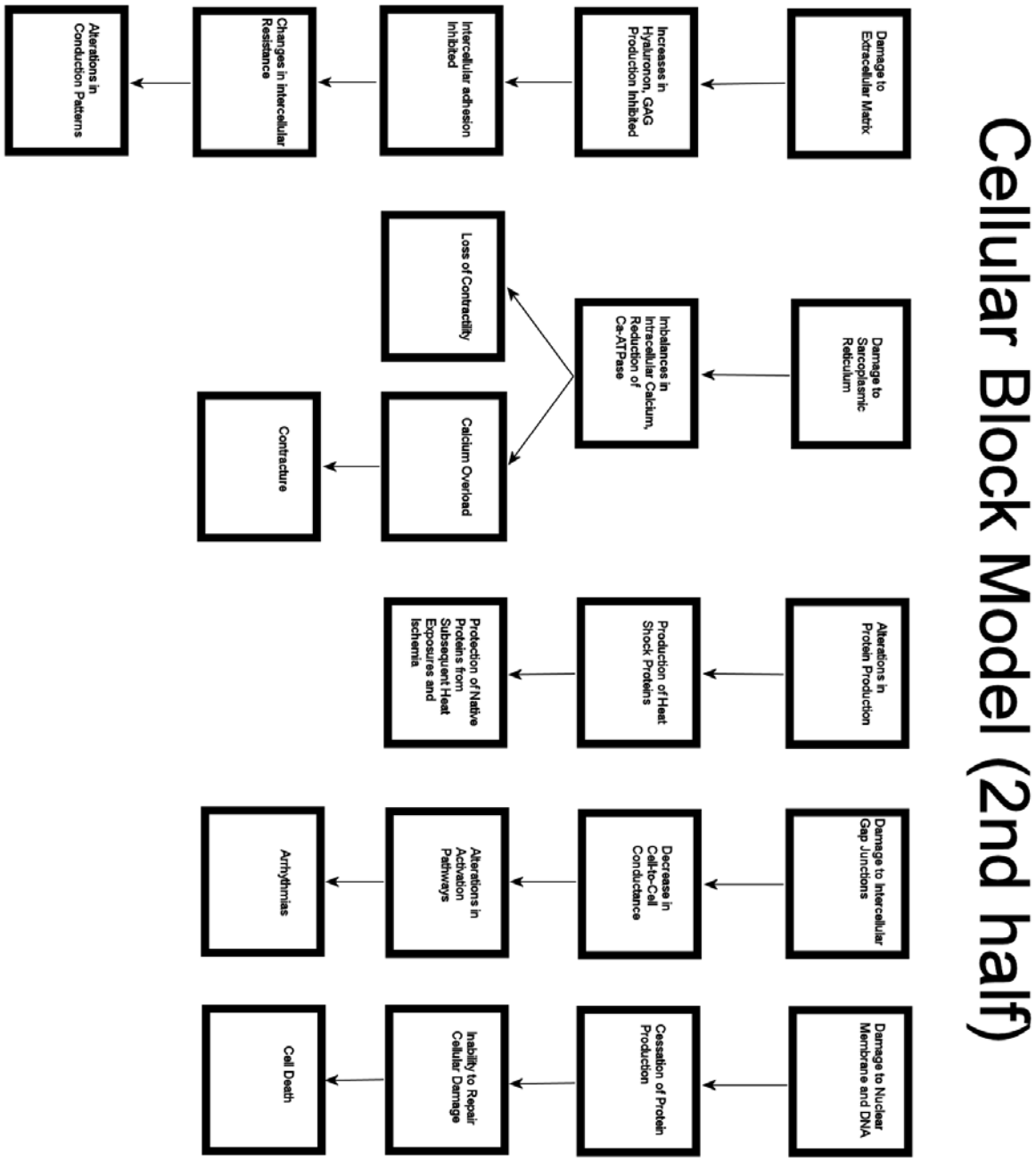


**Figure 1.2** Myocardial model for cell damage following exposure to hyperthermia (second half)

### *B. Effects of Ablation upon the Microvasculature*

During radiofrequency (RF) ablation, the tissue is heated through two distinct mechanisms (Joule and thermal). Joule heating occurs primarily due to the flow of radiofrequency current through the high-resistance electrode-tissue interface near the ablation electrode tip. Thermal heating is a result of passive heat conduction occurring from the site of Joule heating to the surrounding tissue. Thermal heating produces the majority of the tissue damage, and Joule heating produces acute coagulation necrosis near the ablation electrode, with tissue damage gradually decreasing with increasing distance from the ablation electrode contact site. Studies by Nath et al[17,21] indicate that damage to the myocytes as well as to the microvasculature extends outside the region of acute necrosis, and that dynamic changes in these regions may be responsible for late success or failure of ablation surgeries aimed at blocking conduction. Although studies of the effects of RF ablation on cardiac microvasculature are somewhat scarce, there are numerous studies involving cancerous tissue (mostly liver) which describe the effects of the microvasculature upon RF ablation lesion size and cellular necrosis[84-89], as well as changes in the microvasculature due to ablation[90,91]. Studies conducted on tumors have shown that blood flow in the microvasculature increases with mild heating, but then begins to decrease as temperatures reach approximately 46º C[92], eventually resulting in stasis[93]. Following ablation, reductions in myocardial blood flow have been shown for regions up to 6 mm away from RF ablation lesions. More specifically, regions 0-3 mm away from the region of acute necrosis showed a reduction of 52% with respect to normal flow, while regions 3-6 mm away showed a reduction of 18%[17]. These values indicate that regions outside the zone of acute coagulation necrosis suffer from hypoxia.

The endothelial cells are thought to play an important role in the thermal injury of the microvasculature[94]. Gross structural alterations to microcirculatory endothelium have been reported both within and adjacent to the region of acute necrosis, including degeneration of vascular walls, irregular endothelial wall surfaces, and the presence of fibrin[93]. Damage to endothelial cell plasma membranes, nuclear membranes, nuclear chromatin, transport vesicles, endoplasmic reticula, and gap junctions has also been reported[17]. Structural damage to endothelial cells contributes to a variety of metabolic and inflammatory processes which affect the surrounding tissue. Damage to the endothelial wall may also alter the hemodynamics within the damaged vessels due to changes in vessel geometry and decreases in the diameter of the vessel lumen.

Damage to the vascular endothelium is often the result of ischemia in the border adjacent to the zone of acute coagulation necrosis. In regions near the ablation site where mild to moderate hyperthermia occurs, the microvasculature and surrounding tissue may be subject to ischemia-reperfusion injury. Due to increased vascular permeability that occurs during hyperthermia and as a result of inflammatory reaction to endothelial damage, neutrophil accumulation occurs following ischemia and reperfusion, and has been shown to play a significant role in microvascular endothelial injury[95-98]. The accumulation of neutrophils in the microvasculature ultimately results in the production and release of reactive oxygen species (ROS) of which the vascular endothelium is a sensitive target. The group of ROS formed following neutrophil invasion are highly diversified, and affect a wide range of components vital to cardiac function, including membrane lipids and membrane ionic channels[98]. Although neutrophil accumulation is thought to account for the majority of deleterious effects on the vascular endothelium, there is also recent evidence that other types

of blood cells play an important role in post-ischemic endothelial injury, and may act to promote neutrophil-induced injury[99-103]. Thus in addition to the affects of hyperthermia, vessel damage and subsequent ischemia, the immune response is also though to result in significant damage to the walls of the microvasculature. These later effects following RF ablation surgery may be responsible for long-term complications associated with increasing lesion size, such as complete AV block following the correction of atrioventricular nodal reentrant tachycardia[104].

Partial blockage of microvessels, coupled with decreased compliance caused by fibrosis, may lead to large decreases in blood flow and an inability to properly regulate blood flow in tissue adjacent to RF ablation lesions. Accumulation of neutrophils following inflammatory reaction[105] may further act to reduce effective diameter within the microvasculature. In order to appreciate the impact of such changes, it is instructive to consider the physics of flow through a cylindrical pipe. Poiseuille's law dictates that small changes in the diameter of a vessel lead to large changes in the blood flow rate, since the rate of flow is proportional to the radius of the vessel raised to the fourth power[106]. This may lead to ischemic conditions in tissue near RF ablation lesions, particularly during periods of increased stress, where blood flow and energy demands are elevated. The heart may respond by increasing its beat rate and therefore increasing intravascular pressure, but since the structural integrity of the vasculature has been compromised as described above, this pressure increase may lead to hemorrhaging and subsequent extravasation of red blood cells, as reported by Nath et al[21]. Studies of progressive microvascular injury in the liver reveal that peak microvascular and tissue injury occurs approximately 72 hours following treatment via hyperthermia, and that microvasular injury often precedes tissue injury[107]. This highlights the

importance of microvascular injury in the eventual healing or death of tissue located within the border zone (~0-6 mm of the region of acute necrosis).

The larger vessels of the heart are typically avoided during the production of RF ablation lesions, and thus do not play a direct role in lesion production and late tissue death. However, damage to the larger coronary vessels may result in massive damage to the myocardium. A number of dangerous (although somewhat rare) complications are associated with damage to the larger coronary arteries which supply blood to the heart, including severe intimal hyperplasia (a result of the inflammatory response as described above for the microvasculature) and intravascular thrombus[108]. Both of these complications may lead to vessel blockages and subsequent myocardial infarction.

Experimental findings have helped to improve the safety of ablation near coronary vessels, but vessel damage still remains a concern. Several guidelines have been proposed by investigators that have helped to reduce the incidence of complications involving coronary vessels. Based on empirical observations and experimental studies, Sosa et al reported that ablation lesions should be created at least 12 mm from a major coronary artery[109]. D'Avila et al found that susceptibility to damage by RF pulses varied inversely with the coronary vessel size[110], suggesting that larger vessels are protected by the convective heat sink effect provided by greater blood flow in larger vessels. They reported that vessels with diameters greater than 0.51 mm had no significant endothelial lesions, while all vessels with diameters less than 0.24 mm showed signs of significant injury. While in the case of larger arteries it is certainly detrimental to damage the endothelium and endanger the surrounding myocardium, it is likely that in the case of smaller vessels vascular damage may be desirable in order to increase eventual ablation lesion size. Thus it is likely that there exists a "danger zone" of

vessel diameters which must be carefully avoided, below which the vessels are nearly terminal and their destruction acts to aid in increasing lesion size and ensure uniform deactivation of myocytes, and above which the vessels are likely to be protected by the heat sink effect of convective cooling by blood flow.

A recent report by Thyer et al suggests that coronary vessels may be protected by irrigating the vessels with chilled saline[111], however questions still remain regarding the clinical viability of this technique[108], and ischemia-reperfusion injury following infusion with a hypothermic saline solution is a concern[105,112] that must be addressed. The protective effects offered by the saline technique must be weighed against the relatively low incidence of vessel damage reported in the literature (Sosa et al reported only one instance of coronary artery occlusion in 215 procedures[113]). Further, over-cooling of vessels may leave viable myocytes in tissue surrounding vessels, which may allow arrhythmic conduction or act as an arrhythmogenic substrate.

Aside from the more obvious structural damage that may occur in the coronary vessels, such as coagulation necrosis and thromboembolism, endothelial tissue is also subject to the effects of inflammatory reactions that occur in response to hyperthermia and ischemia-reperfusion injury in the microvasculature. Thus in addition to avoiding direct contact with the vessels, care must also be taken to avoid heating the vessels beyond temperatures which may precipitate a potentially damaging inflammatory response.

Both the vasculature and the microvasculature play a critical role in the acute and long-term phases of RF ablation lesion formation. Acute structural damage to the microvasculature results in local ischemia in the lesion border zone, and subsequent inflammatory responses may help to further increase lesion size, although this may result in

the block of conduction necessary for normal cardiac function. While the larger vessels of the heart are typically not as susceptible to acute damage, they may suffer more subtle long-term damage due to the effects of hyperthermia upon the endothelial cells which line the vessels. Also, the larger vessels play an important role in early ablation lesion size, since larger vessels will remove heat from the ablation site by convective cooling. The production of a complete lesion set will depend on the careful consideration of the factors which affect both short-term and long-term effects upon the vasculature and microvasculature of the myocardium.

### *C. Heat Transfer in Perfused Living Tissue*

The Bioheat equation is a modification of the heat equation. The heat equation is based on Fourier's law of heat conduction, which states the following:

1) $$\vec{q}(\mathbf{r},t) = -\kappa \nabla T$$

where $\vec{q}$ is the heat flux vector and corresponds to the direction of heat flow at a position **r** at time *t*, $\kappa$ is the thermal conductivity of the medium (and may depend on both temperature and position within the medium), and T is the temperature of the bulk medium. Under certain conditions, $\kappa$ may be considered a constant, but in general it depends on both temperature and position.

By considering a volume V enclosed by a surface S containing heat sources represented by a function $g(\vec{r},t)$, and then applying the divergence theorem, the standard heat equation may be derived[114]:

2) $$\rho c \frac{\partial T}{\partial t} = \nabla \cdot \kappa \nabla T + g(\mathbf{r},t)$$

where $\rho$ and c are the density and heat capacity of the medium (tissue, in the case of cardiac ablation). The Bioheat equation, originally described by Pennes[115] in 1948, added two source terms to the heat equation:

3) $$c\rho\frac{\partial T}{\partial t} = \nabla \cdot \kappa \nabla T + h_m + h_b$$

4) $$h_b = V \cdot c_b\left(T_a - T_v\right)$$

The additional terms account for heat delivery to the tissue by way of blood circulating through the tissue ($h_b$), and heat production within the tissue ($h_m$) due to increases in metabolism, contraction, and other sources. Equation 4 gives an expression for the rate of heat transfer from the blood to the tissue, where V is the volume of blood flow per unit volume of tissue, $c_b$ is the specific heat of blood, and $T_a$ and $T_v$ are the arterial and venous blood temperatures, respectively[115].

In 1980, Chen and Holmes modified the bioheat equation and provided a firm theoretical basis for the importance of the microvasculature when analyzing small-scale (~10 mm) heat distributions[116] in perfused tissue. The work by Chen suggests that tissue-vessel temperature equilibrium takes place at a higher level of the vasculature than previously assumed, and occurs in the precapillary arterioles rather than the capillaries. Also, he states that larger vessels present in the region should be accounted for individually rather than be lumped together in a continuum, and gives the following expression for the blood perfusion term ($h_b$):

5) $$h_b = \rho_b c_b \sum_i T_{bi} u_i A_i \sin\left(\theta_i\right)$$

where $\rho_b$ and $c_b$ are the density and specific heat of blood, $T_{bi}$ is the "flow-weighted" average temperature of the $i^{th}$ vessel, $u_i$ is the mean velocity of blood in the $i^{th}$ vessel, $A_i$ is the flow

area of the $i^{th}$ vessel, and $\theta_i$ is the angle between the vessel and the exiting or entering surface of the tissue volume.

Chen and Holmes also stressed the importance of the characteristics of the blood flow in each individual vessel of the microvasculature (velocity as well as thermal conductivity in the microvessels). He describes the governing equations as follows:

6) $$x_{ei}\frac{dT_{bi}}{dx} = T_s + T_{bi}$$

7) $$x_{ei} \equiv \frac{A_i \rho_b c_b u_i}{U_i P_i}$$

Equation 6) defines how individual vessels equilibrate with the solid tissue. $T_s$ is the temperature of the solid tissue, not including the vasculature. The tissue temperature of the bulk medium (solid tissue and vasculature), T, may be significantly different than $T_s$. $x_{ei}$ represents the length over which the temperature difference between the blood and the solid temperature will be reduced by a factor of 1/e. $U_i$ and $P_i$ are the heat transfer coefficients and circumference of the $i^{th}$ vessels.

The Weinbaum-Jiji equation was later developed to study heat transfer in a 3-layer model, consisting of a skin layer, intermediate layer, and a deep layer[117,118]. Weinbaum *et al.* subsequently developed a simplified version of their bioheat equation, which described thermal effects of countercurrent convection in artery-vein pairs in terms of the effective conductivity ($k_{eff}$). The details of this model are complex, and the validity of the simplified Weinbaum-Jiji model[119] as a general solution to problems in bioheat transfer is a subject of debate[120-122]. However, it may certainly be said that the work by Weinbaum *et al.* precipitated

work which led to significant improvements to the existing framework (i.e., Pennes' bioheat equation).

These models set the stage for further development of heat transfer in perfused tissues; however they were mainly developed to address problems in arising in hyperthermic therapy of cancerous tissue. Panescu *et al.* used finite element analysis and *in vitro* specimens to specifically address heat distributions occurring during RF ablation of cardiac tissue[123]. Their formulation is a modified version of the Pennes equation, with an additional term to address the delivery of energy by a RF current.

7) $$\rho c \frac{\partial T}{\partial t} = \nabla \cdot \kappa \nabla T + \mathbf{J} \cdot \mathbf{E} - h_b - Q_{el}$$

The current density and electric field generated by the ablation probe are given by **J** and **E**, respectively. Heat contributions due to metabolic heating were neglected in this study. The term $Q_{el}$ is the heat contribution due to conductive transfer between the ablation electrode and the tissue. Although not important for non-irrigated ablation electrodes, this term is significant for liquid-cooled electrodes. Liquid-cooled electrodes were designed to allow heat diffusion throughout the tissue without charring the tissue surface, and have been shown to create larger lesion sizes[124].

### *D. Optical Mapping of Cardiac Ablation Lesions*

Optical mapping techniques with transmembrane voltage-sensitive dyes have been used successfully to study electrical phenomena in hearts, including the influence of defibrillation shocks, the spatio-temporal distribution of transmembrane potentials, effects of tissue heterogeneity on conduction, and the role of electroporation in defibrillation[125-131]. Optical techniques have advantages over electrical measurements for the study of the electrical behavior of excitable tissues, such as the ability to take simultaneous action potential recordings from many sites without requiring cellular impalements. Also, optical recordings of activation are not subject to the effects of far-field activations or polarization. However optical mapping also has limitations for studies of transmembrane potentials, including the lack of a direct voltage calibration, the inability to map three-dimensionally, the presence of artifacts produced by heart movement, and averaging effects which affect upstroke velocities of cardiac action potentials[132].

In cardiac optical mapping studies, a transmembrane voltage-sensitive dye such as di-4-ANEPPS is typically used to map electrical activity on the surface of the epicardium. When cells in the tissue undergo an action potential, which may be due to external pacing or sinus rhythm, transmembrane voltage changes due to depolarization shift the emission spectrum of the dye toward shorter wavelengths[133]. This causes an increase in the fluorescence intensity at short wavelengths and a simultaneous decrease at long wavelengths.

Each of these wavelength bands is also sensitive to movement of the tissue, as is evident from the movement artifacts that have been found during the heartbeat. Movement will cause a similar change, either an increase or decrease, in both wavelength bands. We have found that the ratio of these two, computed as the short wavelength fluorescence intensity divided by the long wavelength intensity, is mainly sensitive to the transmembrane potential[133,134].

### *E. Electrogram Recordings of Ablation Lesions*

Extracellular potential recordings occur due to the flow of ionic currents between the intracellular and extracellular domains that occur during activation of cardiac myocytes[135,136]. There are numerous issues which arise while recording extracellular potentials to determine activation times, some of which are common to both unipolar and bipolar electrodes, while others are unique to only one of the two recording methods. Since our method for evaluation of conduction latency does not currently necessitate electrode mapping of the myocardium, this discussion will be limited to electrode configurations which map activation at a single tissue region.

In contrast to intracellular transmembrane voltage recordings, such as microelectrode recordings, extracellular recordings may be significantly affected by activation of cells at sites distant from the recording electrodes. Durrer and others[136-141] report that unipolar recordings are particularly vulnerable to far-field activation, and that in some cases these components may interfere with detection of a local activation. For example, large far-field activations may obscure the exact timing of a depressed local activation, such as those that occur following a healed myocardial infarct or RF ablation. Since extracellular electrograms report electrical activity of a tissue region rather than individual cells, amplitudes of such waveforms may be significantly diminished if there is damaged tissue in the recording region, leaving only a fraction of the original viable tissue. A simulation study by Steinhaus[142], which examined unipolar and bipolar electrograms in thin strips of tissue, revealed extracellular waveforms with amplitudes of less than 10 μV, illustrating the importance of viable tissue dimensions during collection of extracellular electrograms. This is important for both unipolar and bipolar recordings, as low amplitude waveforms found in

severely damaged tissue may be hidden beneath electrical noise levels found in typical laboratory settings. Studies performed during normal propagation in non-damaged tissue suggest that timing of the negative deflection is not significantly affected by distant activations, although minima and maxima of activation waveforms may be altered[137].

Unipolar electrode recordings are particularly vulnerable to effects of polarization, which may cause the baseline signal to rise outside of the range of the recording amplifier. This phenomenon is due to changes in the half-cell potential which occur as a result of current flow through the electrode-electrolyte interface. These changes are due to ohmic, concentration and activation overpotentials, and all act to produce changes in the half-cell potential from its equilibrium value. Ohmic overpotentials are a result of voltage drops from the recording electrode to the reference electrode across the electrolyte bath. Concentration overpotentials result from changes in ionic concentration in the vicinity of the electrode-electrolyte interface. Activation overpotentials occur as a result of differences in activation energy barriers between oxidation and reduction of metal cations, one of which predominates during a given direction of current flow[143]. Effects of polarization during unipolar electrode recordings may be minimized by the use of a nonpolarizable metal/anion electrode, such as the AgCl electrode[143]. The procedure for optimal chloriding of the AgCl electrode has been described by Geddes et al[144]. Also, baseline drift due to polarization or other factors may be reduced by high-pass filtering (>0.5 Hz), which may also help reduce effects of low-frequency motion due to variable electrode contact and/or cardiac contraction[141]. Higher cutoff high-pass and band pass filters may further reduce system noise and AC line noise, however high-pass filtering at higher cutoffs (>30 Hz) also tends to alter waveform morphology[141]. When identifying the main local activation this filtering may be desirable,

since distant activations which may obscure local activations tend to produce peaks with lower maxima and longer durations[145], however lower frequency peaks may also be important indicators of local tissue damage.

Bipolar recordings may be susceptible to effects of activation at non-local sites, however these effects will be lessened due to the fact both the recording and the reference electrode are positioned adjacent to each other, hence their difference will reject far-field signals. The degree to which far-field effects will be lessened is a function of both the interelectrode distance as well as the distance between the activation and the recording site[136,141]. As the interelectrode distance in a bipolar electrode configuration increases, the effects of distant activity increase. This is logical, since increasing interelectrode distances will eventually approximate the unipolar electrode configuration.

Bipolar recordings are typically more difficult to interpret than unipolar recordings, due to the fact that the bipolar waveform is often more complex and generally have higher morphological variability. While there is a general consensus that the negative deflection in the unipolar electrogram represents activation, there is some disagreement as to which parameter ($dV/dt_{max}$, maximum amplitude, waveform onset, etc.) best indicates activation in a bipolar electrode configuration. A study by Paul et al[146] found that the maximum amplitude best indicates activation as determined by unipolar maximum slope (typically the negative deflection), however this study had no gold standard (i.e. microelectrode recordings) with which to definitively measure activation times. The study also examined maximum slope and the onset of activity in the bipolar electrogram as possible activation indicators, however neither of these parameters correlated with the negative deflection as well as the maximum amplitude.

The term "fractionated activity" has been used to describe peaks with small deflections (<1 mV) and long durations (>100 ms), which are typically found during acute ischemia and in healed myocardial infarcts[145]. Ischemia may occur following ablation therapy due to coagulation and subsequent blockage in the microvasculature[21], which may lead to infarcts and subsequent fractionated electrograms. Fractionation of electrical activation is thought to be due to highly discontinuous conduction[147], which may occur due to fibrosis or other events which lead to tissue discontinuities and/or structural deformities in adjacent myocyte strands. Additional peaks found in electrograms showing fractionated activity may complicate the identification of the "true" activation during non-ideal conditions in the heart. Although most investigators now believe that fractionated activity represents true abnormalities in conduction of activation, and may help to indicate the presence of reentrant circuits or a predisposition to ventricular tachycardia[145], others have proposed that the additional peaks may simply be recording artifacts such as motion[148] and/or effects of filtering[149]. Motion artifacts described by Ideker et al were small (100-200 μV) in magnitude, but did resemble fractionated activity. They were eliminated by ensuring secure contact between epicardial surface and the recording electrode[148]. Errors due to filtering may be minimized by filtering minimally while taking recordings, so that the effects of filtering may be seen during post-processing of data. The extent to which electrograms should be filtered depends on what type of data the investigator wishes to observe, and there are tradeoffs involved in increasing the amount of filtering. For instance, high-pass filtering at a lower cutoff frequency in the unipolar electrogram may allow observation of the site of earliest activation; however far-field activations will also be present in the recording. Raising the

cutoff reduces far-field effects, but does not allow reliable identification of wavefront propagation direction[141].

Another factor which may affect extracellular recordings is the direction of wavefront propagation with respect to the recording electrode(s). Unipolar electrodes used to record extracellular potentials will show a steep negative deflection regardless of the angle of approach of an activation wavefront. The morphology of the unipolar electrode may be significantly altered if the recording electrode is near the origin or termination of an activation wavefront, but the negative deflection will still be found[150]. Bipolar electrodes, however, will record a waveform with amplitudes which vary according to the angle of approach of the propagating wavefront. A wavefront which propagates in the same direction as a line connecting the bipolar electrodes (parallel or anti-parallel) will show the maximum bipolar signal for a particular wavefront, while a wavefront which propagates at some other angle will show a reduction in amplitude. Thus in contrast to unipolar recordings, bipolar electrograms in damaged tissue cannot reliably give information regarding wavefront propagation direction with respect to the electrode(s). Theoretically, a symmetric (plane, spherical, etc.) wavefront which approaches from a direction perpendicular to the electrode axis should produce no electrical waveform since both electrodes will record the same voltage and give a difference of zero. However, this is rarely reported in practice. A study by Blanchard et al[151] showed significant reductions in amplitude for near-perpendicular propagation of bipolar waveforms, and also revealed that these smaller amplitude waveforms were more likely to contain multiple peaks. However the incidence of zero amplitude electrograms in this study seemed low, since for peak-to-peak amplitude waveforms the baseline voltage was approximately two standard deviations from the mean.

While extracellular recordings have significant advantages over intracellular recordings, such as being non-invasive to cells, having the ability to more easily record activations from a large number of closely spaced sites, and being much simpler to position, they tend to be more susceptible to activity occurring outside the local recording region and also tend to show effects related to wavefront orientation. The additional effects found in extracellular recordings may complicate identification local activation in some cases, however these effects may also serve as important indicators of tissue health and as a guide for ablation of accessory pathways[152] and other surgical techniques which require rapid localization of reentrant[153] and focal sources (i.e. drivers)[154] of activation.

### *F. Conduction Velocity and Changes in Normal Propagation*

Reports by Sano *et al.* and others demonstrated that the speed of an activation wavefront may vary considerably, according to factors such as fiber orientation[130,155-158], temperature[156,159], wavefront curvature[130,160], ischemia[155], and depth[156,161] within the myocardial wall. When predicting whether conduction block will occur across an incomplete lesion, these factors must be carefully considered.

Cabo *et al.* have examined the effects of various factors upon the minimum width of viable tissue necessary to support conduction ("critical gap width")[160]. They showed, using both models and experiments, that increases in pacing frequency increase the critical gap width, while parallel arrangement of cardiac fibers with respect to the tissue isthmus decreases the critical gap width.

The safety factor, originally described by Rushton[162], may be qualitatively described as the ratio of the current source (e.g., depolarized cells) over the current sink (downstream resting cells which have not been activated). Most factors which alter the critical gap width are ultimately the result of a change in the safety factor, and block within excitable tissue typically occurs due to an insufficient excitatory current from adjacent cells. For instance, if fibers are oriented perpendicular to an activation path through a gap, the critical gap width will be larger than the case where fibers are oriented along the path through a gap. This is due to a decrease in source current because of higher resistance connections across fibers. When the frequency of the stimulus is increased, the duration between stimuli may be insufficient for sodium channels to fully recover. Thus fast sodium currents may be reduced, resulting in a decrease in the safety factor.

### *G. Changes in Conduction Velocity Due to Ischemia*

Occlusion of coronary vessels and subsequent hypoxia results in immediate changes in cellular and tissue properties. Myocytes have little reserve capacity of high-energy phosphate compounds (ATP), and these are exhausted within approximately 30 seconds of normal cellular metabolism. Exhaustion of high-energy compounds leads to altered metabolic pathways, which result in ionic imbalances, acidosis, and changes in gap junctional conductance[163]. Using computer simulations, Jongsma and Wilders showed that halving gap junctional conductance results in a longitudinal conduction velocity decrease of only 13%, but decreases the transverse conduction velocity by 36%[164]. Experimental studies by Gutstein et al show that knockout mice with decreases in Cx43 (connexin 43) expression of 95% have marked reductions in both longitudinal and transverse conduction velocities. In these experiments, conduction velocity was reduced by 55% for the transverse direction and 42% in the longitudinal direction[165]. Others, such as Eloff et al[166] and Lerner et al[167], have demonstrated that significant changes in conduction velocity occur with less severe reductions in Cx43 expression (~50%). Further, Eloff also reported no change in the anisotropic ratio of longitudinal to transverse conduction velocity reduction. Although it has been recognized that gap junctions play a crucial role in the conduction of activation, the precise quantitative effect of gap junction reductions upon conduction velocity is still a subject of debate.

Following 2-3 minutes of ischemia, a slight depolarization of the resting transmembrane potential occurs, and the resting potential decreases from -80 to approximately -65 mV. During early ischemia, the APD is prolonged, but this is followed by a shortening of the APD. Although the APD is shortened, the atrial effective refractory

period (AERP) is lengthened during ischemia. In addition, the APA and $dV_m/dt$ are significantly reduced. Reductions in APA lead to a reduction of the safety factor, which causes reductions in conduction velocity and may lead to conduction block. Reductions in $dV_m/dt$ (presumably due to damage to sodium and other fast ion channels) also lead to reductions in conduction velocity.

Conduction velocity is affected by both active and passive changes in the myocardium. Since ischemia has effects upon both, the extent of ischemic injury following cardiac ablation must be carefully considered when using a metric which depends upon either conduction properties or passive electrical properties.

## CHAPTER 2

## TRANSLESION STIMULUS-EXCITATION DELAY AS A METRIC FOR RADIOFREQUENCY ABLATION LESIONS IN HEARTS

### *A. INTRODUCTION*

Since Dr. Melvin Scheinman performed the first catheter ablation to halt a supraventricular cardiac arrhythmia in 1981, various methods have been developed to block conduction in cardiac tissue[168-176]. Radiofrequency (RF) has emerged as the preferred energy source for both endocardial and epicardial tissue ablation[169,177-181]. Epicardial RF ablation for the treatment of atrial fibrillation (AF) has several advantages over catheter-directed endocardial RF ablation. The risk of a thromboembolic event is less with epicardial techniques[182] and more complete and continuous ablation lines are obtained with surgical ablation than with catheter-directed approaches[183].

Radiofrequency ablation for AF is frequently performed during cardiac surgery while the heart is arrested[179,184,185]. However, confirmation of complete conduction block on an arrested heart is not currently available. Advancements in minimally invasive surgical techniques have allowed the application of RF ablation to the epicardium of the beating heart[186,187]. While the heart is beating, it may be possible to verify that lines of ablation are indeed transmural and produce complete and continuous block of electrical conduction. The immediate evaluation of epicardial ablation lesions can confirm success and eliminate the need for repeat or additional procedures.

Delay in the time required to conduct an electrical impulse around an ablation lesion may be measured before removing the RF electrode probe to determine if the ablation is sufficient. This can be accomplished by placing stimulation and recording electrodes directly on the ablation probe on opposite sides of the lesion, eliminating the need for an additional mapping catheter. Alternatively, a separate diagnostic device containing four electrodes (two on each side of the lesion separated by a fixed distance) may be used to measure the activation time delay across the lesion. The creation of a significant time delay may unambiguously demonstrate trans-lesion conduction block, and therefore lesion completeness. Marked increase in time delay may also provide a quantitative indication that the lesion ends have extended to anatomical barriers. The relationship between time delay and path length of viable tissue post-ablation may be predictable, based on the conduction velocity of an action potential in the cardiac tissue. This may allow establishment of a target increase in time delay that indicates a sufficient increase in pathway length resulting from continuous, transmural lesions. This topic is examined in chapter 3.

## *B. METHODS*

*Rabbit Heart Preparation*

Fresh hearts isolated from New Zealand rabbits (N = 11) of either gender were perfused through the aorta with Tyrode's solution (129 mM, NaCl, 5.4 mM KCl, 1.8 mM $CaCl_2$, 1.1 mM $MgCl_2$, 26 mM $NaHCO_3$, 1 mM $Na_2HPO_4$, 11 mM Dextrose, and 0.6 μM bovine serum albumin). The solution was bubbled with 95% $O_2$ and 5% $CO_2$, and maintained at 37 ± 0.2ºC. Hearts were stained with 50 μl injections of a 0.0021 M solution of di-4-ANEPPS, a transmembrane voltage-sensitive fluorescent dye used in detecting the action potential across membranes of nerve and cardiac muscle cells. The dye was dissolved in ethanol, and injected into the arterial perfusion tube.

Lesions (N = 29 total) were produced on the heart by RF ablation (100-1200 J/cm²). Two to three lesions were made on each heart, and approximately 60 minutes passed between the creation of each lesion. The animal was sacrificed approximately 30 minutes before the creation of the first lesion.

Before and after each ablation, a glass plate was gently held on the region to facilitate optical mapping. During each ablation procedure, the plate was removed and a prototype RF ablation probe was positioned in the middle of the region (Fig. 2.1). The effects of ablation were studied in regions of the left ventricular free wall epicardium, or in the anterior or posterior epicardium near the ventricular septum, were studied. Ventricular regions were studied instead of atrial regions because the wall thickness of rabbit ventricles is more comparable to that of human atria.

*Electrical Pacing and Recording*

One pair of electrodes (electrodes 1-anode, and 2-cathode, Fig. 2.1) was used to deliver bipolar pacing stimuli from an isolated stimulator (Isostim A320, World Precision Instruments, Sarasota, FL). The pacing amplitude was set at twice the pacing threshold or at 10 mA if the threshold was ≥ 5 mA; pacing pulse width was 3 msec; pacing interval was chosen just above the resting heart rate and ranged from 340 to 660 msec. The other electrode pair (electrodes 3-negative and 4-positive) was used to record a bipolar electrogram. All signals (stimulus and electrogram) were conditioned with an isolation amplifier (AD210AN, Analog Devices, gain 100, low pass <16 kHz), and digitized at 10 kHz using Labview and a DAQPad 6070E data acquisition board (National Instruments, Austin TX). Inter-electrode spacing for each pair was 1-2 mm and spacing between the pairs was 10 mm. During optical mapping, stimulation and electrogram recording electrodes were Ag-AgCl (diameter 0.25 mm, length 2 mm). When electrograms were recorded without optical mapping, the pacing and recording electrodes were stainless steel (contact area with heart ~1 $mm^2$ per electrode), and were attached to the RF probe and positioned in a line at 90 degrees from the ablation probe (Fig. 2.1).

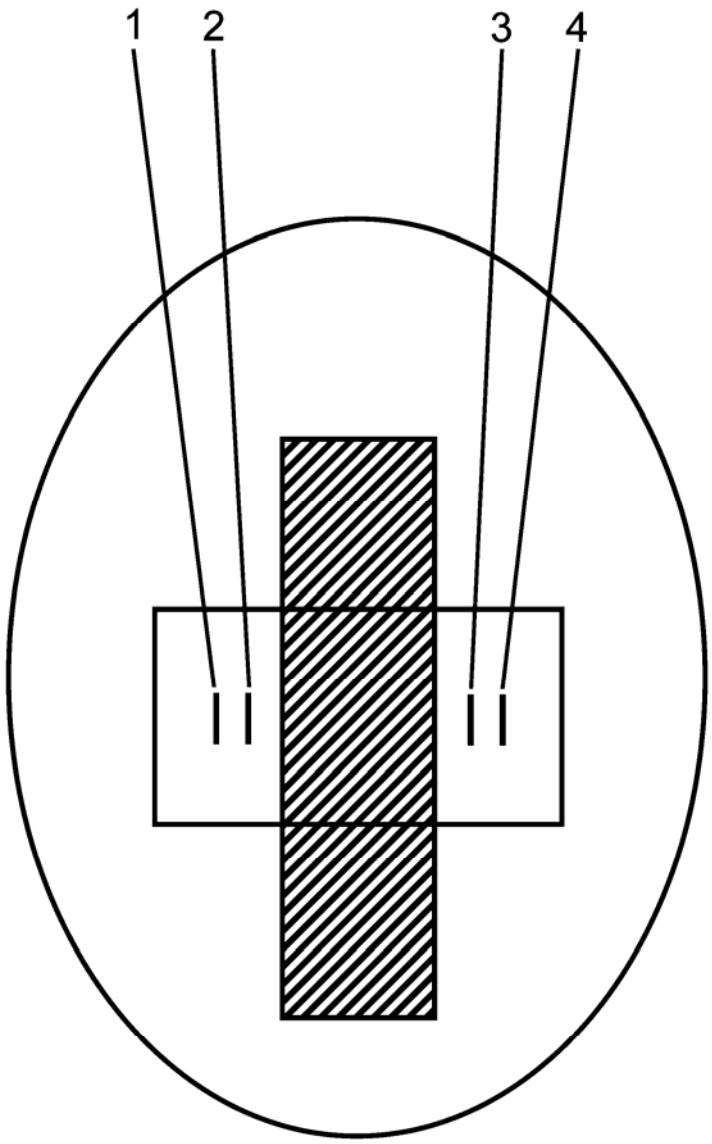


**Figure 2.1** Diagram showing the arrangement of the ablation probe and electrogram recordings on the heart. Ablation probe for continuous lesion is indicated in cross-hatched area. The open rectangle indicates the area mapped optically. Electrodes 1 and 2 were used for bipolar pacing; 3 and 4 were used for bipolar electrogram recording.

*Fluorescence Recording*

An argon ion laser with a wavelength of 488 nm was used to scan a 9x19 mm grid of 128 laser spots. Average light power on the heart surface was 20 mW. Red and green

fluorescence (wavelengths >590 nm and 510-570 nm, respectively) were collected simultaneously with two photomultiplier tubes located in front of the heart. Each fluorescence signal was digitized at a rate of 1 kHz at each spot. Laser scanning and recording were controlled by a microprocessor system (M67, Innovative Integration, Simi Valley, CA) within a PC. To diminish effects of cardiac motion on the recordings, the green fluorescence signal was divided by the red signal[133]. The ratiometric signal was used to measure activation times in tissue at the laser spots.

*Ablation Procedures*

Electrogram and optical measurements were taken before ablation on each heart (baseline). A prototype ablation device (nContact Surgical, Inc.) was used to create a lesion through the middle of the optical grid and between the stimulation and recording electrodes. RF energy was applied for 20-60 seconds at a power of 10-20 Watts using a 480 kHz generator. Lesions were created by application of RF energy using a 2-cm ablation electrode. Lesions extended from the apex to the atrioventricular annulus. Incomplete lesions were created by discrete applications of the ablation probe separated 1-7 mm apart to produce a gap, or by using a lower power level to produce non-transmural lesions. Before and after each ablation, recordings were taken to examine the effects of ablation on the stimulus-excitation time delay.

*Analysis of Stimulus-Excitation Time Delay*

The activation time for optical recordings was defined as the time of the maximum upstroke velocity ($dV_m/dt_{max}$). The activation time for electrogram recordings was defined as the time at which the magnitude of the bipolar electrogram was greatest.

The stimulus-excitation time delay across the lesion was measured in two ways. For optical mapping, it was the difference between activation times at a spot near the pacing electrode and a spot near the recording electrode at the opposite side of the lesion. For electrogram recordings, the stimulus-excitation time delay was measured from the stimulus pulse to the activation time in the electrogram recorded on the opposite side of the lesion. This time delay included the time from the application of the stimulus pulse to excitation of cells near the stimulation electrode, which was measured to be 6-7 msec.

*Viable Tissue Staining*

After completion of all recordings, hearts were perfusion stained with 2,3,5-triphenyltetrazolium chloride (TTC, Sigma-Aldrich, Inc.; 2.1 g of TTC in 150 ml of 0.9% NaCl) to determine histologically the location and completeness of each lesion. After staining with TTC, viable tissue appeared red and non-viable tissue appeared grey (Fig. 2.2). Lesions were bisected to obtain digital photographs and to measure lesion width, depth, and length.

*Statistical Analysis*

Significance of differences in time delay was determined using Student's t-test. For complete lesions, time delay was compared with pre-ablation baseline measurements using a one-tailed test to determine if the delay increased significantly. For incomplete lesions, a two-tailed test was used to determine if a time delay change occurred. Paired t-tests were used to compare delays for the same region measured pre and post-lesion. Non-paired t-tests were used to compare delays for incomplete lesions vs. complete lesions. All results are given as the mean ± standard error of the mean (SEM).

## *C. Results*

*Examination of TTC-stained Hearts*

Photographs were taken of representative incomplete and complete lesions, and stained immediately post-procedure with TTC (Fig. 2.2). The incomplete lesions contained a gap between two discrete, transmural segments, or were not transmural. The complete lesions were continuous and transmural. The average length for complete lesions was 26.17 ± 1.37 mm. For all lesions, the average width was 7.1 ± 0.20 mm; depth was 3.1 ± 0.2 mm. Of 15 incomplete lesions, 12 were non-continuous, and 3 were non-transmural. Individual gap widths were 1.0, 1.5, 1.5, 1.0, 5.5, 4.0, 3.0, 7.0, 3.0, 2.0, 4.0, 3.0 mm, and had a mean of 3.0 ± 0.5 mm.

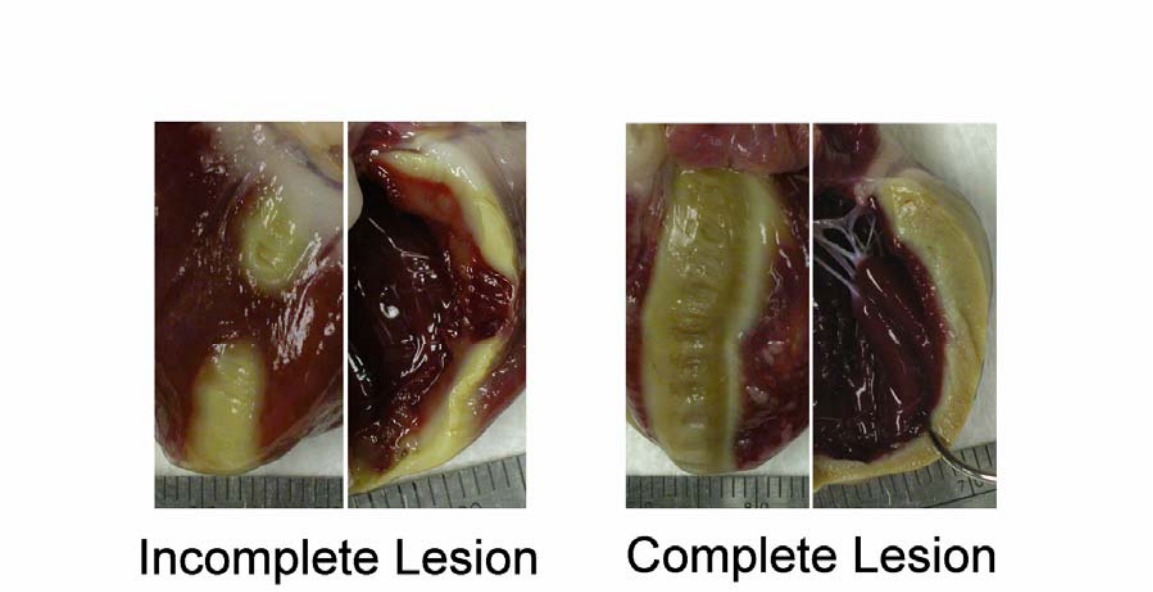


**Figure 2.2** Photographs of incomplete and complete lesions. The two photographs on the left show an epicardial view and a transmural section of an incomplete lesion in the posterior ventricular septal region. The two photographs on the right show these views for a complete lesion in the left ventricular free wall. Viable tissue is stained red; ablated tissue appears as a lighter color. Divisions on rulers at the bottom of the photographs indicate mm.

*Electrograms*

Electrograms were obtained before ablation and after production of complete and incomplete lesions (Fig. 2.3). For incomplete lesions, time delay did not change (21 msec pre-lesion and 21 msec post-lesion). After the formation of a complete lesion, time delay increased from 28 msec pre-lesion to 89 msec post-lesion.

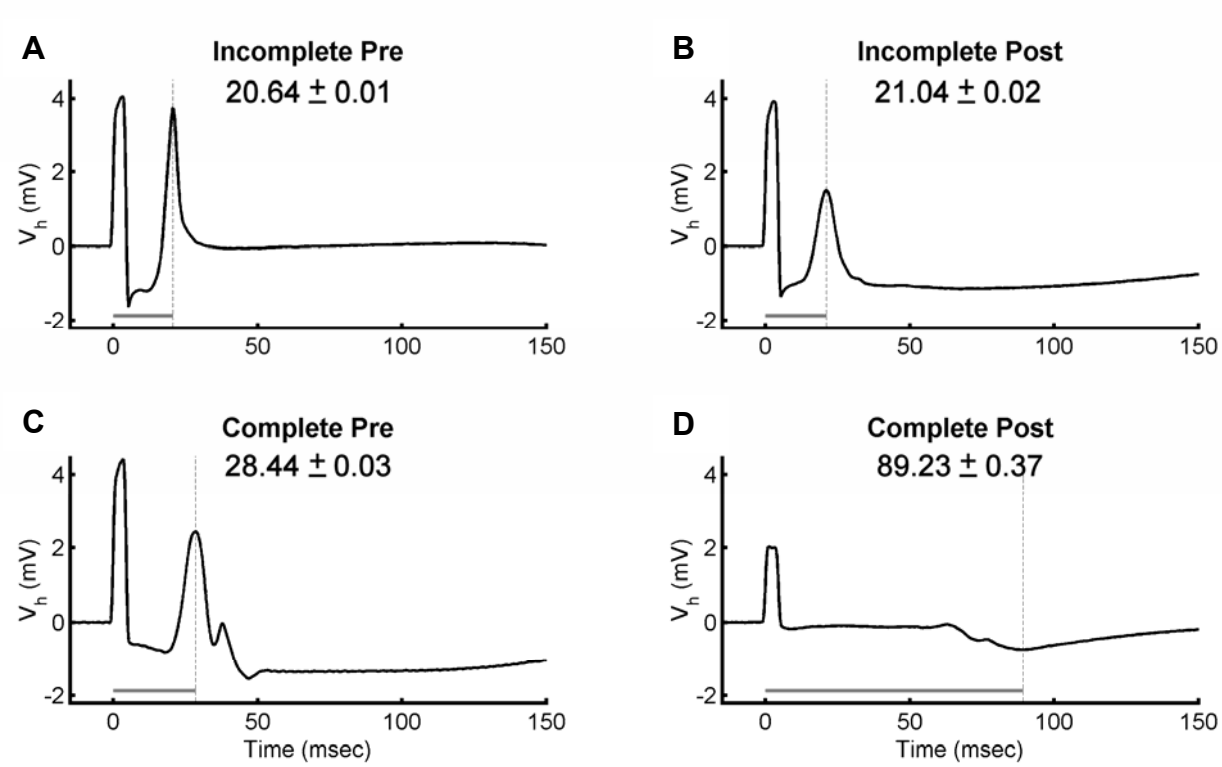


**Figure 2.3 Electrograms for incomplete and complete lesions. The electrograms in Row I were recorded before (A) and after (B) an incomplete ablation. Electrograms in Row II show recordings before (C) and after (D) a complete lesion. The mean conduction delay reported for each plot is an average time delay from 27 individual recordings (beats). The length of the colored horizontal bar at the bottom indicates the time delay from the stimulus on one side of the lesion to excitation on the opposite side (expressed as the mean +/- SEM for 27 beats).**

*Optical Maps*

Representative isochronal maps and associated action potentials are shown before ablation (baseline; Fig. 2.4), after the production of an incomplete lesion (Fig. 2.5), and after a complete lesion (Fig. 2.6). Upper plots in each figure show activation isochrones produced by pacing on the left side of the mapped region. The numbers represent the time, in milliseconds, of excitation relative to the stimulation pulse. The map in Fig. 2.4 demonstrates uniform conduction of the impulse from left to right across the epicardium, traversing the grid in 30 msec. The lower portions of the figures show the optical signals from all laser spots in 150 msec segments that begin at the onset of stimulation. In the incomplete lesion, the impulse traveled across the epicardium from left to right in the center of the gap but conduction was restricted to the gap by the ablated regions on either side of the wavefront. With the incomplete lesion, the total time to activate the mapped region was slightly greater than that of the pre-lesion (35 vs. 30 msec). In the areas of transmural ablation, the optical signal waveforms showed no amplitude deflection indicating no activations in these areas. For the complete lesion (Fig. 2.6), the stimulus began on the left, but was blocked by the ablation lesion. The optical signal waveforms in this area of ablation did not show a detectable activation. The right part of the mapped region showed activation much later (average 75 msec) than that of the pre-lesion recordings.

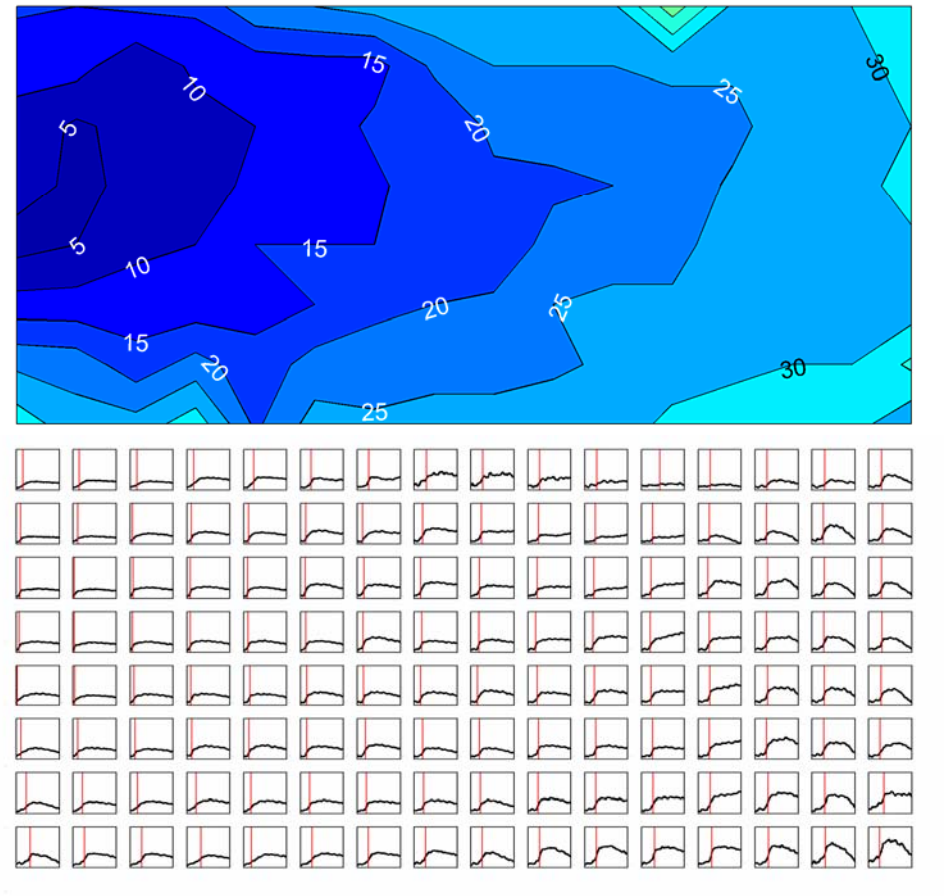


**Figure 2.4** Activation contour map and action potential recordings before RF ablation. Upper plot shows activation isochrones produced by pacing on the left side of the mapped region. Times shown in msec are relative to the onset of the stimulation pulse. Lower portion of the figure shows optical signals from all laser spots. For each spot, a 100 msec segment is plotted that begins at the onset of stimulation. The vertical scale is the same for all spots to illustrate differences in the relative amplitudes of deflections among spots. Activation times are indicated with vertical lines. Activation times for optical signals were averaged from 27 beats.

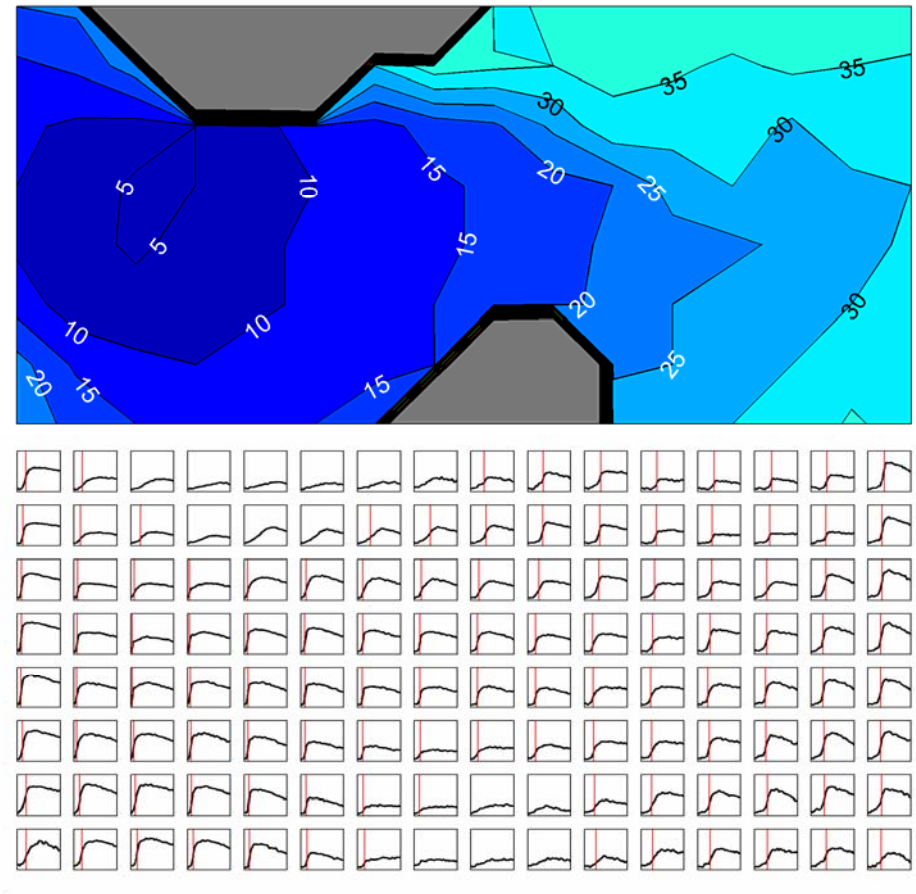


**Figure 2.5** Activation contour map and action potential recordings after production of an incomplete lesion.

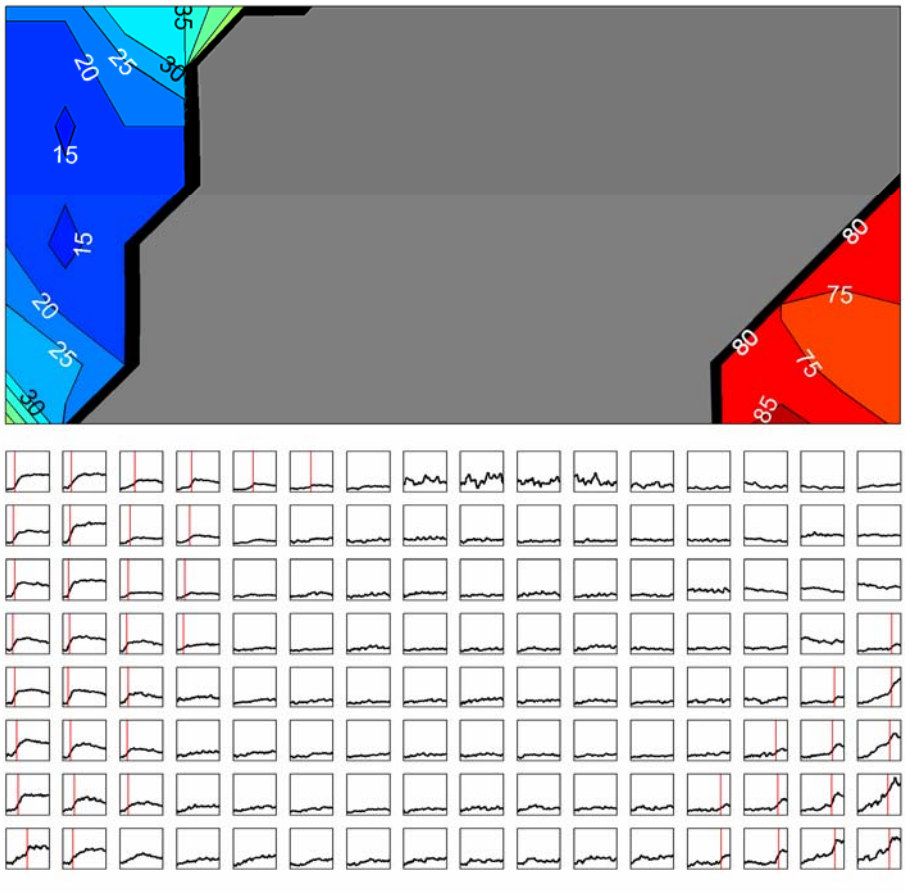


**Figure 2.6** Activation contour map and action potential recordings after production of a complete lesion.

*Time Delay*

The time delays for complete and incomplete lesions as measured by electrogram and optical recordings are shown in Tables 2.1 and 2.2, and graphically in figure 2.7.

For incomplete lesions, post-lesion time delay did not differ significantly from the pre-lesion delay. The difference in post-lesion and pre-lesion mean time delay was 3 msec for electrogram measurements and 23 msec for optical recordings.

For complete lesions, the mean post-lesion time delay was significantly greater than the mean pre-lesion delay, for both electrogram (70 msec) and optical (65 msec) recordings ($p<0.05$). In addition, the post-lesion time delays were significantly longer for the complete lesions than they were for the incomplete lesions ($p<0.05$).

Electrogram measurements of the time delays produced lower SEM for incomplete lesions and a larger disparity in time delay measurements between complete and incomplete lesions than optical recordings.

In three experiments, time delay was measured at two time points after ablation to assess recovery over time. In one lesion with a small epicardial gap of 1 mm, the conduction delay doubled when measured within 10 minutes post ablation, but recovered to near baseline after one hour. For experiments in which complete lesions were assessed, conduction time delay increased 3- to 4-fold after ablation. In contrast to the pattern observed with the incomplete lesion, neither of the continuous, transmural lesions exhibited marked recovery when measured more than two hours after ablation. The effects of recovery on post-lesion time delay are examined more thoroughly in chapters 4 and 5.

**Table 2.1 -** Time Delay Measured by Electrogram Recordings

| ELECTROGRAM | Pre-lesion (msec) | Post-lesion (msec) | n |
|---|---|---|---|
| Incomplete | 45 ± 12.20 | 48 ± 10.45 | 12 |
| Complete | 33 ± 3.97 | 103 ± 10.59[a,b] | 14 |

**Table 2.2 -** Time Delay Measured by Optical Recordings

| OPTICAL | Pre-lesion (msec) | Post-lesion (msec) | n |
|---|---|---|---|
| Incomplete | 33 ± 10.11 | 56 ± 16.44 | 9 |
| Complete | 28 ± 8.59 | 93 ± 10.51[a,b] | 9 |

[a] $p<0.05$ for post-lesion vs. pre-lesion

[b] $p<0.05$ for incomplete lesion vs. complete lesion

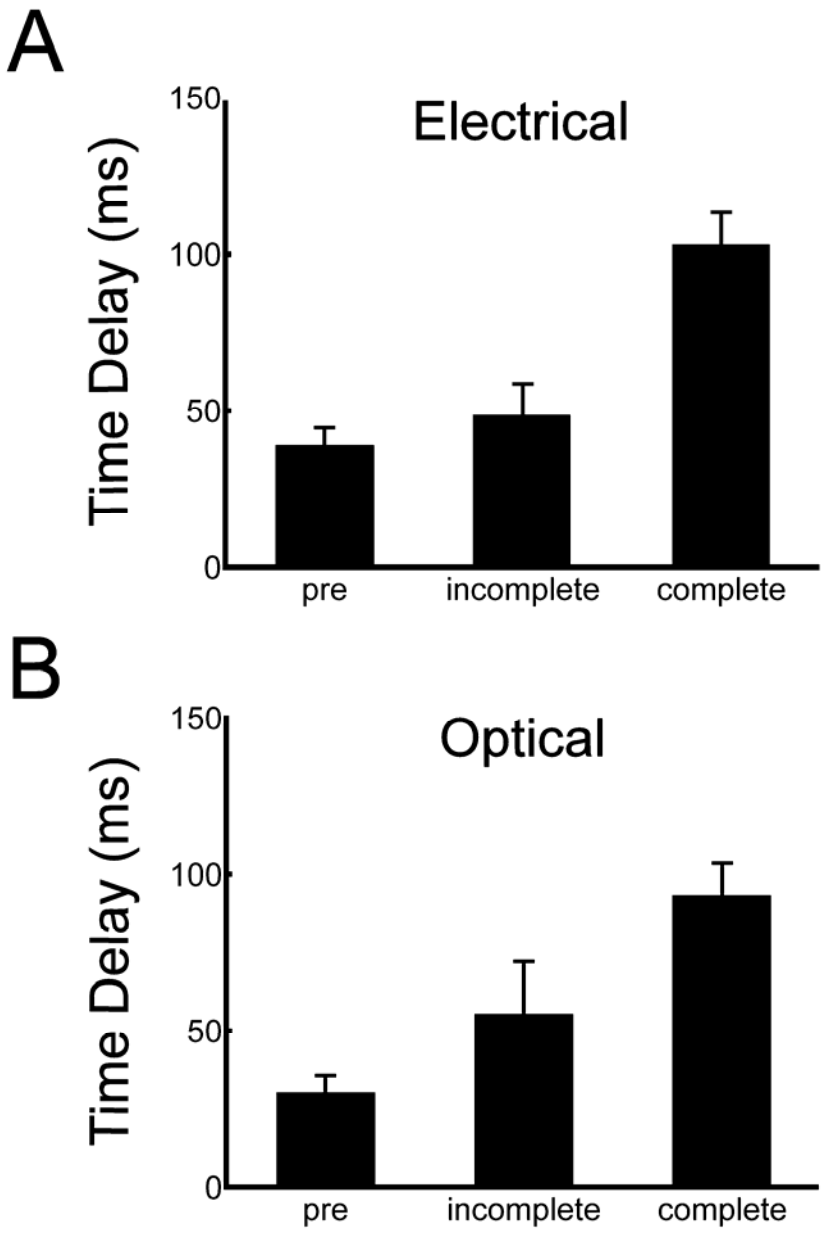


**Figure 2.7** Electrical and optical time delays measured before lesion creation, and for incomplete and complete lesions. Mean values are shown, with standard errors of each mean indicated by error bars.

## *D. DISCUSSION*

Methods used to determine presence of conduction block after RF ablation include P wave changes after ablation of the cavotricuspid isthmus for atrial flutter[188], detailed electrogram mapping with or without electrical stimulation[189,190], changes in electrogram amplitude[191], and double potentials[192]. Many of these methods use intravascular catheter approaches and require several catheters for pacing and electrogram recordings, usually with continuous repositioning of the probe.

Endocardial ablation techniques for creating linear lesions for the treatment of atrial fibrillation using intravascular catheters have reported success rates of 20-60% despite established techniques for evaluating conduction block within the pulmonary veins[193]. Both surgical and catheter approaches for the treatment of atrial fibrillation have been hampered by the inability to create continuous and transmural lesions. Incomplete lesions have been associated with the recurrence of atrial fibrillation or the development of reentrant atrial tachyarrhythmias[194].

### *Epicardial Approach*

The epicardial techniques described here introduce a new and promising method of myocardial ablation and intraoperative confirmation of lesion completeness. Epicardial ablation with new ablation devices may obviate the need for cardiopulmonary bypass support therefore allowing the procedure to be performed while the heart is beating. As such, electrical signals throughout the heart are active and lesion completeness can be evaluated during the ablation procedure.

A diagnostic device incorporating bipolar pacing and recording electrodes capable of measuring time delay as described here should accurately assess ablation line continuity and transmurality, provide a metric for determining lesion completeness intraoperatively, and improve outcomes after atrial fibrillation treatment. Alternatively, diagnostic electrodes could be incorporated in the ablation device to simultaneously create the lesion and evaluate its completeness.

*Time Delay*

The results demonstrated recovery of time delay for lesions with gaps, whereas complete lesions had a low extent of recovery. This recovery may be due to revival of stunned tissue at the perimeter of ablated tissue[188,189,192,196,197]. For complete lesions, recovery may produce only a small decrease in the post-lesion path length (e.g., at the lesion ends), whereas recovery of tissue in an epicardial gap region may produce a large decrease in path length since conduction may again occur directly across the lesion. Increases in time delay were significantly larger for complete lesions and the magnitude of increase may predict stability of time delay. Complete lesions showed a greater than two-fold increase in time delay, and did not recover, indicating that the delay must exceed a threshold to avoid recovery of conduction post-ablation. A greater than two-fold increase in delay may indicate production of a complete lesion that was incapable of recovery.

Strategies to incorporate measurement of time delay into ablation systems may be advantageous. Ablation lines that appear acutely transmural can reveal gaps during follow-up[198]. Even so, metrics that predict outcomes either by confirming conduction block of

anatomic structures or demonstrating the inability to induce an arrhythmia with known pacing techniques have been shown to predict long term success[199].

The value of lesion completeness is a current topic of debate. It has been suggested that ablation lesions of myocardium may not need to be complete (continuous and transmural) and that over time lesions grow and outcomes improve. Results presented here suggest that incomplete lesions maintain trans-lesion conduction, which may account for the acknowledged high recurrence rates reported for catheter and surgical ablation of atrial fibrillation. This is further evidenced by Melby et al[200], where electrical propagation persisted through narrow gaps in lesions created on isolated canine atria, even when conduction velocities were significantly slowed. Although atrial fibrillation required larger gaps for 1:1 propagation, their data suggest that even narrow gaps may conduct AF, and that to ensure total block, complete lines of ablation must be created. Alternatively, studies performed by Cabo *et al.* show that increasing pacing frequency increases the critical gap width size[160], suggesting that small lesion gaps may not conduct activation of high-frequency activation which occurs during atrial fibrillation. However, lower frequency components may also be present during atrial fibrillation which may conduct through small gaps.

The increase in time delay from pre- to post-lesion formation is a critical factor for immediate assessment of lesion completeness. The demonstrated difference in time delay increase from baseline provides a clear distinction between complete and incomplete lesions. Results showed a greater than two-fold increase in trans-lesion time delay post-ablation compared to pre-ablation, which confirms conduction block across linear lesions.

# CHAPTER 3

# ABILITY OF MINIMUM ACTIVATION PATH LENGTH TO PREDICT TRANSLESION TIME DELAY

## *A. INTRODUCTION*

In typical lesion sets used to block and/or isolate arrhythmic conduction, activation path length is difficult to determine. However activation paths around simple linear lesions may be approximated and compared with pre-lesion pathways. These linear lesions may serve as building blocks for more complex lesion sets.

Estimation of conduction pathways around linear lesions would give an expected value of time delay based on pre-lesion conduction velocity, and may give additional confidence in time delay as an accurate predictor of lesion completeness.

Heterogeneities within the myocardium are known to affect conduction velocity[147,155-158,161,201-206], and may cause substantial deviations from expected time delays according to the nature and severity of the heterogeneity.

The aim of this report is to determine the reliability of minimum activation path length (APL) in predicting expected time delays, and thus provide additional evidence that a complete lesion has been formed. Also, identification of the path length as a cause of increases in time delay decreases the likelihood that the increases are caused by slow conduction through the ablation lesions.

## *B. METHODS*

*Rabbit Heart Preparation*

Fresh hearts isolated from New Zealand rabbits (N = 11) of either gender were perfused through the aorta with Tyrode's solution (129 mM, NaCl, 5.4 mM KCl, 1.8 mM $CaCl_2$, 1.1 mM $MgCl_2$, 26 mM $NaHCO_3$, 1 mM $Na_2HPO_4$, 11 mM Dextrose, and 0.6 μM bovine serum albumin). The solution was bubbled with 95% $O_2$ and 5% $CO_2$, and maintained at 37 ± 0.2ºC.

Lesions (N = 11) were produced on the hearts by RF ablation (100-1200 J/cm²). Two to three lesions were made on each heart, and approximately 60 minutes passed between the creation of each lesion. The animal was sacrificed approximately 30 minutes before the creation of the first lesion. Following perfusion with Tetrazolium Chloride (TTC), lesions were identified by their light gray appearance while viable tissue appeared dark red.

*Electrical Pacing and Recording*

One pair of electrodes (electrodes 1-anode, and 2-cathode, Fig. 2.1) was used to deliver bipolar pacing stimuli from an isolated stimulator (Isostim A320, World Precision Instruments, Sarasota, FL). The pacing amplitude was set at twice the pacing threshold or at 10 mA if the threshold was ≥ 5 mA; pacing pulse width was 3 msec; pacing interval was chosen just above the resting heart rate and ranged from 340 to 660 msec. The other electrode pair (electrodes 3-negative and 4-positive) was used to record a bipolar electrogram. All signals (stimulus and electrogram) were conditioned with an isolation amplifier (AD210AN, Analog Devices, gain 100, low pass <16 kHz), and digitized at 10 kHz using Labview and a DAQPad 6070E data acquisition board (National Instruments, Austin

TX). Inter-electrode spacing for each pair was 1-2 mm and spacing between the pairs was approximately 10 mm.

*Ablation Procedures*

Electrograms were taken before ablation on each heart (baseline). A prototype ablation device (nContact Surgical, Inc.) was used to create a lesion through the middle of the optical grid and between the stimulation and recording electrodes. RF energy was applied for 20-60 seconds at a power of 10-20 Watts using a 480 kHz generator. Complete lesions were created discrete and overlapping applications of RF energy using a 2-cm ablation electrode. Lesions extended from the apex to the atrioventricular annulus. Incomplete lesions were created by discrete applications of the ablation probe separated 1-7 mm apart to produce a gap, or by using a substantially lower power level to produce non-transmural lesions. Before and after each ablation, recordings were taken to examine the effects of ablation on the stimulus-excitation time delay.

*Analysis of Stimulus-Excitation Time Delay*

The activation time for optical recordings was defined as the time of the maximum upstroke velocity ($dV_m/dt_{max}$). The activation time for electrogram recordings was defined as the time at which the magnitude of the bipolar electrogram was greatest.

The stimulus-excitation time delay across the lesion was measured in two ways. For optical mapping, it was the difference between activation times at a spot near the pacing electrode and a spot near the recording electrode at the opposite side of the lesion. For electrogram recordings, the stimulus-excitation time delay was measured from the stimulus

pulse to the activation time in the electrogram recorded on the opposite side of the lesion. This time delay included the time from the application of the stimulus pulse to excitation of cells near the stimulation electrode, which was measured between 6-7 msec.

*Viable Tissue Staining*

After completion of all recordings, hearts were perfusion stained with 2,3,5-triphenyltetrazolium chloride (TTC, Sigma-Aldrich, Inc.; 2.1 g of TTC in 150 ml of 0.9% NaCl) to determine histologically the location and completeness of each lesion. After staining with TTC, viable tissue appeared red and non-viable tissue appeared grey (Fig. 3.1). Lesions were bisected to obtain photographs and to measure lesion width, depth, and length, and the minimum path length of viable tissue from the stimulation site to the recording site on the opposite side of the lesion.

*Minimum Activation Path Length Determination*

The minimum path length for conduction was measured along viable tissue highlighted after TTC staining from the stimulation site to the recording site on the opposite side of the lesion. For all pre-lesion recordings, the minimum path length between the two spots on the optical grid or between the stimulus and electrogram electrodes was defined as the straight-line distance between the spots or between the electrodes. For incomplete lesions, the minimum path length was measured as the total distance from the stimulus electrode to the lesion gap center, and from the lesion gap center to the recording electrode. For complete lesions, the minimum path length was the total distance from the stimulus electrode to the end of the lesion nearer the apex (conduction was blocked on the basal end of the lesion by

the annulus) and from there to the recording electrode position. Activation path length for an incomplete lesion is shown in figure 3.1. Optical time delays along with their respective activation path lengths were used to determine conduction velocities. If the optical time delay was not available for a particular lesion, the electrical time delay was used. An alternate method for predicting time delay which incorporates fiber direction is presented in an appendix following chapter 5.

**Figure 3.1** Photograph showing the minimum activation path length. Bipolar pacing and recording electrodes are shown as white circles, while white dotted line indicates the activation path length.

## *C. RESULTS*

A direct relationship was demonstrated between conduction time delay and the activation path length (Fig. 3.2) across linear lesions. The complete lesions produced longer time delays, which correlated with longer minimum path lengths. The longer the length of minimum path length of viable tissue around the lesion, the longer the stimulus-excitation time delay. Linear regression of the results produced a slope of 2.29 msec/mm, an intercept near 0 (1.63 mm) and a correlation coefficient (R) value of 0.89, showing high correlation of time delay and minimum path length. In contrast, there was no difference in APL or in stimulation-excitation time delay between the non-treated cardiac tissue and incomplete lesions (Fig. 3.2).

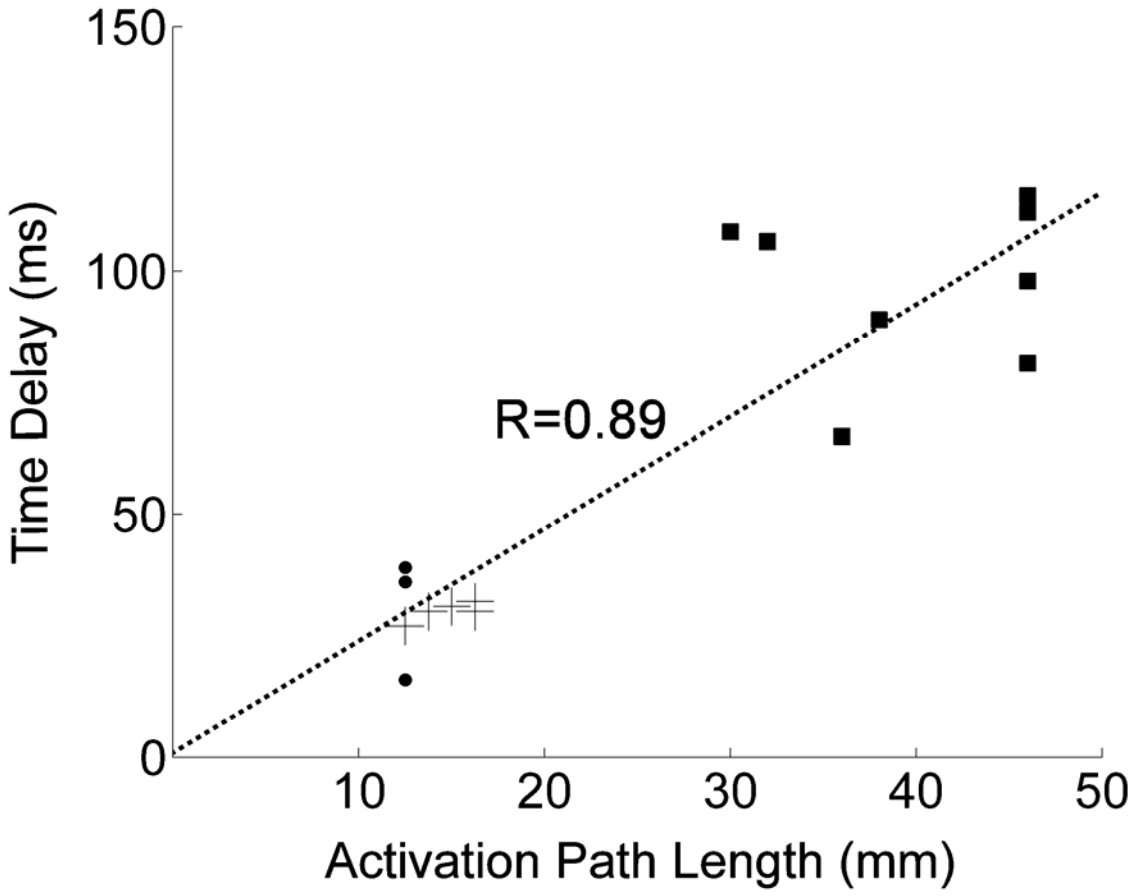


**Figure 3.2** Stimulus to excitation time delays as a function of minimum activation path length. Pre-lesion values are shown as plus signs, incomplete lesion values are shown as solid circles, and complete lesion values are shown as solid squares. The dotted line indicates the best-fit curve as determined by linear regression.

## *D. DISCUSSION*

Activation path length may not predict delays in diseased atria, or in tissue containing anti-arrhythmic drugs that alter propagation velocity anisotropy. Variations in factors such as fiber direction and complexity of the conduction path, which may have greater chance to affect conduction for complete lesions due to longer minimum path length, may produce deviations from the linear relationship observed in this study. However, the high ratios of post-ablation to baseline values of activation path length observed for complete lesions may be predictive even in complex cases. An attempt has been made to account for the effect of fiber direction in the appendix following chapter 5.

# CHAPTER 4

# RECOVERY OF TISSUE WITHIN SMALL GAPS OF LINEAR RADIOFREQUENCY CARDIAC ABLATION LESIONS

## *A. INTRODUCTION*

Trans-venous catheter ablation procedures have been shown to halt various forms of atrial fibrillation and atrial tachycardias. However these procedures are technically challenging to perform, and success rates vary widely according to operator experience, the specific nature of the arrhythmia present, and the type of procedure being attempted.

Approximately 90% of patients with paroxysmal atrial fibrillation can be cured by pulmonary vein isolation, however only a small percentage of patients with chronic atrial fibrillation may be treated with this technique[183]. For patients with chronic atrial fibrillation, more extensive lesion sets are desired, such as those required for the Maze III procedure. For the Maze III, a series of linear lesions are required in order to break up arrhythmic conduction in the left atrium, isolate the pulmonary veins, isolate or remove both atrial appendages, and form a corridor ("Maze") which directs sinus activation toward the atrioventricular node[170], and breaks up wavelets which sustain fibrillation.

The linear lesion is an important building block for the formation of a Maze III lesion set. Thus the ability to form complete (i.e., continuous and transmural) linear lesions is critical to achieving success during ablation procedures. Due to the complexity of temperature distributions in the heart during ablation, difficulty in maintaining consistent contact and position on the myocardial wall, and variability in atrial anatomy, gaps in

catheter ablation lesions are not uncommon. Such gaps may recover over time following ablation, and may allow arrhythmic conduction to propagate across a lesion and sustain atrial fibrillation. Further, lesions which are incomplete may form new arrhythmic substrates for anatomically based macroreentrant circuits.

Cabo *et al.* performed experiments and simulations in order to characterize the minimum width of cardiac tissue slices necessary to support conduction[160]. They reported considerable variability in this "critical isthmus width", which depended on pacing frequency and fiber direction. Cabo's study addressed the importance of viable tissue width, however radiofrequency ablation lesions are complicated by the fact that partial damage to both endothelial cells within the microvasculature as well as to the myocytes may occur at distances up to 6 mm from the site of coagulation necrosis[17,21]. Further, a recent report by Perez *et al.* demonstrates the importance of gap geometry in discontinuous lesions[209], and reveals that "angled gaps" (i.e., gaps which contain an approximately 90º turn in the path of conduction) are more likely to block conduction than either bifurcated gaps (~45º turn, but in two directions) or straight gaps. These factors suggest that additional complexity is present due to hyperthermic injury following radiofrequency ablation which may cause deviations from previous studies.

In addition to the above factors, it is likely that transient conduction block in injured myocardial cells may lead to early block followed by later recovery. Simmers et al have reported that both heating and RF ablation may cause transient (<5 minutes) and permanent block in superfused sections of myocardium[204,205], however it is likely that the response of whole-heart preparations is more complex. We hypothesized that ablation lesions containing

a small gap may acutely recover within one hour following ablation, and that after this time period has passed, acute recover is highly improbable.

Characterization of recovery over time in lesion gaps may lead to a better understanding of acute changes in conduction through incomplete linear lesions, which are important in the formation of the Maze lesion set as well as other ablation procedures. This would provide clinicians with an estimate of the time involved to ensure stable conduction block in individual linear lesions.

## *B. METHODS*

*Rabbit Heart Preparation*

Fresh hearts isolated from New Zealand rabbits (N = 7) of either gender were retrograded perfused through the aorta with Tyrode's solution (129 mM, NaCl, 5.4 mM KCl, 1.8 mM $CaCl_2$, 1.1 mM $MgCl_2$, 26 mM $NaHCO_3$, 1 mM $Na_2HPO_4$, 11 mM Dextrose, and 0.6 μM bovine serum albumin). The solution was bubbled with 95% $O_2$ and 5% $CO_2$, and maintained at 37 ± 0.2º C.

Lesions (N = 9) were produced on the heart by RF ablation (300-600 J/cm², 30 seconds). Two to three lesions were made on each heart, and approximately 60 minutes passed between the creation of each lesion. The animal was sacrificed approximately 30 minutes before the creation of the first lesion. The effects of ablation in epicardial regions of the anterior or posterior ventricular septum were studied. Also, control recordings were made on non-ablated epicardium to examine the stability of control recordings over time.

*Electrical Pacing and Recording*

One pair of electrodes (electrodes 1 and 2, anode and cathode, Fig. 4.1) was used to deliver bipolar pacing stimuli from an isolated stimulator (Isostim A320, World Precision Instruments, Sarasota, FL). The pacing amplitude was set at twice the pacing threshold or at 10 mA if the heart captured at ≥ 5 mA; pacing pulse width was 3 msec; pacing interval was chosen just above the resting heart rate and ranged from 340 to 660 msec. The other electrode pair (electrodes 3 and 4, negative and positive, Fig. 4.1) was used to record a bipolar electrogram. All signals (stimulus and electrogram) were conditioned with an isolation amplifier (AD210AN, Analog Devices, gain 100, low pass <16 kHz), and digitized

at 10 kHz or 1kHz using Labview and a DAQPad 6070E data acquisition board (National Instruments, Austin TX). Inter-electrode spacing for each pair was 1-2 mm and spacing between the pairs was 10 mm. Pacing and recording electrodes were stainless steel rings (contact area with heart ~1 $mm^2$ per electrode), and were attached to the RF probe and positioned in a line 90 degrees from the ablation probe (Fig. 4.1).

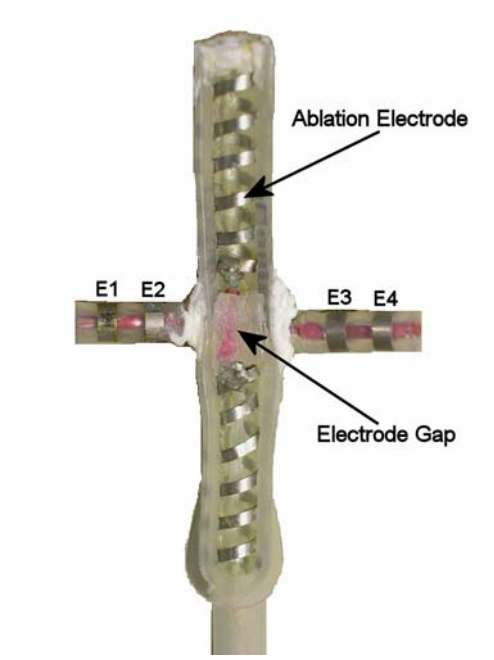


**Figure 4.1** Five cm ablation probe with silicone gap. Helical stainless steel coil was used for ablation, while stainless steel ring electrodes were used to deliver bipolar pacing and record bipolar electrograms.

*Ablation Procedure*

A prototype ablation device (nContact Surgical, Inc., Fig. 4.1) was used to create a lesion through the middle of the optical grid and between the stimulation and recording electrodes. RF energy was applied for 30 seconds at a power of 30-40 Watts using a 480 kHz generator. Lesions were created with a single application of RF energy using a 2-cm or a 5-cm ablation electrode. Lesions extended from the apex to the atrioventricular groove.

Incomplete lesions were created by discrete applications of the 2-cm ablation probe separated approximately 5 mm apart to produce a gap, or by the 5-cm ablation probe as shown in figure 4.1 which contained a gap in the ablation electrode. Control recordings were taken prior to ablation, and then post-ablation recordings were taken to examine the effects of ablation on the stimulus-excitation time delay over a 60-minute period.

*Selection of Activations in Fractionated Electrograms*

Following injury to the myocardium, heterogeneities within the tissue lead to discontinuous propagation resulting in fractionated electrograms with multiple peaks of varying amplitudes. Since early activations indicate propagation through an incomplete lesion which may allow arrhythmic conduction, the first discernable activation was chosen as the activation with which to determine time delay measurements. The first deflection greater than 1 mV from the baseline was labeled as the activation. The peak of this deflection was chosen as the activation time[146]. Since it was possible that this new criterion for selection of activations may affect previous results, the new method was also used to analyze results from chapter 2. Results using the new method showed that it does not change any of the conclusions found in chapter 2. Specifically, time delays for control recordings were not different from time delays following incomplete lesions, time delays for control recordings were different from time delays for complete lesions, and time delays for incomplete lesions were different from time delays for complete lesions. Also, time delays calculated using electrical recordings were not different from those calculated using optical recordings.

*Indication of Recovery*

Slight shifts in electrode position may result in beat-to-beat variability, as well as small changes in the magnitude of time delay. However large increases or decreases in time delay were not observed due to the small shift in electrode position with our apparatus (< 1mm), and are likely due to significant changes in the activation path length. Results from chapters 2 and 3 of this work suggest that a doubling of time delay indicates that the path length has been significantly increased.

*Classification of Recovery*

Several distinct features were present in post-lesion electrograms which indicated recovery within the myocardium. Full recovery, partial recovery, and recovery of the activation complex were observed in post-lesion electrograms. A late increase in time delay was also observed.

Full recovery was defined as a greater than 2-fold increase in time delay followed by a decrease to within 5 percent of the control value. The time of 50% or 90% recovery was identified as the time at which time delay fell below 50% or 90% of the difference between its maximum and the final recording taken at 60 minutes.

Partial recovery was defined as a greater than 2-fold initial increase in time delay followed by a >10 percent decrease from the maximum time delay. The time of 50% or 90% recovery was defined as the time at which time delay fell below 50% or 90% of the difference between the maximum and the final recording taken at 60 minutes.

Recovery of the activation complex in post-lesion electrograms was defined by the late appearance of an activation peak(s) in the electrogram following lesion production,

which precluded the identification of the original post-ablation peak in subsequent recordings. Recovery of the activation complex was defined as the time at which the first morphological change precluded identification of the first peak chosen following ablation.

*Rate of Change in Time Delay*

The time rate of change for those lesions showing partial recovery and late conduction decrease was determined in the following manner. For each set of consecutive time delays, the difference in time delay was divided by the difference in time that elapsed between the two recordings. Rates of change for each lesion were compared against rates of change found during the control recordings to examine the significance of the rates of change.

*Data Processing*

All electrograms were filtered using a 4 ms boxcar filter. Electrograms were signal averaged by aligning consecutive stimulation pulses over a 10 second period. Time delay was determined using these signal-averaged electrograms by locating the first post-stimulation peak which exceeded 1 mV.

*Statistical Analysis*

All values were presented as the mean ± SEM (standard error of the mean). In order to determine whether the rate of change in time delay during partial recovery and/or a late conduction decrease were significant, the unpaired one-sided Student's t-test was used. A p-

value less than 0.05 was considered significant. The binomial sign test was used to determine if the probability of observation of various types of recovery was different than 50%.

## *C. RESULTS*

*Control Recording*

In order to ensure that changes in time delay were due to effects of RF ablation, a control recording was taken over a 1-hour period (Fig. 4.2). Although small variations were observed in the control recording (~5 ms), there was no trend seen in the control measurements which indicated that influences of the measurement system or animal model resulted in significant changes in time delay over a 60-minute post-ablation period. The mean value of the time derivative of time delay was $0.10 \pm 0.19$.

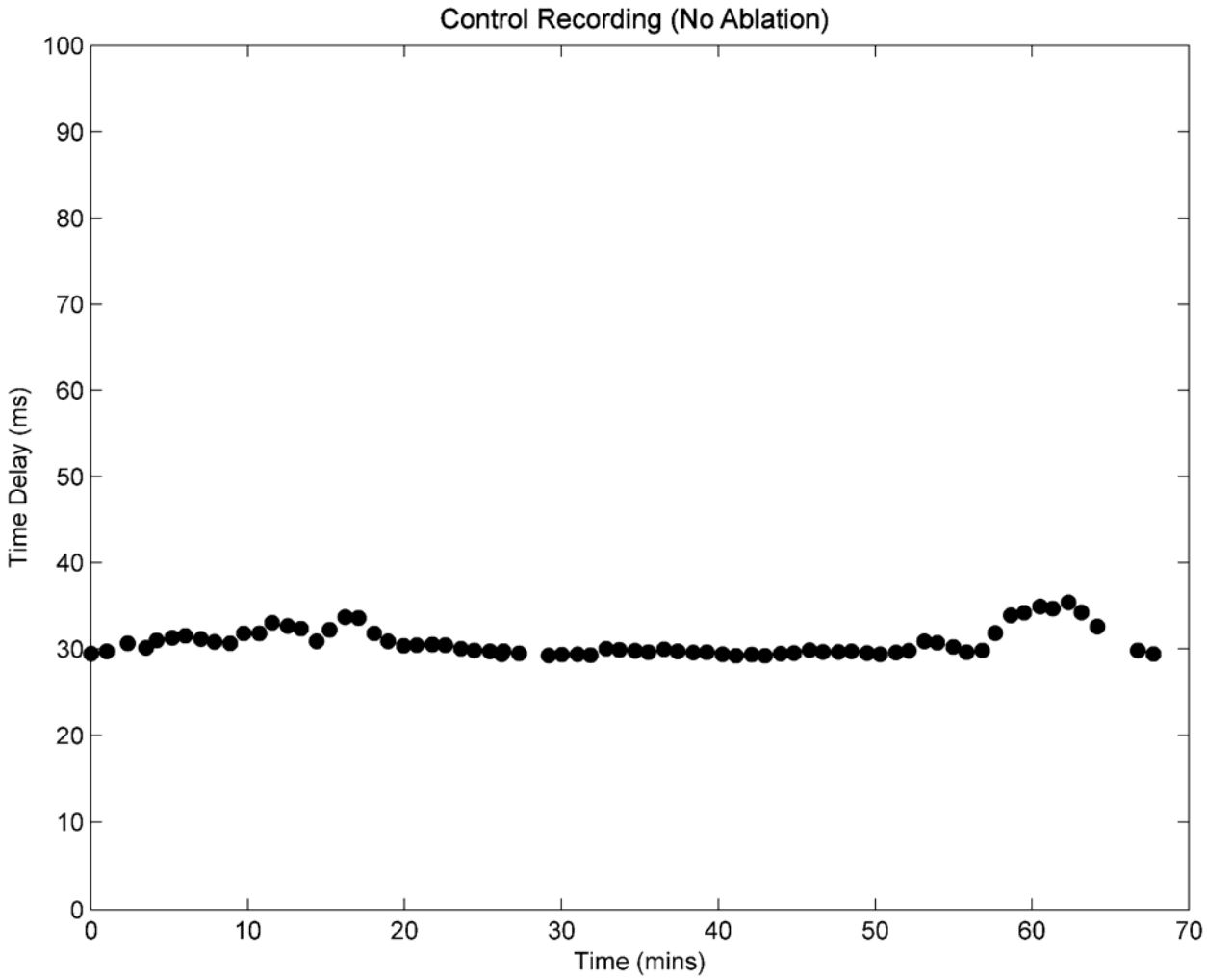


**Figure 4.2** Control recording of time delay over a 1-hour period. Filled circles represent individual recorded values for time delay. A time of zero indicates the time of the first control recording.

*Recovery of the Activation Complex*

In 4 of 9 lesions, electrograms showed cases where changes in morphology precluded the identification of a distinct peak throughout the full duration of the time recording (figures 4.3 and 4.4). Since activation peaks were not present during all measurements, the time course of activation for these lesions was not tracked, and attention was given to the timing of the first morphological change that took place. Figure 4.3 shows an example of tissue recovery indicated by morphological changes. Early after ablation (<20 mins.), recordings

show an electrogram of long duration (>100 ms) with high beat-to-beat variability as demonstrated by high standard error on signal-averaged beats (> 0.5 ms). After 30 minutes, the emergence of a small peak may be seen, and then by 40 minutes 2 small peaks have appeared. After 50 minutes, only a single peak is seen. The remaining peak has a short duration (10 ms) and a large reduction in the standard error (approximately 5-fold reduction). In summary, changes in morphology were found at 23.7 ± 7.9 (N=4) minutes following RF ablation. Individual values for all 4 cases are listed in table 4.2.

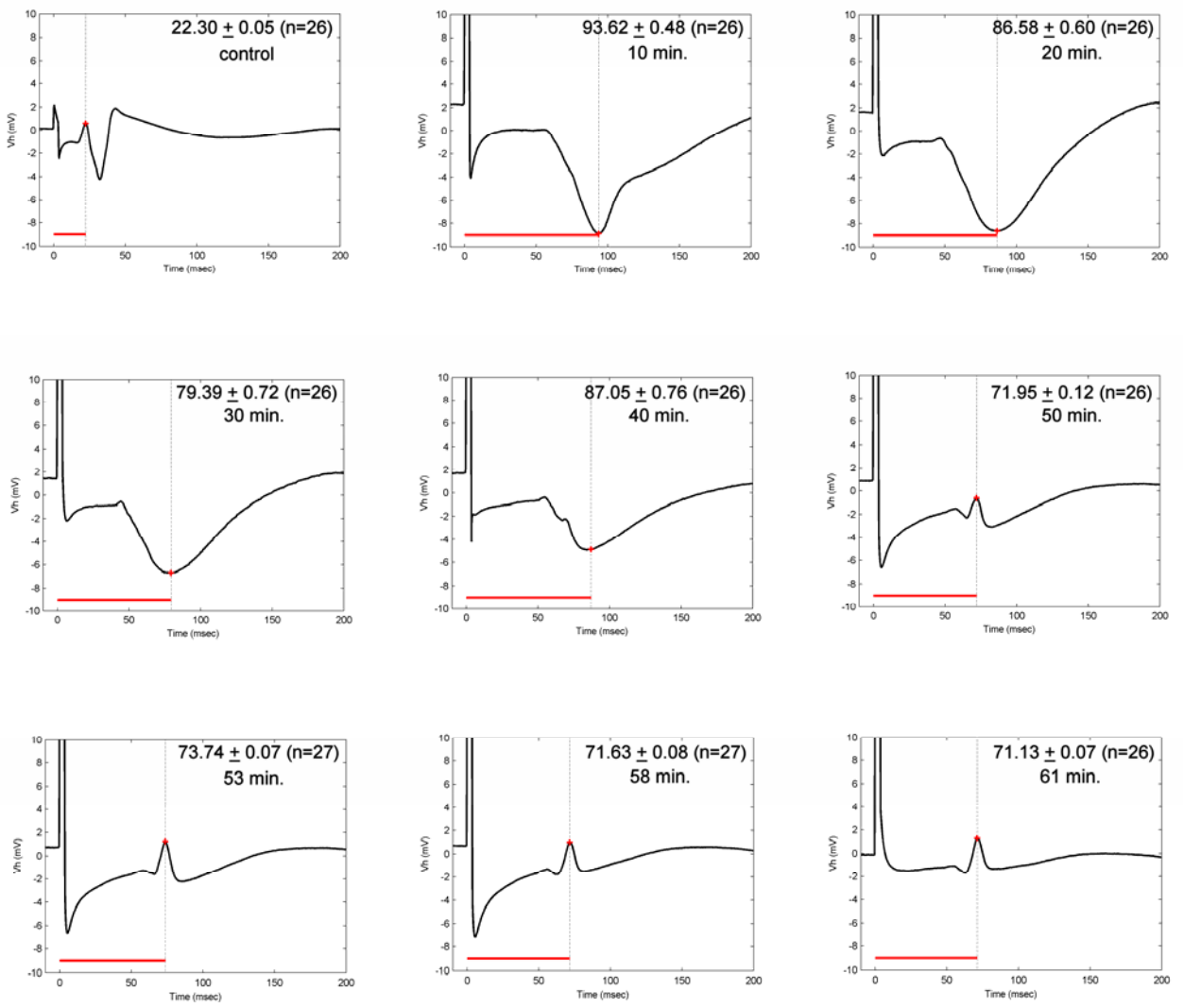


**Figure 4.3** Example of activation complex recovery following an RF ablation lesion, over a period of 61 minutes. Red bar indicates the duration of time delay. Means and standard error are given for each recording. Time of recording following ablation is given in minutes.

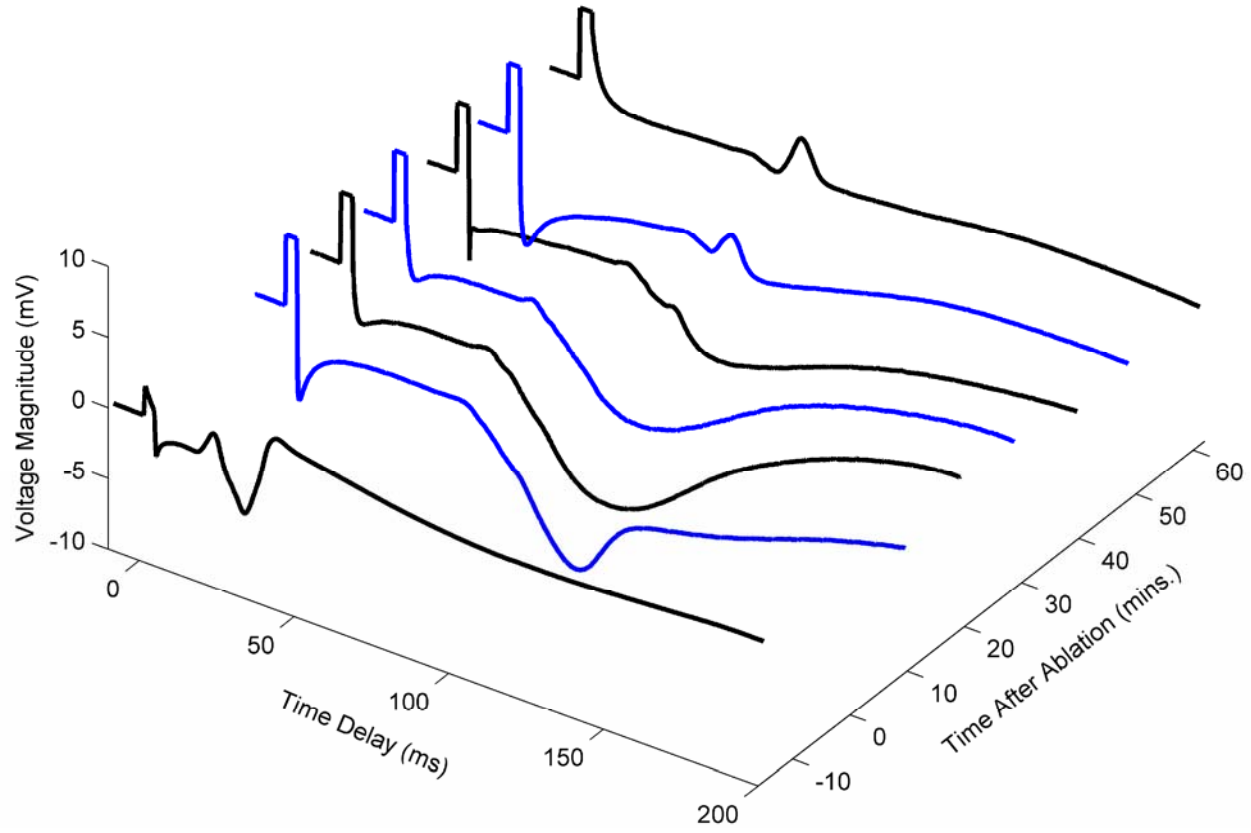


**Figure 4.4** Three-dimensional view of morphological changes following ablation indicating recovery of activation complex, for the electrograms shown in figure 4.3. Colors of adjacent electrograms are alternated in black and blue so that they may be distinguished. In cases where the stimulation signal was greater than 5 mV, the stimulation signal was truncated to 5 mV for plotting purposes.

*Complete Recovery of Conduction*

Complete recovery was observed in 1 of 9 lesions which showed post-lesion block. The time at which both 50% and 90% recovery occurred was 5.4 minutes.

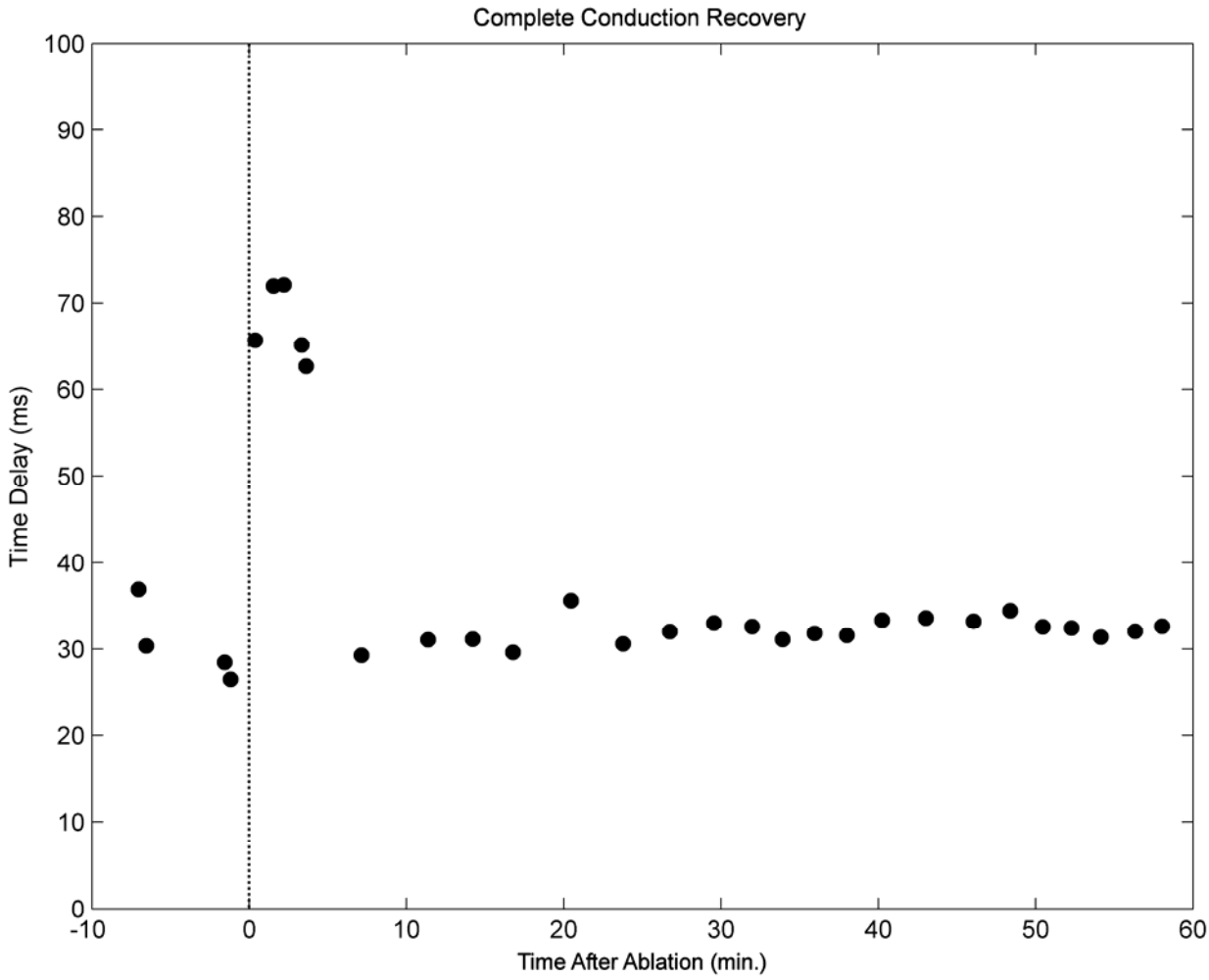


**Figure 4.5** Complete recovery following an ablation lesion. Dotted vertical line marks the end of the RF ablation.

Immediately following ablation, an early (0.4 minutes) electrogram taken during complete recovery (Fig. 4.5) shows an increase in time delay by 147% and an inversion of the activation peak. The peak is inverted again at 1.5 and 2.2 minutes, and then inverted again 3.3 and 3.6 minutes. At 7.1 minutes, the peak is again upright, and the time delay has returned to within 3 ms of the control value.

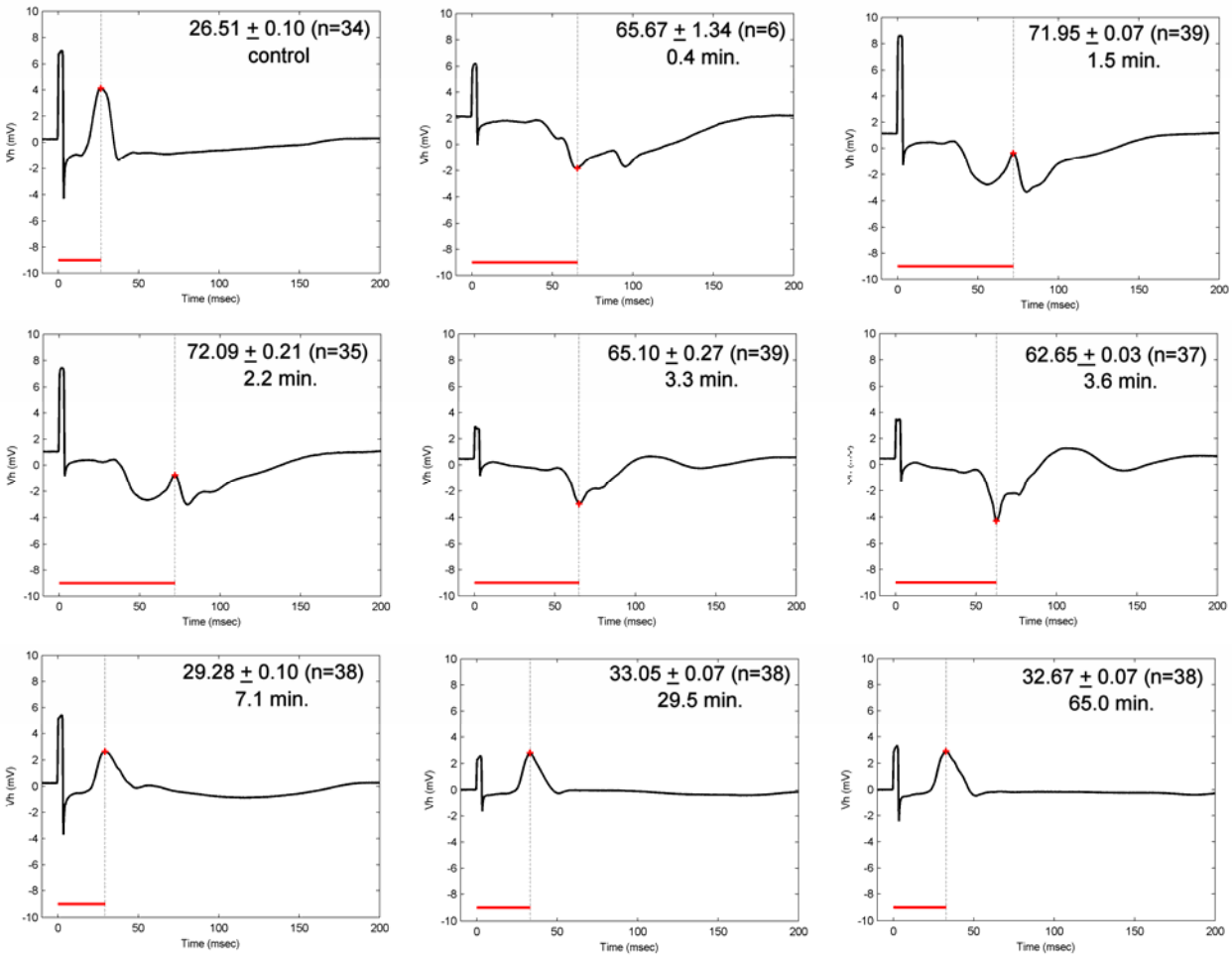


**Figure 4.6** Electrograms taken during complete conduction recovery. Mean and standard error of time delay are shown for each electrogram, along with the number of beats used to generate the signal-averaged electrogram shown. Red horizontal bar indicates the duration of the time delay.

*Partial Recovery of Conduction*

Partial conduction recovery was observed in 3 of 9 lesions. The point of 50% recovery for these lesions was 14.4 ± 1.0 minutes, and the point of 90% recovery was 23.7 ± 4.3 minutes. For the lesion shown in figure 4.7, 50% and 90% recovery were 16.3 and 30.3 minutes, respectively. Times for the example in figure 4.7 were measured from the end of the second ablation, indicated by the rightmost vertical dotted line.

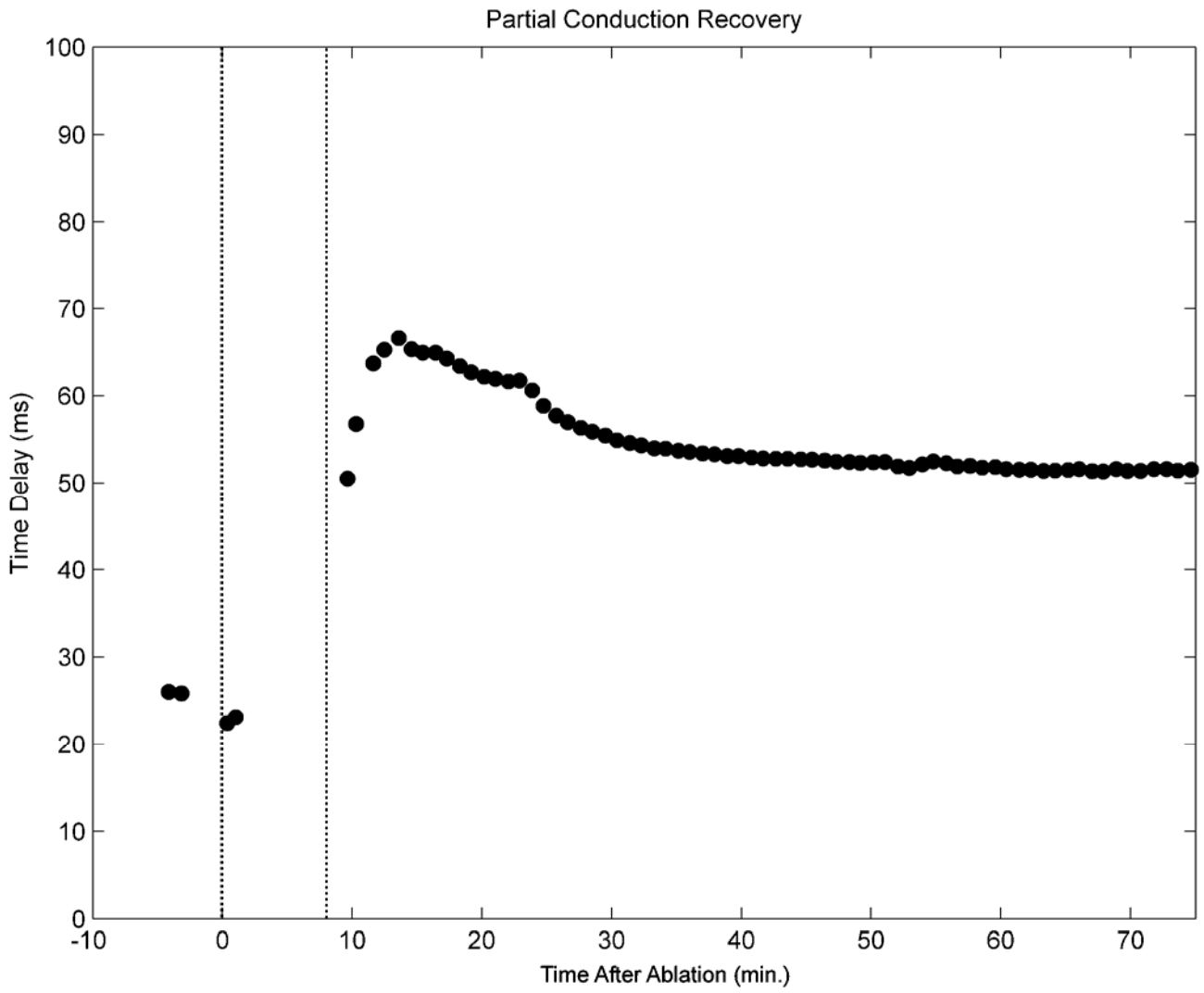


**Figure 4.7** Partial conduction recovery in a complete lesion. Vertical dotted lines indicate the end of an RF ablation.

Electrograms shown in figure 4.8 indicate block, as demonstrated by a greater than 2-fold increase in conduction delay and an inversion of the activation peak with respect to the control recording. Maximum time delay is seen at approximately 10 minutes after the first ablation, followed by a slow decline in time delay over the next 50 minutes.

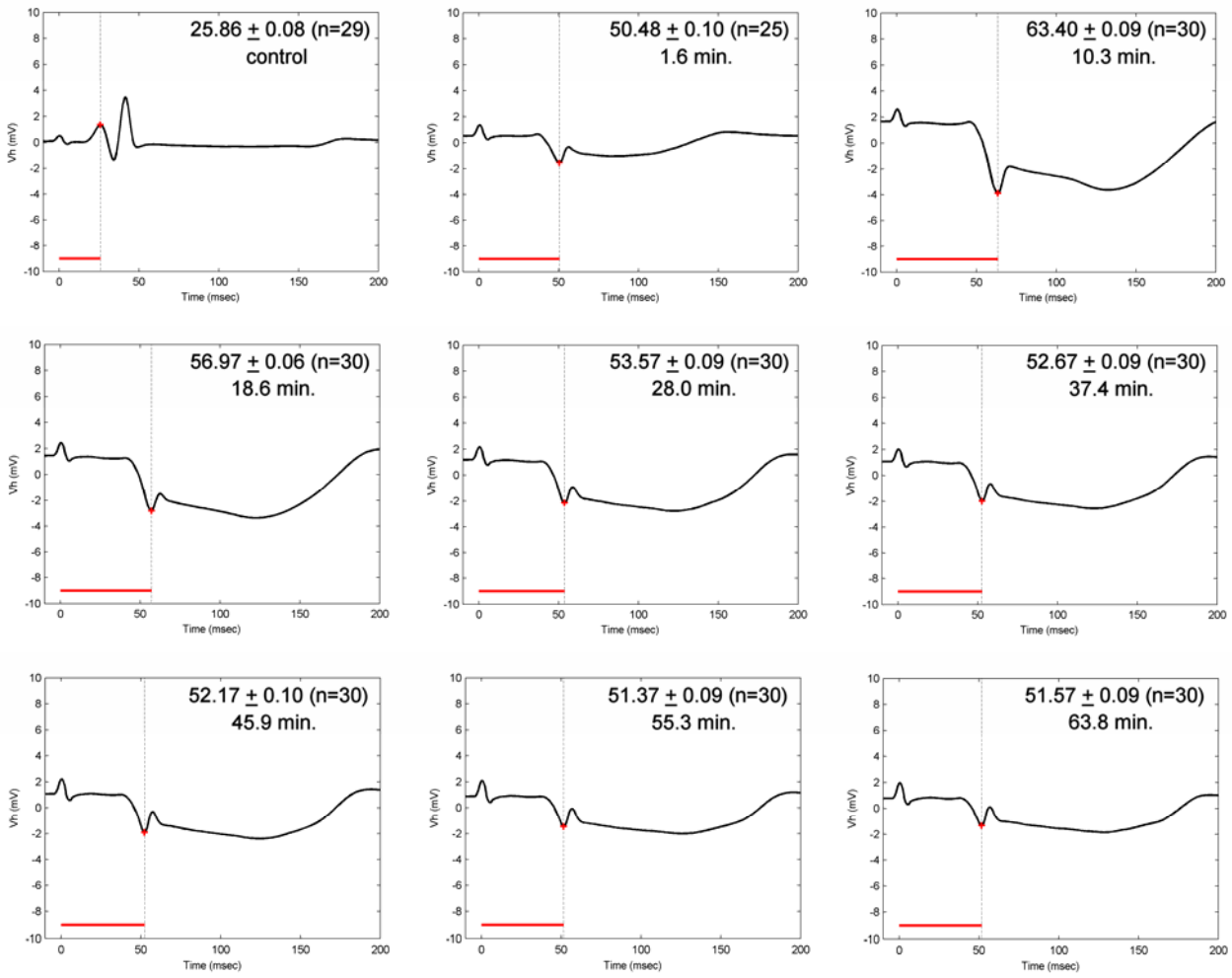


**Figure 4.8** Electrograms for partial conduction recovery in an incomplete lesion.

*Late Worsening of Conduction*

In 1 of 9 lesions, a late increase in time delay was observed, as illustrated in figure 4.9. For this lesion, time delay rose to 50% of the difference between its post-ablation and final value at 41.1 minutes, and 90% of the difference at 49.6 minutes. The results for recovery for all lesion types are summarized in tables 4.1 and 4.2.

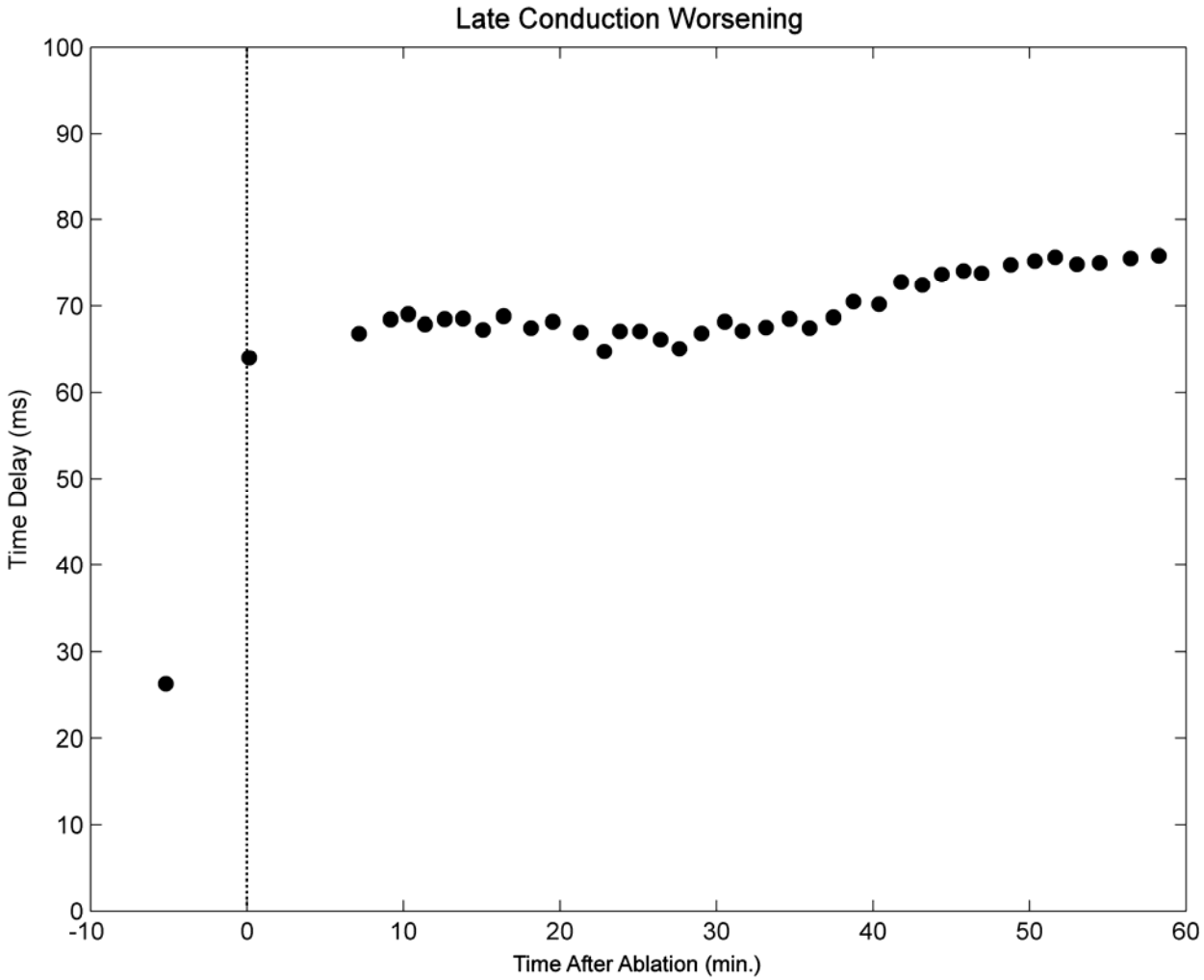


**Figure 4.9** Late conduction worsening following RF ablation. Vertical dotted line indicates end of RF ablation.

| Type of Recovery | $t_{50}$ (mins.) | $t_{90}$ (mins.) | Lesion Number | Gap Size (mm) |
|---|---|---|---|---|
| Complete Recovery | 5.4 | 5.4 | 2 | 1.0 |
| Partial Recovery | 13.0 | 19.5 | 3 | 2.5 |
| Partial Recovery | 13.8 | 19.4 | 1 | 0.5 |
| Partial Recovery | 16.3 | 32.3 | 2 | 0.5 |
| Conduction Decrease | 38.1 | 47.9 | 2 | 1.0 |

**Table 4.1 –** Summary of recovery times (50% and 90%) for all lesion types except those showing morphological changes post-ablation.

| Type of Recovery | $t_R$ (mins.) | Lesion Number | Gap Size (mm) |
|---|---|---|---|
| Recovery of Activation Complex | 19.7 | 1 | 1.0 |
| Recovery of Activation Complex | 46.9 | 3 | 4.0 |
| Recovery of Activation Complex | 16.8 | 1 | 3.0 |
| Recovery of Activation Complex | 11.2 | 2 | 1.5 |

**Table 4.2 -** Times of activation complex recovery occurring post ablation.

*Rate of Change During Partial Recovery and Conduction Worsening*

In order to determine whether time delay decreases were different from deviations found during control, rates of change during partial recovery and conduction decrease were compared to those of control. For all three cases of partial recovery, the rate of decrease in time delay was significantly greater than that of the control recording. For the one lesion where a late conduction worsening was observed, the rate of increase in time delay was not statistically different than that of the control recording. Means and p-values for slopes of time delay during partial recovery and late conduction decrease are given in table 4.3.

| Type of Recovery | Average Slope of Time Delay (ms/min.) | p-value (vs. control) |
|---|---|---|
| Partial Recovery Lesion | -0.55 ± 0.18 | 0.0172 (n=8) |
| Partial Recovery Lesion | -0.17 ± 0.10 | 0.0205 (n=61) |
| Partial Recovery Lesion | -0.32 ± 0.06 | 0.0002 (n=50) |
| Late Conduction Decrease | 0.20 ± 0.14 | 0.2673 (n=38) |
| Control Recording | 0.10 ± 0.19 | 0.5000 (n=65) |

**Table 4.3 -** Averaged slopes of time delay for lesions showing partial recovery and late conduction worsening.

*Probability of Observing Different Lesion Types*

To test the probability of observing various types of recovery while recording electrograms adjacent to incomplete lesions, the binomial sign test was used. For complete recovery and worsening of conduction, $p < 0.05$, indicating that the probability of observing either of these phenomena was significantly less than 50%. For partial recovery and recovery of the activation complex, p values were less than 0.05, indicating that the occurrences of these two phenomena were not significantly different from 50%.

## *D. DISCUSSION*

This study demonstrates that the time course of conduction recovery following RF ablation is highly variable in the whole heart Langendorff rabbit model. Acute complete recovery of RF ablation lesions was observed in only 1 of 9 lesions, suggesting that it is a relatively rare phenomenon following the confirmation of initial block by an increase in time delay. Partial recovery was more common, occurring in 3 of 9 lesions, however lesions which showed partial recovery never recovered below 2x the initial value of time delay, indicating that conduction block remained despite partial recovery. Data for partial recovery suggests that cells located on the periphery of the lesion may recover and lead to a slight decrease in the path length of activation. In one case, a late decrease in time delay occurred following conduction block, suggesting that injury to cells around the lesion periphery may also lead to progressive cell death and subsequent conduction path length increases. Apoptosis is one mechanism which may result in progressive cell death.

Both partial and complete recovery may be explained by temporary inexcitability of cells near the lesion perimeter. Increases in temperature have been shown to result in temporary as well as permanent loss of excitability, both in the context of standard hyperthermia[204] as well as RF-induced hyperthermia[205]. For partial recovery, the amount of cells which recovered within the lesion gap was not sufficient to allow trans-gap conduction of the activation wavefront. In this scenario, time delay was only affected by those cells which recovered near the lesion perimeter, resulting in a slight decrease in time delay. For complete recovery, recovery of cells within the lesion gap led to a gap widening which was sufficient to support trans-gap conduction of the activation wavefront.

From a cellular perspective, it is likely that damage to connexins has a significant impact upon conduction following RF-induced hyperthermia. Ultrastructural observations by Nath et al have shown that the most extensive damage to cardiac myocytes occurs at the plasma membrane and the region of the gap junctions[21]. It is likely that the temperature dependence of sodium channels also plays a significant role in the time-dependent behavior of time delay. Rosen has shown that sodium channel activation kinetics exhibit highly nonlinear behavior with changes in temperature. He also states that increases in membrane fluidity at higher temperatures may play an indirect role in sodium current modulation by altering interactions between membrane lipids and channel proteins[210].

Significant changes in electrogram morphology were observed in 4 of 9 lesions which indicated recovery of the activation complex. In all 4 cases, these morphological changes were accompanied by the presence of a peak or trough of long duration (>100 ms), suggesting the presence of injury as described by Deleze[211]. Cardiac myocytes which have sustained severe membrane damage by RF ablation may be electrically coupled to the extracellular space. This results in an intracellular current flowing away from injured cells during diastole, and an intracellular current flowing toward the injured cells during systole. This current my produce the peaks of long duration observed in cases of activation complex recovery. After healing, the myocytes are no longer coupled to the extracellular space, and electrograms in the vicinity of the recording electrodes may no longer be dominated by injury current. Thus a typical bipolar activation may then be seen (<20 ms), indicating recovery of tissue near the recording electrode.

Examination of the recording electrode configuration with respect to the lesion location also suggests that injury and subsequent healing may play a significant role in

phenomenon we have described as recovery of the activation complex following RF ablation. First, we examine figure 4.1 and find that the negative recording electrode is near the ablation electrode while the positive recording electrode is further away (~2 mm further). If injury occurs in the region near the ablation electrode resulting in intracellular/extracellular electrical coupling and a transmembrane potential of zero, intracellular current due to injury will flow from cells in the region of electrode 3 toward those in the region of electrode 4. In other words, intracellular current will flow toward downstream cells which are able to maintain their normal diastolic transmembrane potential of -80 mV. This in turn implies that extracellular current during diastole will flow from electrode 4 to electrode 3, resulting in an increase in the baseline extracellular potential with respect to control values. During systole, when the transmembrane potential becomes positive (+20 mV), the direction of the injury current is reversed throughout the entire duration of the action potential plateau phase. Thus during activation, a prolonged negative deflection (> 100 ms) would be expected to follow the initial rapid signal rise caused by the fast sodium current, which may be smoothed by downstream injured cells. Figures 4.3 and 4.4 show this behavior in early recordings (< 40 minutes), and then show the return of a single rapid signal (< 20 ms), presumably due to the electrical sealing of the damaged cells by the process known as “healing over”.

## CHAPTER 5

## TIME COURSE OF TEMPERATURE WITHIN STUNNED MYOCARDIUM ADJACENT TO LINEAR RADIOFREQUENCY ABLATION LESIONS

### *A. INTRODUCTION*

It is well-known that cardiac tissue subjected to temperatures greater than ~50º C will be irrevocably damaged and no longer capable of normal conduction[18,28,204,205], while temperatures in the 37-45 ºC range typically show metabolic increases and increases in conduction velocity. However, previous studies using superfused sections of myocardium underestimate the anatomical and thermal complexity of lesion formation, which may be important in a more realistic clinical setting.

We hypothesized that acute recovery within a lesion gap is dependent upon the epicardial gap temperature. Assuming that the temperature within the lesion gap does not exceed a critical temperature (~50 ºC), recovery of the gap tissue may depend upon the maximum epicardial gap temperature and/or the rate of temperature decrease following ablation. Since the detection of lesion incompleteness depends on intra-gap conduction, it is important to characterize those parameters which may affect tissue recovery and allow tissue to conduct. In this study we examine the time course of epicardial gap temperature immediately following the formation of incomplete lesions, and attempt to determine the relationship between epicardial gap temperature and tissue recovery following RF ablation.

## *B. METHODS*

*Rabbit Heart Preparation*

Fresh hearts isolated from New Zealand rabbits (N = 6) of either gender were perfused through the aorta with Tyrode's solution (129 mM, NaCl, 5.4 mM KCl, 1.8 mM $CaCl_2$, 1.1 mM $MgCl_2$, 26 mM $NaHCO_3$, 1 mM $Na_2HPO_4$, 11 mM Dextrose, and 0.6 μM bovine serum albumin). The solution was bubbled with 95% $O_2$ and 5% $CO_2$, and maintained at 37 ± 0.2º C.

Lesions (N = 8) were produced on the heart by RF ablation (300-600 J/cm², 30 seconds). Two to three lesions were made on each heart, and approximately 60 minutes passed between the creation of each lesion. The animal was sacrificed approximately 30 minutes before the creation of the first lesion. In cases where initial conduction block was not observed, multiple applications of RF energy were applied to achieve block. The effects of ablation in regions of the anterior or posterior epicardium near the ventricular septum were studied.

*Electrical Pacing and Recording*

One pair of electrodes (electrodes 1 and 2, Fig. 4.1) was used to deliver bipolar pacing stimuli from an isolated stimulator (Isostim A320, World Precision Instruments, Sarasota, FL). The pacing amplitude was set at twice the pacing threshold or at 10 mA if the heart captured at ≥ 5 mA; pacing pulse width was 3 msec; pacing interval was chosen just above the resting heart rate and ranged from 340 to 660 msec. The other electrode pair (electrodes 3 and 4, Fig. 4.1) was used to record a bipolar electrogram. All signals (stimulus and electrogram) were conditioned with an isolation amplifier (AD210AN, Analog Devices,

gain 100, low pass <16 kHz), and digitized at 10 kHz or 1 kHz using Labview and a DAQPad 6070E data acquisition board (National Instruments, Austin TX). Inter-electrode spacing for each pair was 1-2 mm and spacing between the pairs was 10 mm. The pacing and recording electrodes were stainless steel (contact area with heart ~1 $mm^2$ per electrode), which were attached to the RF probe and positioned in a line 90 degrees from the ablation probe (Fig. 5.1).

*Temperature Measurements*

The mid-lesion gap temperature was measure immediately following ablation by a thermocouple probe (Thermalert TH-5, Physiotemp, Clifton, NJ) on the surface of a silicone wedge which was placed within the ablation probe to cause a lesion gap. The thermocouple probe was held securely against the epicardium by the silicone wedge, which was pressed against the epicardium by vacuum suction on either side of the wedge. The probe, which contained the ablation electrode, pacing and recording electrodes, and the thermocouple probe, is shown in figure 5.1.

Temperature was measured immediately following the end of ablation for 100 seconds, and was digitized at a sampling rate of 1 kHz. Typically, the gap temperature returned to its equilibrium value within 100 seconds (11 of 12 temperature time constants measured were below 70 seconds).

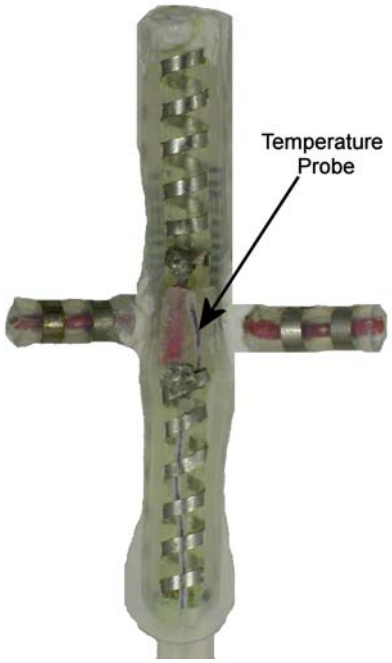


**Figure 5.1** Photograph of ablation probe with temperature probe attached near gap region.

*Temperature Time Constant*

The time constant of temperature following ablation was measured by determining the amount of time which must pass following ablation in order for the temperature to rise one time constant above its original equilibrium value (the "1/e" point). The time constant $\tau$ was calculated using the following expression:

1) $$T(\tau) = (T_{\max} - T_{\min})(1/e) + T_{\min}$$

where $T_{max}$ is the maximum temperature, $T_{min}$ is the minimum temperature, $\tau$ is the time constant, and e is Euler's number. After $T(\tau)$ was determined, the first time $t_1$ for which $T(t_1) \leq T(\tau)$ was recorded as the time constant $\tau$.

*Time Response of Temperature Probe*

The time response of the probe was measured by immersing approximately 1 inch of the thermocouple into 1 L of water of a constant temperature. To generate the data shown in figure 5.2, the probe was first moved abruptly (<0.1 s) from the cold water container (room temperature, 23.0° C) to the hot water container (50.4° C), where it remained for 5 seconds. The probe was then moved back to the cold water container, which caused the temperature decline at approximately 6 seconds (Fig. 5.2). The time constant of the probe was determined using equation 1, and was found to be 0.35 seconds.

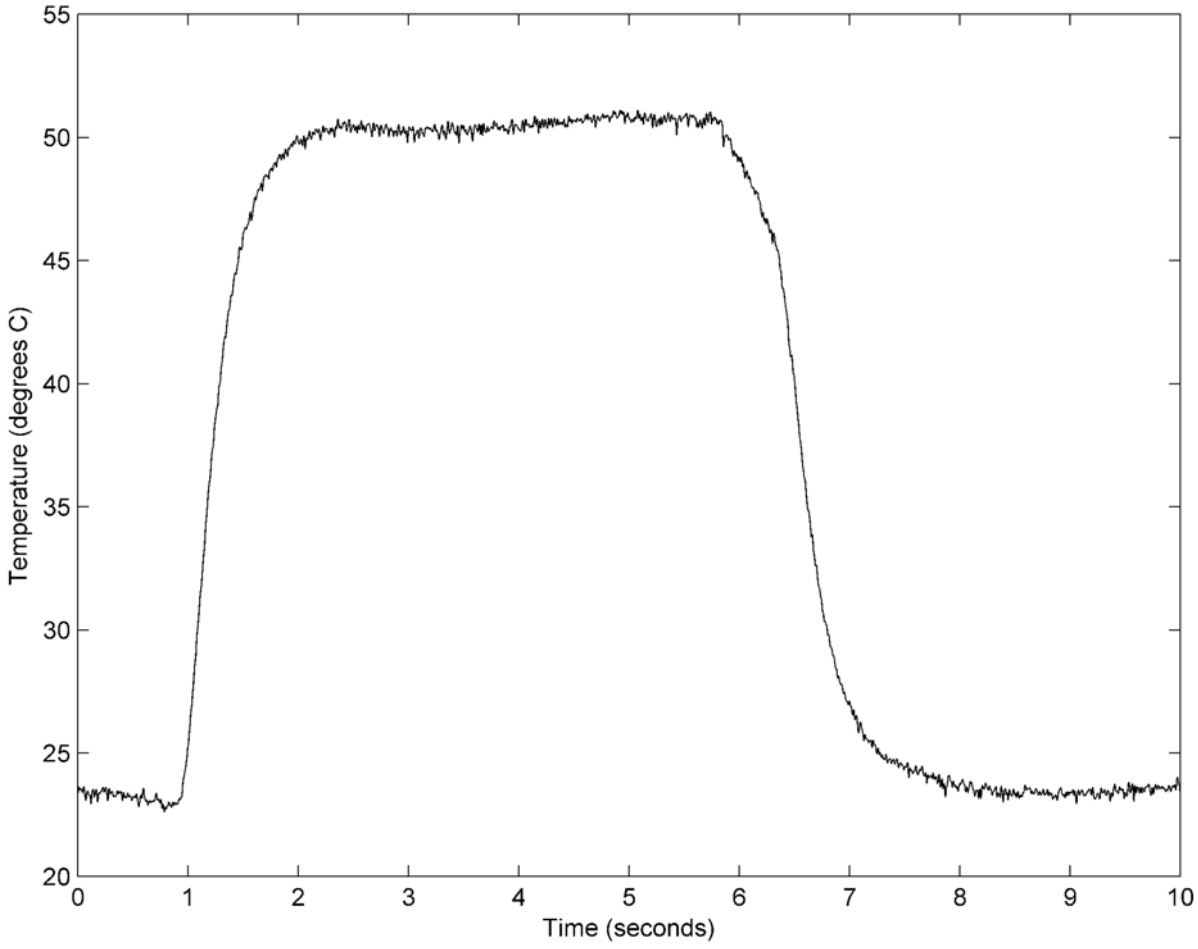


**Figure 5.2** Time response of temperature probe.

*Classification of Recovery*

Several distinct features were present in post-lesion electrograms which indicated recovery within the myocardium. Full recovery, partial recovery, and recovery of the activation complex were observed in post-lesion electrograms.

Full recovery was defined as a greater than 2-fold increase in time delay followed by a decrease to within 5 percent of the control value. The time of 50% or 90% recovery was identified as the time at which time delay fell below 50% or 90% of the difference between its maximum and the final recording taken at 60 minutes.

Partial recovery was defined as a greater than 2-fold initial increase in time delay followed by a >10 percent decrease from the maximum time delay. The time of 50% or 90% recovery was defined as the time at which time delay fell below 50% or 90% of the difference between the maximum and the final recordings taken at 60 minutes.

Recovery of the activation complex in post-lesion electrograms was defined by the appearance or disappearance of peaks in the electrogram following lesion production, which precluded the identification of the peak in subsequent recordings. The time of recovery as indicated by morphological changes was defined as the time at which the first morphological change precluded identification of the first activation peak chosen following ablation.

*Supernormal Conduction*

In some lesions, post-ablation measurements of time delay revealed that conduction block did not occur. Rather, heating due to RF ablation caused a transient decrease in time delay immediately following the completion of the ablation. The extent of supernormal conduction was quantified by the maximum percent decrease from control in time delay following ablation, and the time of the minimum time delay was also determined. The

maximum temperature and time constant for ablations was also calculated. Also, the correlation between temperature and post-minimum time delays was examined using linear regression.

*Data Processing*

All electrograms were filtered using a 4 ms boxcar filter. Electrograms were signal averaged by aligning consecutive stimulation pulses over a 10 second interval. Since the pacing rate was not constant for all experiments, the number of beats for a given signal-averaged electrogram varied. On average, approximately 30 beats were used to create a signal-averaged electrogram. Time delay was determined using these signal-averaged electrograms by locating the first post-stimulation peak which exceeded 1 mV. Temperature recordings were filtered using a 3 ms boxcar filter.

*Statistical Analysis*

All values were presented as the mean ± SEM (standard error of the mean). Linear regression was used to determine the relationship between post-minimum time delays and temperature in the 35-41 degree range, following RF ablation that did not produce initial block.

## *C. RESULTS*

*Summary of Temperature Results*

The maximum temperature within the lesion gap showing initial block followed by complete recovery was 63.4° C, with a time constant of 22.2 seconds. For lesions which showed block followed by partial recovery, the maximum temperature within the lesion gap was 58.9 ± 4.2° C (N=3), with a time constant of 29.0 ± 11.8 seconds. For lesions showing supernormal conduction, the maximum temperature within the lesion gap was 59.5 ± 2.5° C (N=5), with a time constant of 44.1 ± 12.2 seconds. An example of the post-ablation gap temperature is shown in figure 5.3.

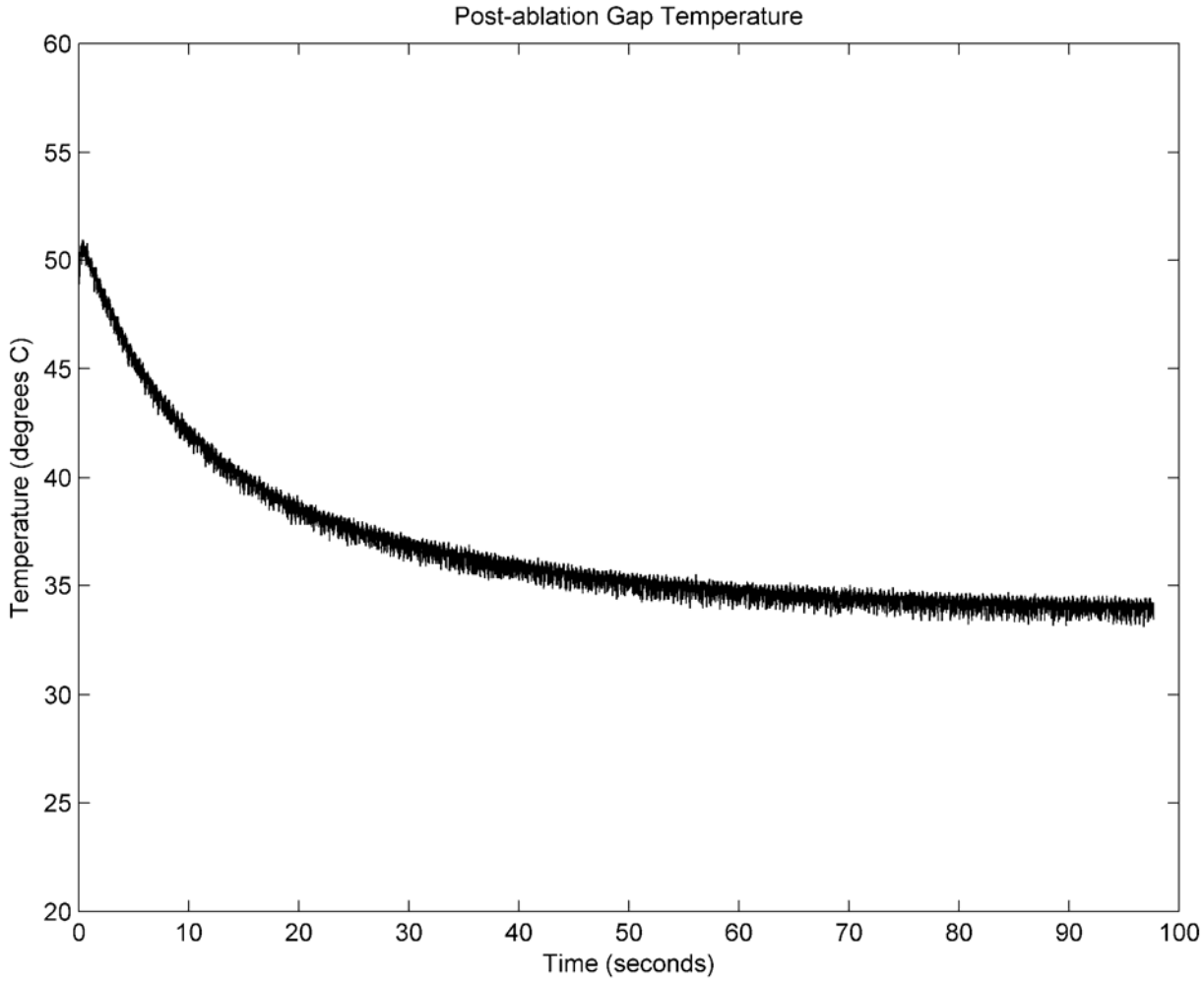


**Figure 5.3** Gap temperature following RF ablation. The peak of the curve represents the peak ablation temperature within the epicardial gap.

*Temperature During Control Recordings*

In one heart, time delay and temperature were monitored for 60 minutes before a lesion was formed. The purpose of this was to ensure that changes in time delay and temperature were due to RF ablation lesion formation, rather than to physiological changes which occur normally over the course of the experiment.

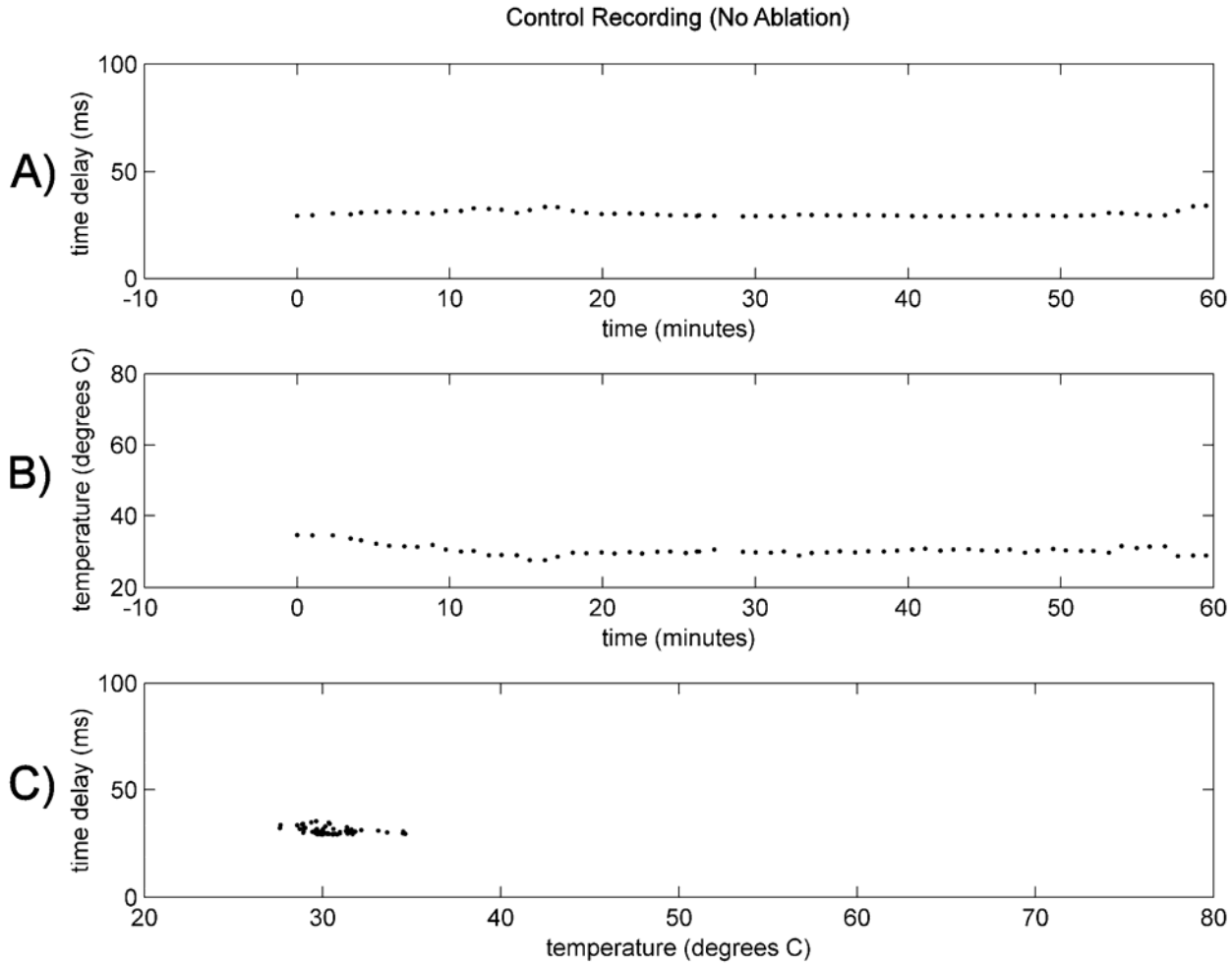


**Figure 5.4** Control recording of time delay and temperature for a 60-minute period.

Control time delay and temperature remained stable compared to post-ablation measurements (figures 5.5 and 5.6). Plot C of figure 5.4 shows that time delay and temperature measurements remain confined to a small area of the plotting surface.

*Temperature During Complete Recovery*

For the lesions which showed complete recovery, figure 5.5 shows that the initial rise in temperature is associated with conduction block. However, the temperature decreased to its resting value within 1 minute (time constant = 22.7 seconds) while conduction block

remained until approximately 5 minutes post-ablation. Hysteresis occurred and is shown in panel C, where time delay rises above 60 ms as temperature rises above 40 degrees, but then remains above 60 ms until approximately 4 minutes after the temperature has fallen to 35 degrees.

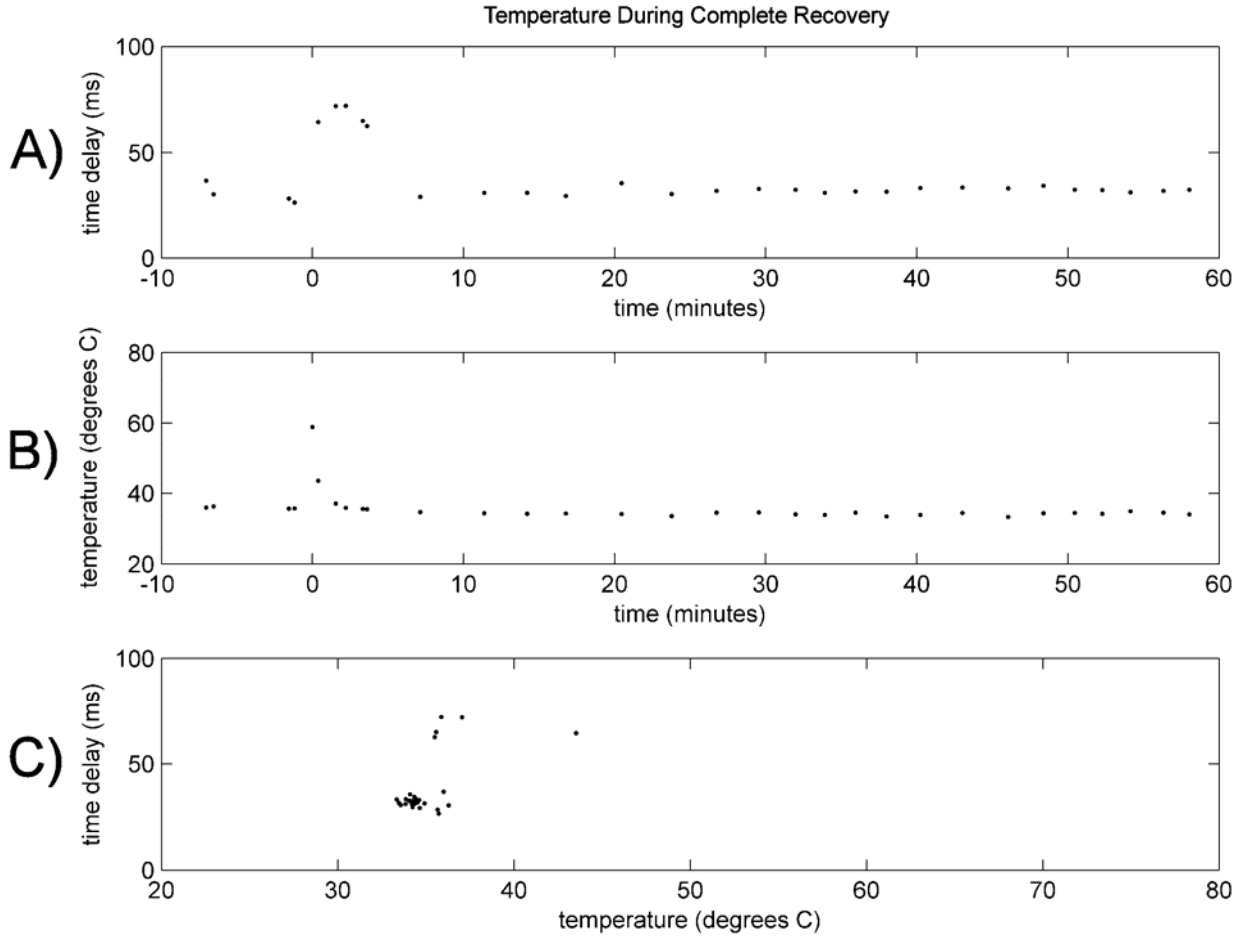


**Figure 5.5** Graphs illustrating the relationship between time delay and temperature for a lesion showing complete recovery.

*Temperature During Partial Recovery*

During partial recovery, the initial rise in temperature was associated with a concurrent rise in time delay indicating conduction block. However partial recovery occurred

after the temperature had returned to its equilibrium value, and 50% and 90% recovery occurred at 14.4 ± 1.0 and 23.7 ± 4.3 minutes, respectively. For the example shown in figure 5.6, 50% and 90% recovery occurred at 13.8 and 19.4 minutes.

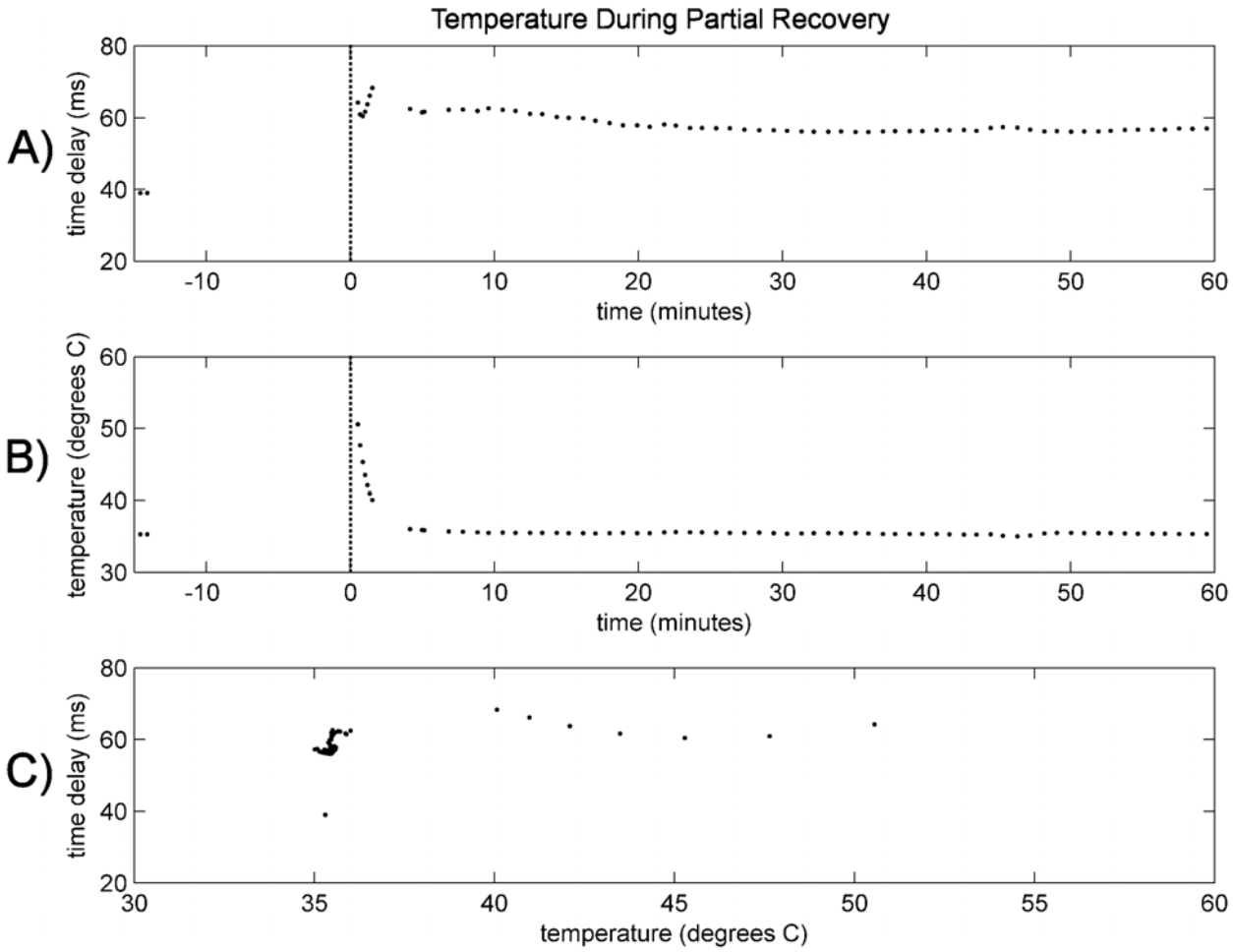


**Figure 5.6** Graphs illustrating the relationship between time delay and temperature for a lesion showing partial recovery.

*Temperature During Changes in Activation Complex*

Morphological changes in the post-ablation electrogram occurred in 1 of 8 lesions. Immediately following ablation, the first activation peak greater than 1 mV was chosen for

time delay measurements as described previously. After 11.2 minutes, this peak is no longer present.

| Type of Recovery | $T_{max}$ (°C) | τ (sec) | $t_{50}$ (mins.) | Lesion Number | Gap Size (mm) |
|---|---|---|---|---|---|
| **Complete Recovery** | **63.44** | **22.2** | **5.4** | **2** | **2.0** |
| **Partial Recovery 1** | **50.97** | **16.87** | **13** | **3** | **2.5** |
| **Partial Recovery 2** | **60.57** | **52.68** | **13.8** | **1** | **0.5** |
| **Partial Recovery 3** | **65.29** | **17.51** | **16.3** | **2** | **0.5** |
| **Recovery of Activation Complex (burn 2)** | **73.87** | **50.87** | **11.2*** | **2** | **1.5** |

**Table 5.1 -** Summary of maximum temperatures ($T_{max}$), time constants (τ), and times for 50% recovery ($t_{50}$).

*50% recovery for the morphological change indicates the amount of time that elapsed between the final ablation and the recovery of the activation complex.

*Temperature During Supernormal Conduction*

Supernormal conduction immediately following RF ablation was observed in 4 lesions. For one lesion in which RF was applied twice, supernormal conduction was observed twice, for a total of 5 observations. Time delay for those lesions showing supernormal conduction decreased by 5.5 ± 1.3 ms (N=5) to their minima, which equated to a 17.8 ± 2.6% decrease from control. Minima for time delay occurred 28.0 ± 4.0 seconds after the end of ablation. Two examples of supernormal conduction are shown in figure 5.7. The results for supernormal conduction are summarized in table 5.2.

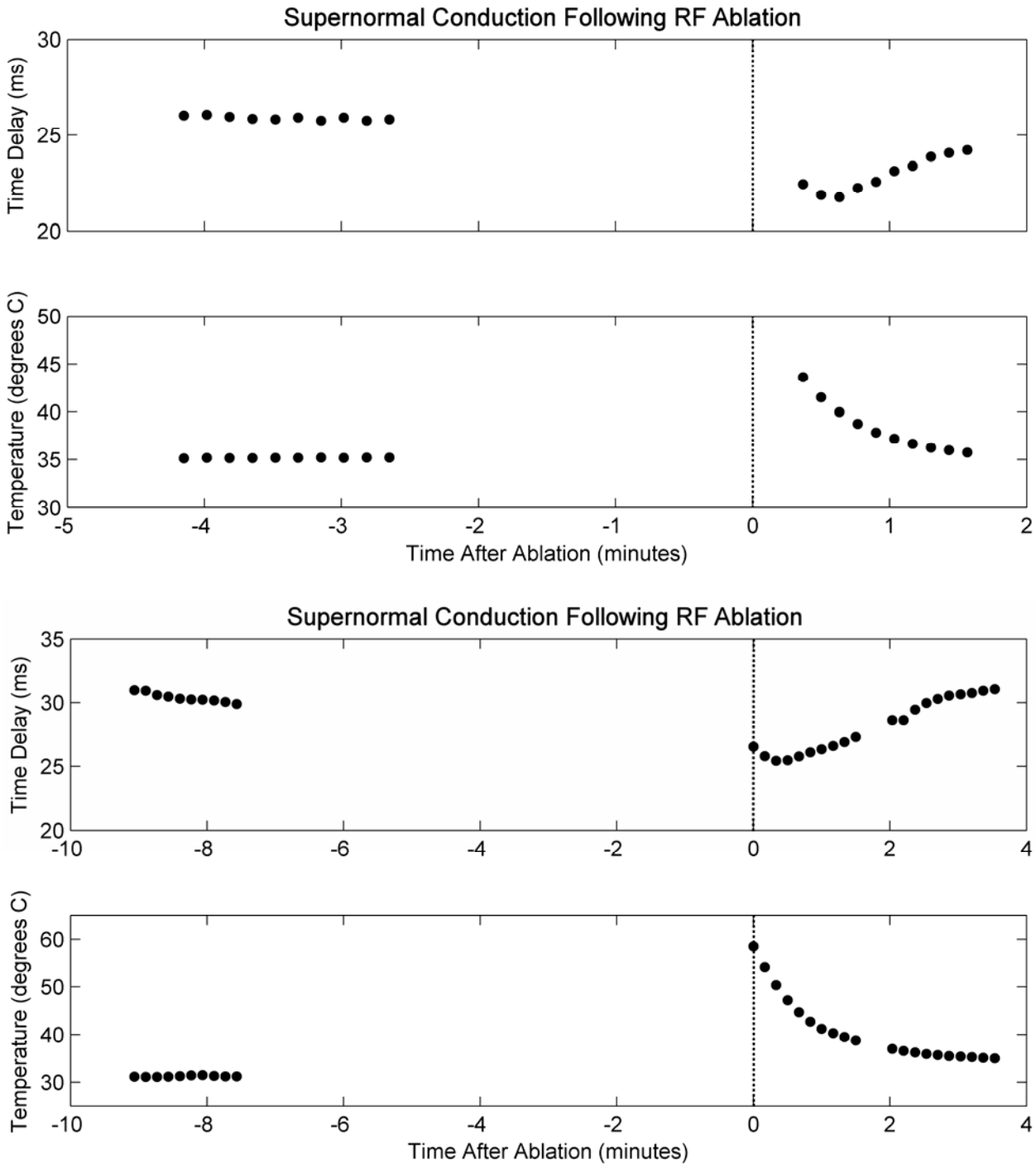


**Figure 5.7** Supernormal conduction immediately following RF ablation (end of RF ablation indicated by the dotted vertical line).

| $TD_{min}$ (ms) | $\Delta TD_{decrease}$ (%) | $t_{min}$ (sec) | $T_{max}$ (°C) | τ (sec) | Lesion Number | Gap Width (mm) |
|---|---|---|---|---|---|---|
| 20.81 | 10.88 | 17.4 | 50.97 | 16.87 | 3 | 2.5 |
| 26.06 | 24.18 | 30 | 63.01 | 66.44 | 2 | N/A* |
| 26.37 | 23.28 | 35 | 57.59 | 76.35 | 3 | 0.5 |
| 21.76 | 15.76 | 37.8 | 65.29 | 17.51 | 2 | 1.5 |
| 25.43 | 14.9 | 20 | 60.9 | 43.32 | 2 | 1.5 |

**Table 5.2 -** Parameters describing supernormal conduction. $t_{min}$ indicates the time of the minimum time delay relative to the end of the ablation.

*For this lesion, opposite sides of the lesion were bridged by a papillary muscle.

After ablations which did not cause conduction block, a decrease in time delay was observed. For the example shown in figure 5.7, late decreases (>30 seconds) in temperature correspond to increases in time delay, however earlier decreases in temperature (<30 seconds) correspond to a decrease in time delay, indicating the presence of a "phase lag" for the dependence of time delay upon temperature.

*Correlation between Time Delay and Temperature during Supernormal Conduction*

Immediately following the ablation burn, time delay changes in a biphasic manner (figure 5.7), and it is apparent that time delay is not linearly correlated with temperature over the entire post-ablation range. However, following the minimum value of time delay observed at approximately 30 seconds after ablation, a linear relationship was observed for data points within the 35-40 degree range. Figure 5.8 shows a strong correlation between temperature and time delay for this range of temperatures.

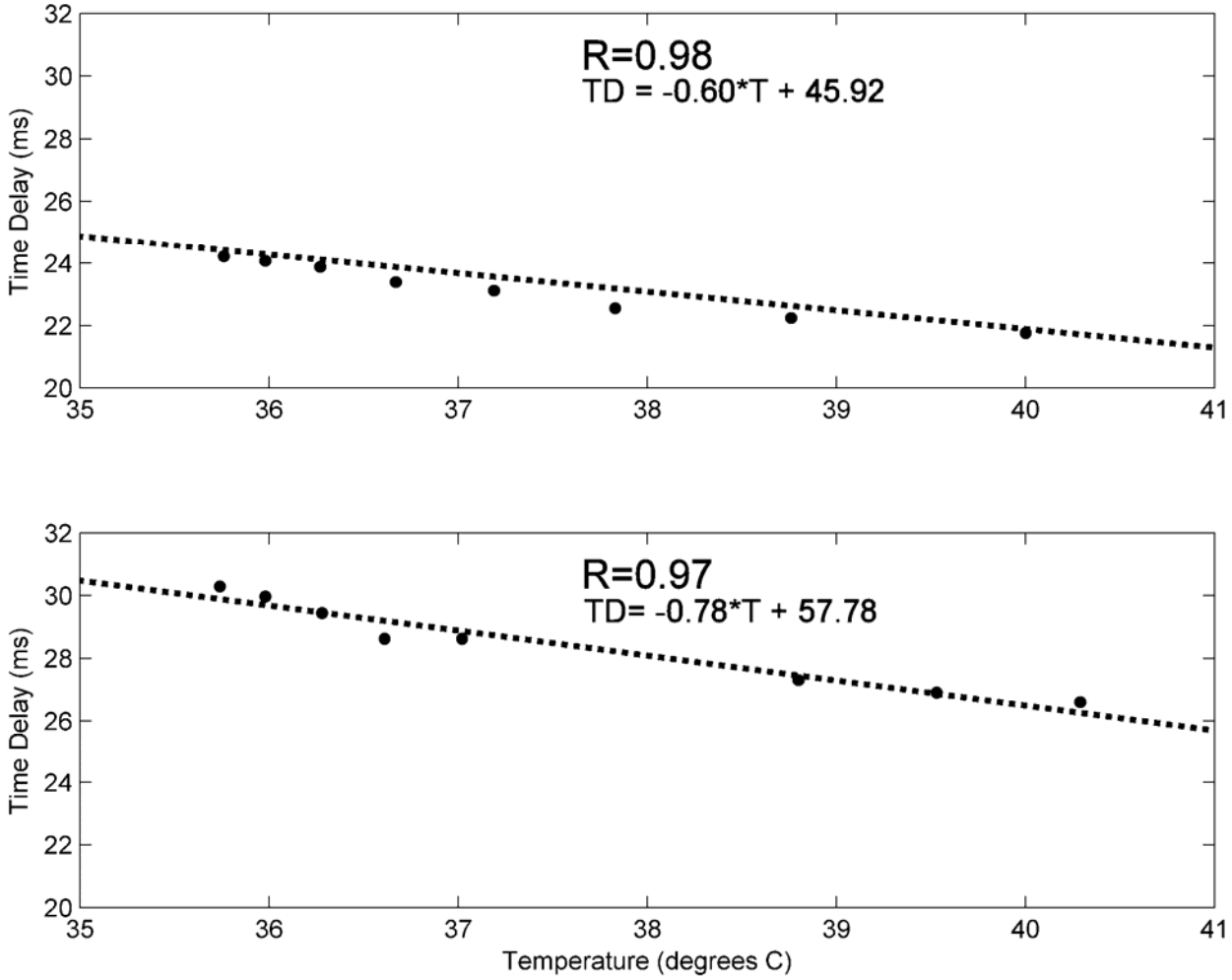


**Figure 5.8** Relationship between temperature and time delay during supernormal conduction, shown for the same lesions as in figure 5.7. Filled circles represent experimental values. Dotted line represents the best-fit line as determined by linear regression.

*Summary of Temperature Dependence of Recovery*

Figure 5.9 illustrates the case of complete recovery. The diagram shows an initial increase in time delay concurrent with an increase in temperature (arrow 1), indicating block following ablation. As temperature decreases, time delay remains constant (arrow 2). As time passes, time delay eventually returns to its control value (arrow 3).

Figure 5.10 gives a diagram for partial recovery. Initially, the same behavior is observed as for complete recovery (arrows 1 and 2). However, as time passes, time delay

does not return to control values, and only small decreases in time delay are observed over time (arrow 3).

For supernormal conduction (figure 5.11), temperature increases were not sufficient to produce post-ablation block. Time delay decreased following ablation (arrow 1), and continued to increase for approximately 30 seconds after temperature began to decrease (arrow 2). With further temperature decreases, time delay began to return to control values (arrow 3).

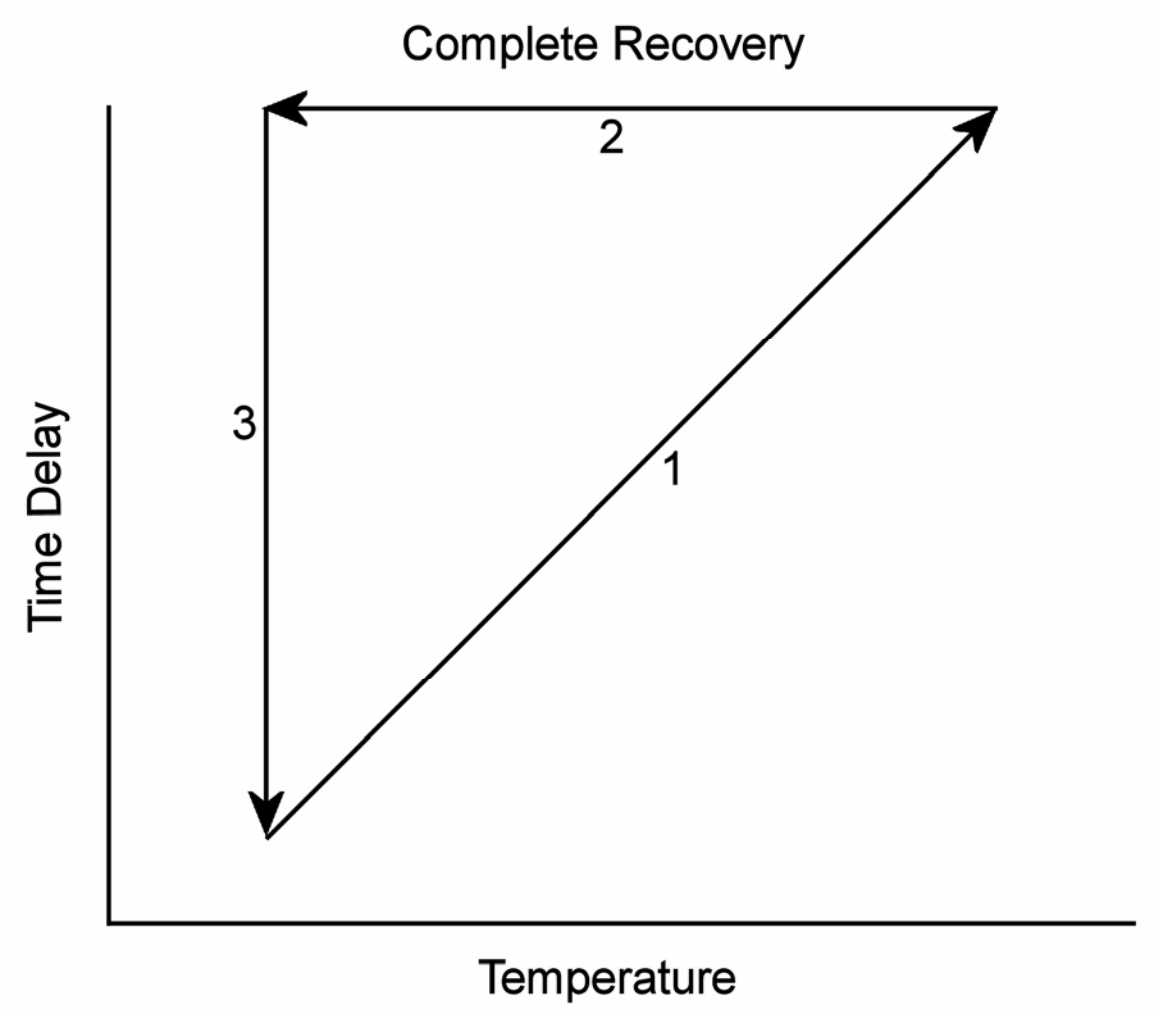


**Figure 5.9** Diagram for complete recovery. Numbers indicate the time order of events, and the direction of arrows represents the flow of time.

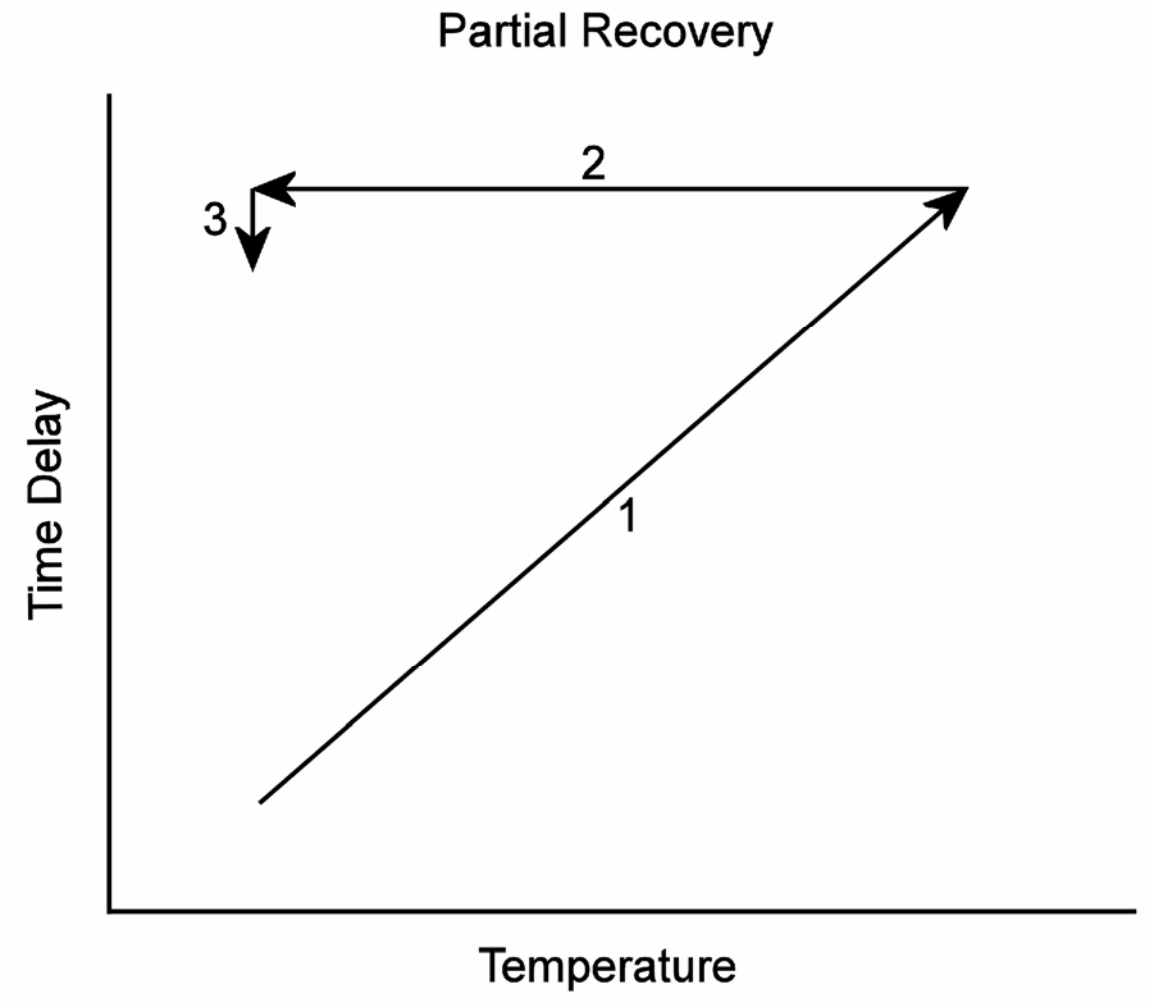


**Figure 5.10** Diagram for partial recovery. Numbers indicate the time order of events, and the direction of arrows represents the flow of time.

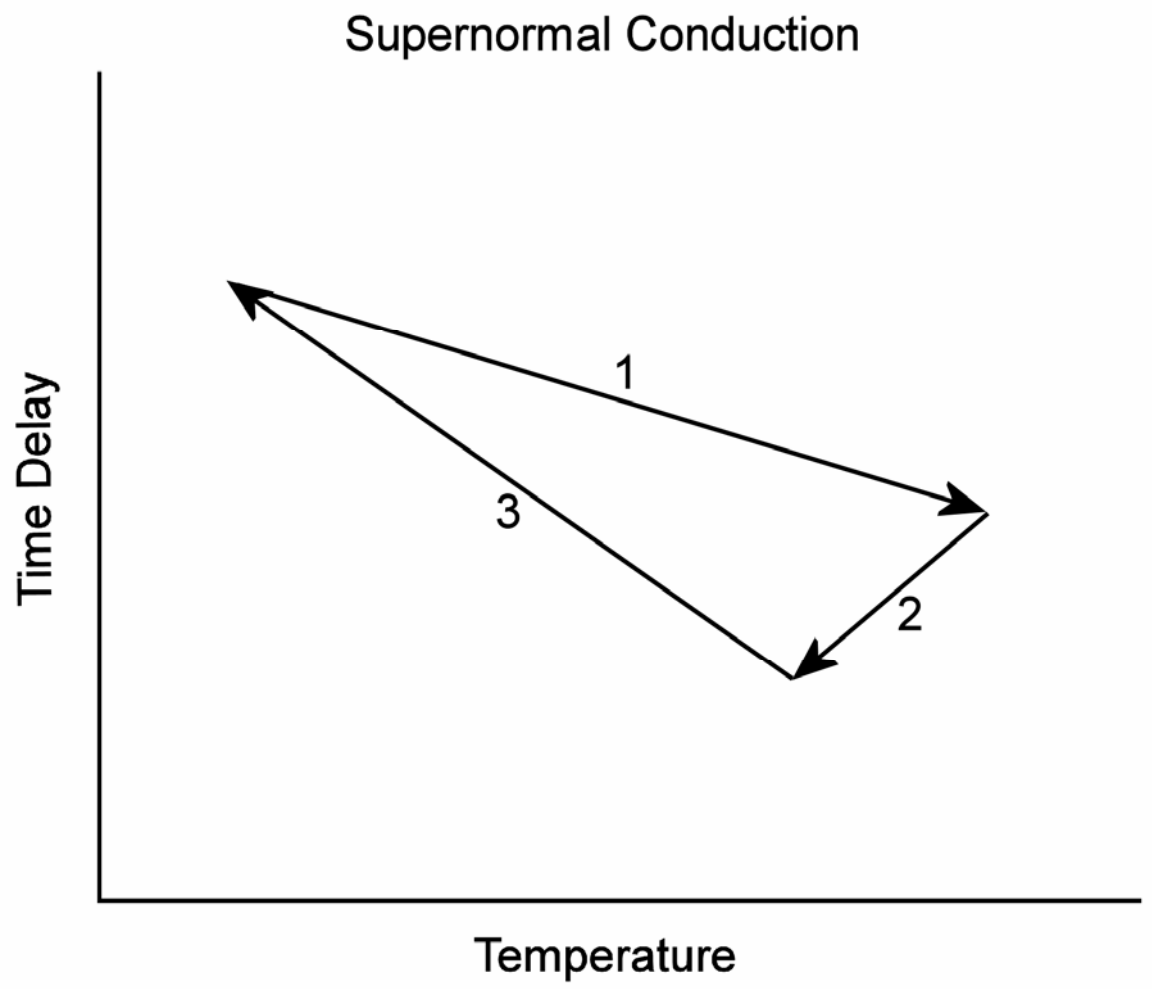


**Figure 5.11** Diagram for supernormal conduction. Numbers indicate the time order of events, and the direction of arrows represents the flow of time.

## *D. DISCUSSION*

The main findings of this study are the following:

1) Initial rises in temperature are temporally correlated with initial conduction block, as indicated by increases in trans-lesion conduction delay immediately following ablation. However, decreases in temperature are not necessarily correlated temporally with decreases in time delay.
2) Complete recovery of time delay from a greater than 2-fold increase to pre-ablation values occurred within a five minute period, but did not temporally correspond to decreases in temperature.
3) Incomplete recovery occurred tens of minutes following ablation, and did not correspond temporally with decreases in post-ablation temperature.
4) Supernormal conduction may occur following ablations which do not produce block. An inverse relationship existed between temperature and time delay following the minimum value of time delay. However early decreases in time delay (<30 seconds) following ablation were not inversely related to temperature, and the response of the tissue to temperature decreases following ablation was associated with a phase lag of approximately 30 seconds. Following the phase lag, a linear inverse relationship existed between temperature and time delay.

It is well-known that temperature increases will increase the rate of biochemical reactions, and that beyond critical temperatures protein denaturation leads to failure of critical biological processes. In this study, we have observed processes which occur in both

the mildly hyperthermic realm of temperatures (38 – 50° C) as well as those leading to irreversible protein denaturation ( > 50° C).

The effect of temperature upon slices of superfused myocardium has been described previously by Simmers et al[204]. This study showed that temperatures in excess of 54° C are required in order to ensure complete block. However this study used thin (~2 mm) superfused slices of myocardium rather than a whole heart preparation, where conduction of activation and heat distributions are complicated by complex fiber orientation significantly greater anatomical complexity. Clinically, it is important to understand the response of tissue conduction to epicardial lesion temperature in the whole heart, as epicardial temperature is an accessible parameter during ablation procedures.

Our study shows that the timing of temperature decline following the production of conduction block was not closely related to subsequent decreases in time delay. The time constant of temperature decay was on the order of tens of seconds, while complete and partial recovery occurred at 5 and 15-30 minutes, respectively. This suggests that the processes governing conduction react rapidly to initial temperature increases but react relatively slowly to temperature decreases.

Time delay for lesions which do not produce initial block shows a strong temporal correlation to both increases and decreases in epicardial temperature. In the case of no initial block, time delay decreases following a temperature increase, and then increases linearly as temperature returns to its equilibrium value. However this change in the sign of the time delay derivative does not perfectly coincide with the change in the sign of the temperature derivative. Even after the temperature begins to decrease following ablation, time delay continues to decrease for approximately 30 seconds, and then time delay begins to rise back

to its control value. Although it is possible that this is merely an artifact of heat conduction patterns in the tissue following ablation, it is also possible that this 30-second "phase lag" truly represents the time response of the tissue to heat efflux. This phase lag may indicate a time-dependent recovery process of either sodium and/or connexin channels which modulate the speed of the activation wavefront.

Considering the strong dependence of time delay upon temperature as demonstrated in figures 5.7 and 5.8, it is likely that hyperthermia is the most significant factor which contributes to supernormal conduction. However there are other possible causes which may decrease time delay. While the fast sodium current is primarily responsible for the early activation of myocytes, other currents may also modulate the action potential upstroke. Sugiura and Joyner showed that the introduction of a calcium channel blocker (nifedipine) caused an increase in cell-to-cell conduction delay. Further, this delay increased when the intercellular coupling resistance increased[212]. Also, the transient outward current ($I_{to}$) has been shown to modulate conduction velocity by altering early repolarization (phase 1) of the action potential. By rapidly reducing the transmembrane potential immediately following the action potential upstroke, $I_{to}$ reduces the ability of upstream cells to act as a current source. Thus factors which reduce $I_{to}$ will lead to supernormal conduction[213]. As is the case with calcium channel blockers, the effects of $I_{to}$ block upon conduction delay will be markedly pronounced when the intercellular resistance (junctional resistance) is increased. In a coupled myocyte pair where the junctional resistance was increased by 33%, the conduction delay between the two cells increased by a factor of 3.6 (from 12 to 43 ms)[213]. While the L-type calcium current and the transient outward current may play a role in supernormal conduction following ablation, the significance of these currents is thought to be relatively minor, in light

of the fact that changes in junctional resistances due to ischemia take longer amounts of time to develop. There are reports which have shown that connexin 43 decreases in and around the site of ablation[214], however the timing and cause of these decreases is not precisely known.

Another factor which may modulate conduction velocity involves myocardial ischemia induced by damage to the microvasculature. Although acidosis, hypoxia, and extracellular potassium concentration ($[K]_o$) levels all affect conduction velocity, it is the extracellular potassium levels which are thought to play the greatest role[215]. Rises in $[K]_o$ have been shown to be responsible for a biphasic change in conduction velocity, with early rises corresponding to an increase in conduction velocity and further rises corresponding to a decrease in conduction velocity, and eventually resulting in conduction block[215]. Thus ischemia may contribute to decreases in time delay, and may be responsible for the biphasic trend observed in time delay in figure 5.7, although confirmation would require precise knowledge of $[K]_o$ over the course of the experiment.

## *APPENDIX: A Geometric Model for Predicting Time Delay around a Linear Ablation Lesion in a Two-Dimensional Sheet of Myofibers*

The following model is proposed as a "next step" for improving predictions of time delay based on activation path length. The model assumes that the myocardium is composed of a single sheet of myofibers which maintain a constant fiber direction throughout the region of the ablation lesion. The atria have previously been modeled as a two-dimensional sheet[207], but this is thought to underestimate the complexity of conduction paths which may be altered by atrial pectinate muscles[208]. The model also assumes specific lesion geometry, and that propagation is confined to the perimeter of the lesion.

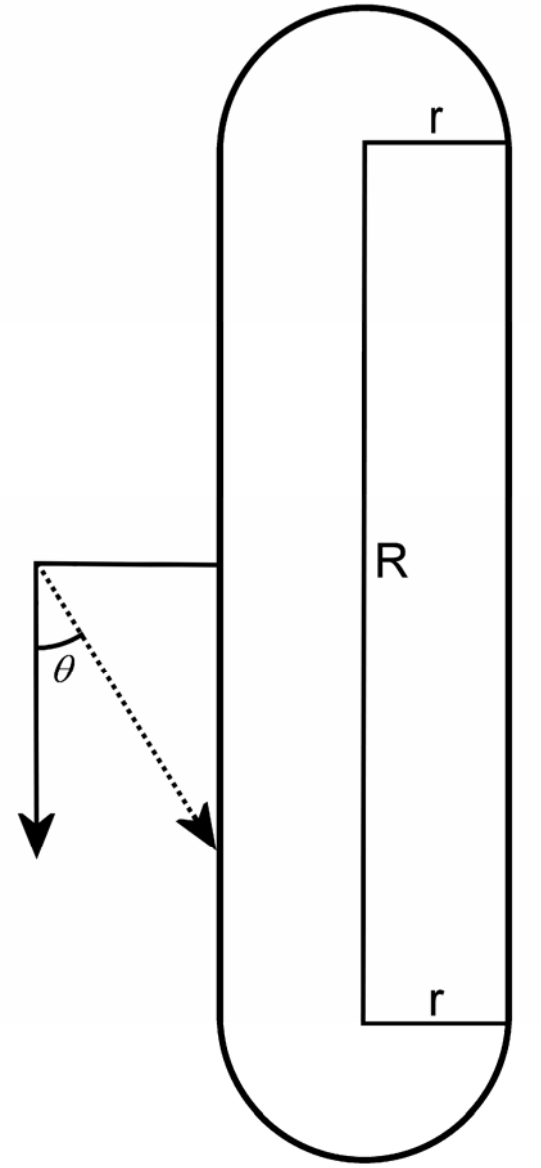


In this model, r represents the radius of the semicircle formed by the end of the lesion, R represents the length of the lesion minus 2r, and θ represents the angle between the fiber direction and the direction of travel of the activation wavefront. The velocity of the wavefront will be modeled as a sinusoid with a constant term (based on figure 2 of Roberts et al[158]):

1) $$v_\theta = v_c + v_f \cos(2\theta)$$

where $v_\theta$ is the velocity of the wavefront as a function of θ, $v_c$ is the constant term of the

wavefront velocity, and $v_f$ is the additional component of velocity which is due to alignment of the direction of propagation with respect to the fiber direction.

The time delay (TD) for a pre-lesion recording is given by the following expression:

2) $$TD_{pre} = \frac{2r}{v_\theta(\theta)}$$

For the time delay while traveling around a complete lesion, the path will be broken up into two terms for illustrative purposes. The first term represents the time delay due to the wavefront traveling down the side of the lesion a distance R/2 and back up the lesion another distance R/2. For these two segments of the activation path, θ will be constant. Time delay for this segment of the path is given by the following expression:

3) $$TD_{post1} = \frac{R}{v_\theta(\theta_o)}$$

For the segment of the path which lies on the circular end of the lesion, θ will change at each consecutive point on the path, thus the velocity must be integrated over with respect to θ. The time delay for this segment of the path is given by the following expression:

4) $$TD_{post2} = \int_{\theta_o - \pi/2}^{\theta_o} \frac{r \cdot d\theta}{v_c + v_f \cdot \cos(2 \cdot \theta)} + \int_{\pi/2}^{\pi/2 - \theta_o} \frac{r \cdot d\theta}{v_c + v_f \cdot \cos(2 \cdot \theta)} + \int_{-\theta_o}^{-\pi/2 + \theta_o} \frac{r \cdot d\theta}{v_c + v_f \cdot \cos(2 \cdot \theta)}$$

where $\theta_o$ is a constant, and represents the angle between the fibers and the initial direction of propagation over the segment being integrated (the solid vertical arrow for the post-lesion case).

Thus if the fiber direction and lesion dimensions are known, time delay can be approximated using this method.

As an example, let r = 3.6 mm, R = 19.0 mm, $v_c$ = .35 mm/ms, and $v_f$ = .15 mm/ms. Values for r and R were taken from the results section of Chapter 2. The control and post-lesion time delays are plotted below as a function of $\theta_o$:

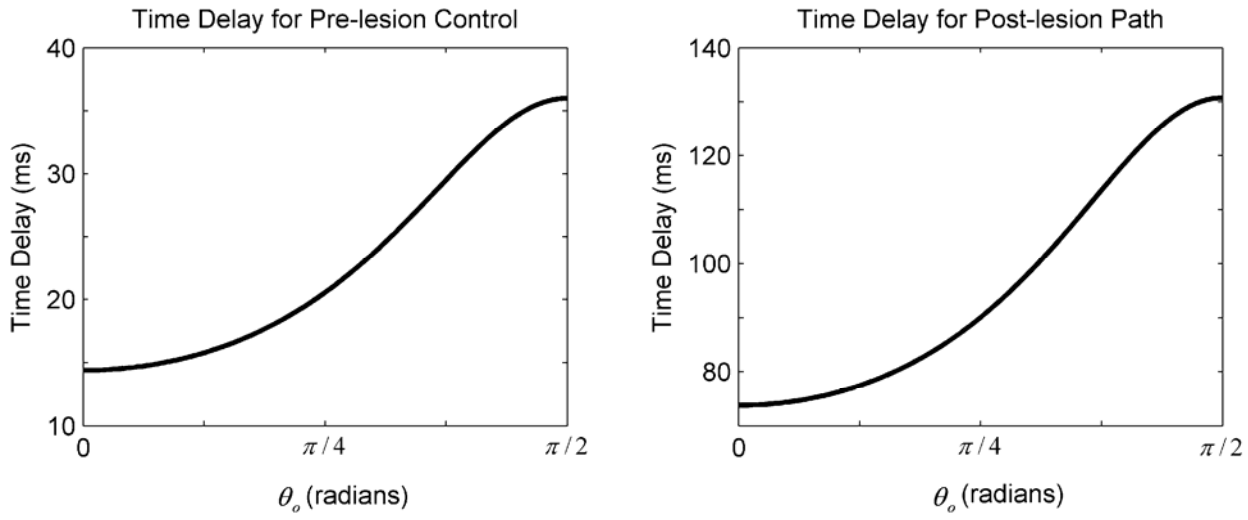


While the straight region ($TD_{post1}$) of the conduction path around the ablation lesion has a sinusoidal dependence upon fiber angle (above), the time delay for the semicircular portion ($TD_{post2}$) of the path is independent of fiber angle.

Substantial differences exist between the model assumptions and the experimental setup of chapter 2, such as the tissue depth and fiber rotation of the ventricles. However the values presented using this simple model are comparable to those in tables 2.1 and 2.2, with both pre and post-lesion (complete) time delay means falling within the ranges shown above.

## REFERENCES


1. Thom T, Haase N, Rosamond W, Howard VJ, Rumsfeld J, Manolio T, Zheng Z-J, Flegal K, O'Donnell C, Kittner S, Lloyd-Jones D, David C. Goff J, Hong Y: Heart disease and stroke statistics--2006 update: A report from the american heart association statistics committee and stroke statistics subcommittee. *Circulation*. 2006;113:e85-e151.

2. Lloyd-Jones DM, Wang TJ, Leip EP, Larson MG, Levy D, Vasan RS, D'Agostino RB, Massaro JM, Beiser A, Wolf PA, Benjamin EJ: Lifetime risk for development of atrial fibrillation: The framingham heart study. *Circulation*. 2004;110:1042-1046.

3. Guyton AC. Heart muscle; the heart as a pump. In: Guyton AC, ed. *Textbook of medical physiology*. Philadelphia, PA: W. B. Saunders Company; 2000:96-106.

4. Wolf PA, Abbott RD, Kannel WB: Atrial fibrillation: A major contributor to stroke in the elderly. *Arch Intern Med*. 1987;147:1561-1564.

5. Wolf PA, Abbott RD, Kannel WB: Atrial fibrillation as an independent risk factor for stroke: The framingham study. *Stroke*. 1991;22:983-988.

6. Benjamin EJ, Wolf PA, D'Agostino RB, Silbershatz H, Kannel WB, Levy D: Impact of atrial fibrillation on the risk of death: The framingham heart study. *Circulation*. 1998;98:946-952.

7. Kinebuchi O, Mitamura H, Shiroshita-Takeshita A, Kurita Y, Ohashi N, Tanimoto K, Fukuda Y, Ieda M, Sato T, Hara M, Takatsuki S, Ogawa S: Temporal patterns of progression and regression of electrical and mechanical remodeling of the atrium. *International Journal of Cardiology*. 2005;98:91-98.

8. Wijffels MCEF, Kirchhof CJHJ, Dorland R, Power J, Allessie MA: Electrical remodeling due to atrial fibrillation in chronically instrumented conscious goats: Roles of neurohormonal changes, ischemia, atrial stretch, and high rate of electrical activation. *Circulation*. 1997;96:3710-3720.

9. Wijffels MCEF, Kirchhof CJHJ, Dorland R, Allessie MA: Atrial fibrillation begets atrial fibrillation: A study in awake chronically instrumented goats. *Circulation*. 1995;92:1954-1968.

10. Schotten U, Duytschaever M, Ausma J, Eijsbouts S, Neuberger H-R, Allessie M: Electrical and contractile remodeling during the first days of atrial fibrillation go hand in hand. *Circulation*. 2003;107:1433-1439.

11. Allessie MA, Konings K, Kirchhof CJHJ, Wijffels M: Electrophysiologic mechanisms of perpetuation of atrial fibrillation. *Am J Cardiol*. 1996;77:10A-23A.

12. Allessie M, Ausma J, Schotten U: Electrical, contractile, and structural remodeling during atrial fibrillation. *Cardiovascular Research*. 2002;54:230-246.

13. Oral H, Chugh A, Ozaydin M, Good E, Fortino J, Sankaran S, Reich S, Igic P, Elmouchi D, Tschopp D, Wimmer A, Dey S, Crawford T, Frank Pelosi J, Jongnarangsin K, Bogun F, Morady F: Risk of thromboembolic events after percutaneous left atrial radiofrequency ablation of atrial fibrillation. *Circulation*. 2006;114:759-765.

14. Wazni OM, Rossillo A, Marrouche NF, Saad EB, Martin DO, Bhargava M, Bash D, Beheiry S, Wexman M, Potenza D, Pisano E, Fanelli R, Bonso A, Themistoclakis S, Erciyes D, Saliba WI, Schweikert RA, Brachmann J, Ravielle A, Natale A: Embolic events and char formation during pulmonary vein isolation in patients with atrial fibrillation: Impact of different anticoagulation regimens and importance of intracardiac echo imaging. *J Cardiovasc Electrophysiol*. 2005;16:576-581.

15. Lee DSY, Dorian P, Downar E, Burns M, Yeo EL, Gold WL, Paquette M, Lau W, Newman DM: Thrombogenecity of radiofrequency ablation procedures: What factors influence thrombin generation? *Europace*. 2001;3:195-200.

16. Seidl K, Schwacke H, Zahn R, Rameken M, Drogemuller A, Senges J: Catheter ablation of chronic atrial fibrillation with noncontact mapping: Are continuous linear lesions associated with ablation success? *PACE*. 2003;26:534-543.

17. Nath S, Whayne JG, Kaul S, Goodman C, Jayaweera AR, Haines DE: Effects of radiofrequency catheter ablation on regional myocardial blood flow: Possible mechanism for late electrophysiological outcome. *Circulation*. 1994;89:2667-2672.

18. Nath S, Carl Lynch I, Whayne JG, Haines DE: Cellular electrophysiological effects of hyperthermia on isolated guinea pig papillary muscle: Implications for catheter ablation. *Circulation*. 1993;88:1826-1831.

19. Haines DE. The biophysics and pathophysiology of lesion formation during radiofrequency catheter ablation. In: Zipes DP, Jalife J, eds. *Cardiac electrophysiology: From cell to bedside*. Third ed. Philadelphia: W. B. Saunders Company; 2000:983-993.

20. Quian L, Song X, Ren H, Gong J, Cheng S: Mitochondrial mechanism of heat stress-induced injury in rat myocyte. *Cell Stress & Chaperones*. 2004;9:281-293.

21. Nath S, Redick JA, Whayne JG, Haines DE: Ultrastructural observations in the myocardium beyond the region of acute coagulation necrosis following radiofrequency catheter ablation. *J Cardiovasc Electrophysiol*. 1994;5:838-845.

22. Bennett MR: Apoptosis in the cardiovascular system. *Heart*. 2002;87:480-487.

23. Debatin K-M, Poncet D, Kroemer G: Chemotherapy: Targeting the mitochondrial cell death pathway. *Oncogene*. 2002;21:8786-8803.

24. Matsuyama S, Llopis J, Deveraux QL, Tsien RY, Reed JC: Changes in intramitochondrial and cytosolic ph: Early events that modulate caspase activation during apoptosis. *Nature Cell Biology*. 2000;2:318-325.

25. Waibel M, Kramer S, Lauber K, Lupescu A, Manns J, Schulze-Osthoff K, Lang F, Wesselborg S: Mitochondria are not required for death receptor-mediated cytosolic acidification during apoptosis. *Apoptosis*. 2006;Epub ahead of print.

26. Wesselborg S, Engels IH, Rossmann E, Los M, Schulze-Osthoff K: Anticancer drugs induce caspase-8/flice activation and apoptosis in the absence of cd95 receptor/ligand interaction. *Blood*. 1999;93:3053-3063.

27. Engels IH, Stepczynska A, Stroh C, Lauber K, Berg C, Schwenzer R, Wajant H, Janicke RU, Porter AG, Belka C, Gregor M, Schulze-Osthoff K, Wesselborg S: Caspase-8/flice functions as an executioner caspase in anticancer drug-induced apoptosis. *Oncogene*. 2000;19:4563-4573.

28. Everett TH, Nath S, Carl Lynch I, Beach JM, Whayne JG, Haines DE: Role of calcium in acute hyperthermic myocardial injury. *J Cardiovasc Electrophysiol*. 2001;12:563-569.

29. Schertzer JD, Green HJ, Tupling AR: Thermal instability of rat muscle sarcoplasmic reticulum $ca^{2+}$-atpase function. *Am J Physiol Endocrinol Metab*. 2002;283:E722-E728.

30. Borelli MJ, Wong RSL, Dewey WC: A direct correlation between hyperthermia-induced membrane blebbing and survival in sychronous g1 cho cells. *J Cell Physiol*. 1986;126:181-190.

31. Coss RA, Linnemans WAM: The effects of hyperthermia on the cytoskeleton: A review. *Int J Hyperthermia*. 1996;12:173-196.

32. Gabai VL, Kabakov AE: Tumor cell resistance to energy deprivation and hyperthermia can be determined by the actin skeleton stability. *Cancer Letters*. 1993;70:25-31.

33. Taylor DL, Wang Y-L: Molecular cytochemistry: Incorporation of fluorescently labeled actin into living cells. *Proc Natl Acad Sci*. 1978;75:857-861.

34. Schuler H, Lindberg U, Schutt CE, Karlsson R: Thermal unfolding of g-actin monitored with the dnase i-inhibition assay: Stabilities of actin isoforms. *Eur J Biochem*. 2000;267:476-486.

35. Ngaage DL, Schaff HV: Mitral valve surgery in non-ischemic cardiomyopathy. *J Cardiovasc Surg*. 2004;45:477-486.

36. Cooper GM. The cytoskeleton and cell movement. In: Cooper GM, ed. *The cell: A molecular approach*. Sunderland, MA: Sinauer Associates, Inc.; 1997:423-466.

37. Lodish H, Baltimore D, Berk A, Zipursky SL, Matsudaira P, Darnell J. Multicellularity: Cell-cell and cell-matrix interactions. In: Lodish H, Baltimore D, Berk A, Zipursky SL, Matsudaira P, Darnell J, eds. *Molecular cell biology*. New York: W. H. Freeman and Company; 1995:1123-1200.

38. Janmey PA: The cytoskeleton and cell signaling: Component localization and mechanical coupling. *Physiological Reviews*. 1998;78:763-781.

39. Katz AM: Cytoskeletal abnormalities in the failing heart: Out on a lim? *Circulation*. 2000;101:2672-2673.

40. Li X-L, Zheng H-F, Jin Z-Y, Yang M, Li Z-L, Xu W-X: Effect of actin microfilament on potassium current in guinnea pig gastric myocytes. *World Journal of Gastroenterology*. 2004;10:3303-3307.

41. Lader AS, Kwiatkowski DJ, Cantiello HF: Role of gelsolin in the actin filament regulation of cardiac l-type calcium channels. *Am J Physiol Cell Physiol*. 1999;46:C1277-C1283.

42. Calaghan SC, Guennec J-YL, White E: Cytoskeletal modulation of electrical and mechanical activity in cardiac myocytes. *Progress in Biophysics & Molecular Biology*. 2004;84:29-59.

43. Sampson LJ, Leyland ML, Dart C: Direct interaction between the actin-binding protein filamin-a and the inwardly rectifying potassium channel, kir2.1. *The Journal of Biological Chemistry*. 2003;278:41988-41997.

44. Piao L, Ho W-K, Earm YE: Actin filaments regulate the stretch sensitivity of large conductance, $ca^{2+}$-activated $k^{+}$ channels in coronary artery smooth muscle cells. *Pflugers Arch - Eur J Physiol*. 2003;446:523-528.

45. Bouchard M, Pare C, Dutasta J-P, Chauvet J-P, Gicquaud C, Auger M: Interaction between g-actin and various types of liposomes: A $^{19}$f, $^{31}$p, and $^{2}$h nuclear magnetic resonance study. *Biochemistry*. 1998;37:3149-3155.

46. Gicquaud C, Wong P: Mechanism of interaction between actin and membrane lipids: A pressure-tuning infrared spectroscopy study. *Biochemical Journal*. 1994;303:769-774.

47. Laszlo A: The effects of hyperthermia on mammalian cell structure and function. *Cell Proliferation*. 1992;25:59-87.

48. Lepock JR: How do cells respond to their thermal environment? *Int J Hyperthermia*. 2005;21:681-687.

49. Lorinczy D, Konczol F, Gaszner B, Belagyi J: Structural stability of actin filaments as studied by dsc and epr. *Thermochimica Acta*. 1998;322:95-100.

50. Gicquaud CR, Heppell B: Three steps in the thermal unfolding of f-actin: An experimental evidence. *Biopolymers*. 2006;Epub ahead of print.

51. Vega-Warner V, Smith DM: Denaturation and aggregation of myosin from two bovine muscle types. *J Agric Food Chem*. 2001;49:906-912.

52. Lehrer SS, Kerwar G: Intrinsic fluorescence of actin. *Biochemistry*. 1972;11:1211-1217.

53. Zolkiewski M, Redowicz MJ, Korn ED, Ginsburg A: Thermally induced unfolding of *acanthamoeba* myosin ii and skeletal muscle myosin: Nucleotide effects. *Archives of Biochemistry and Biophysics*. 1995;318:207-214.

54. Ikeuchi Y, Ito T, Fukazawa T: A kinetic analysis of thermal denaturation of f-actin. *Int J Biochem*. 1981;13:1065-1069.

55. Goodno CC, Harris TA, Swenson CA: Thermal transitions of myosin and its helical fragments. Regions of structural instability in the myosin molecule. *Biochemistry*. 1976;15:5157-5160.

56. Konno K, Yamamoto T, Takahashi M, Kato S: Early structural changes in myosin rod upon heating of carp myofibrils. *J Agric Food Chem*. 2000;48:4905-4909.

57. Bertazzon A, Tsong TY: High-resolution differential scanning calorimetric study of myosin, functional domains, and supramolecular structures. *Biochemistry*. 1989;28:9784-9790.

58. Guthe KF, Brown DES: Reversible denaturation in the myosin adenosine triphosphatase system. *Journal of Cellular and Comparative Physiology*. 1958;52:79-87.

59. Brown DES, Guthe KF, Lawler HC, Carpenter MP: The pressure, temperature, and ion relations of myosin atp-ase. *Journal of Cellular and Comparative Physiology*. 1958;52:59-77.

60. Penny IF: The influence of ph and temperature on the properties of myosin. *Biochemical Journal*. 1967;104:609-615.

61. Wegrowski Y: Effect of hyperthermia on the extracellular matrix. *FEBS*. 1993;334:121-124.

62. Lepock JR: Cellular effects of hyperthermia: Relevence to the minimum dose for thermal damage. *Int J Hyperthermia*. 2003;19:252-266.

63. Thompson CB: Apoptosis in the pathogenesis and treatment of disease. *Science*. 1995;267:1456-1462.

64. Schulze-Osthoff K, Walczak H, Droge W, Krammer PH: Cell nucleus and DNA fragmentation are not required for apoptosis. *Journal of Cell Biology*. 1994;127:15-20.

65. Fortuno MA, Gonzalez A, Ravassa S, Lopez B, Diez J: Clinical implications of apoptosis in hypertensive heart disease. *Am J Physiol Heart Circ Physiol*. 2003;284:H1495-H1506.

66. Diez J, Panizo A, Hernandez M, Vega F, Sola I, Fortuno MA, Pardo J: Cardiomyocyte apoptosis and cardiac angiotensin-converting enzyme in spontaneously hypertensive rats. *Hypertension*. 1997;30:1029-1034.

67. Latchman DS: Heat shock proteins and cardiac protection. *Cardiovasc Res*. 2001;51:637-646.

68. Marber MS, Latchman DS, Walker JM, Yellon DM: Cardiac stress protein elevation 24 hours after brief ischemia or heat stress is associated with resistance to myocardial infarction. *Circulation*. 1993;88:1264-1272.

69. Donnelly TJ, Sievers RE, Vissern FLJ, Welch WJ, Wolfe CL: Heat shock protein induction in rat hearts: A role for improved myocardial salvage after ischemia and reperfusion? *Circulation*. 1992;85:769-778.

70. Hutter MM, Sievers RE, Barbosa V, Wolfe CL: Heat-shock protein induction in rat hearts: A direct correlation between the amount of heat-shock protein induced and the degree of myocardial protection. *Circulation*. 1994;89:355-360.

71. Yellon DM, Pasini E, Cargnoni A, Marber MS, Latchman DS, Ferrari R: The protective role of heat stress in the ischaemic and reperfused rabbit myocardium. *J Mol Cell Cardiol*. 1992;24:895-907.

72. Currie RW, Karmazyn M, Kloc M, Mailer K: Heat-shock response is associated with enhanced postischemic ventricular recovery. *Circ Res*. 1988;63:543-549.

73. Ilangovan G, Osinbowale S, Bratasz A, Bonar M, Cardounel AJ, Zweier JL, Kuppusamy P: Heat shock regulates the respiration of cardiac h9c2 cells through

upregulation of nitric oxide synthase. *Am J Physiol Cell Physiol*. 2004;287:C1472-C1481.

74. Lavoie JN, Gingras-Breton G, Tanguay RM, Landry J: Induction of chinese hamster hsp27 gene expression in mouse cells confers resistance to heat shock. *Journal of Cell Biology*. 1993;268:3420-3429.

75. Pivovarova AV, Mikhailova VV, Chernik IS, Chebotareva NA, Levitsky DI, Gusev NB: Effects of small heat shock proteins on the thermal denaturation and aggregation of f-actin. *Biochemical and Biophysical Research Communications*. 2005;331:1548-1553.

76. Coss RA: Inhibiting induction of heat shock proteins as a strategy to enhance cancer therapy. *Int J Hyperthermia*. 2005;21:695-701.

77. Maulik N, Engelman RM, Wei Z, Liu X, Rousou JA, Flack JE, Deaton DW, Das DK: Drug-induced heat-shock preconditioning improves postischemic ventricular recovery after cardiopulmonary bypass. *Circulation*. 1995;92:II381-II388.

78. Streffer C: Aspects of metabolic change in hyperthermia. *Recent Results in Cancer Research*. 1988;107:7-16.

79. Kobza R, Hindricks G, Tanner H, Schirdewahn P, Dorszewski A, Piorkowski C, Gerds-Li J-H, Kottkamp H: Late recurrent arrhythmias after ablation of atrial fibrillation: Incidence, mechanisms, and treatment. *Heart Rhythm*. 2004;1:676-683.

80. Shah DC, Takahashi A, Jais P, Hocini M, Peng JT, Clementy J, Haissaguerre M: Tracking dynamic conduction recovery across the cavotricuspid isthmus. *J Am Coll Cardiol*. 2000;35:1478-1484.

81. Gaita F, Riccardi R, Calo L: Importance and implications of the occurrence of av block following radiofrequency ablation. *Heart*. 1998;79:534-535.

82. Collins KK, Dubin AM, Chiesa NA, Avasarala K, Hare GFV: Cryoablation versus radiofrequency ablation for treatment of pediatric atrioventricular nodal reentrant tachycardia: Initial experience with 4-mm cryocatheter. *Heart Rhythm*. 2006;3:564-570.

83. Takahashi M, Mitsuhashi T, Hashimoto T, Ebisawa K, Fujikawa H, Ikeda U, Shimada K: Transient complete atrioventricular block occurring 1 week after radiofrequency ablation for the treatment of atrioventricular nodal re-entrant tachycardia. *Circ J*. 2002;66:1073-1075.

84. Goldberg NS, Hahn PF, Tanabe KK, Mueller PR, Schima W, Athanasoulis CA, Compton CC, Solbiati L, Gazelle SG: Percutaneous radiofrequency tissue ablation:

Does perfusion-mediated tissue cooling limit coagulation necrosis? *J Vasc Interv Radiol*. 1998;9:101-111.

85. Patterson EJ, Scudamore CH, Owen DA, Nagy AG, Buczkowski AK: Radiofrequency ablation of porcine liver in vivo: Effects of blood flow and treatment time on lesion size. *Ann Surg*. 1998;227:559-565.

86. Schuder G, Pistorius G, Fehringer M, Feifel G, Menger MD, Vollmar B: Complete shutdown of microvascular perfusion upon hepatic cryothermia is critically dependent on local tissue temerature. *British Journal of Cancer*. 2000;82:794-799.

87. Rossi S, Garbagnati F, Lencioni R, Allgaier H-P, Marchiano A, Fornari F, Quaretti P, Tolla GD, Ambrosi C, Mazzaferro V, Blum HE, Bartolozzi C: Percutaneous radio-frequency thermal ablation of nonresectable hepatocellular carcinoma after occlusion of tumor blood supply. *Radiology*. 2000;217:119-126.

88. Chang CK, Hendy MP, Smith JM, Recht MH, Welling RE: Radiofrequency ablation of the porcine liver with complete hepatic vascular occlusion. *Annals of Surgical Oncology*. 2002;9:594-598.

89. Scott DJ, Fleming JB, Watumull LM, Lindberg G, Tesfay ST, Jones DB: The effect of hepatic inflow occlusion on laparoscopic radiofrequency ablation using simulated tumors. *Surg Endosc*. 2002;16:1286-1291.

90. Kruskal JB, Oliver B, Huertas J-C, Goldberg SN: Dynamic intrahepatic flow and cellular alterations during radiofrequency ablation of liver tissue in mice. *J Vasc Interv Radiol*. 2001;12:1193-1201.

91. Hansler J, Neureiter D, Strobel D, Muller W, Mutter D, Bernatik T, Hahn EG, Becker D: Cellular and vascular reactions in the liver to radio-frequency thermo-ablation with wet needle applicators. Study on juvenile domestic pigs. *Eur Surg Res*. 2002;34:357-363.

92. Dudar TE, Jain RK: Differential response of normal and tumor microcirculation to hyperthermia. *Cancer Research*. 1984;44:605-612.

93. Badylak SF, Babbs CF, Skojac TM, Voorhees WD, Richardson RC: Hyperthermia-induced vascular injury in normal and neoplastic tissue. *Cancer*. 1985;56:991-1000.

94. Fajardo LF, Schreiber AB, Kelly NI, Hahn GM: Thermal sensitivity of endothelial cells. *Radiation Research*. 1985;103:276-285.

95. Hernandez LA, Grisham MB, Twohig B, Arfors KE, Harlan JM, Granger DN: Role of neutrophils in ischemia-reperfusion-induced microvascular injury. *Am J Physiol Heart Circ Physiol*. 1987;253:H699-H703.

96. Hoffmeyer MR, Scalia R, Ross CR, Jones SP, Lefer DJ: Pr-39, a potent neutrophil inhibitor, attenuates myocardial ischemia-reperfusion injury in mice. *Am J Physiol Heart Circ Physiol*. 2000;279:H2824-H2828.

97. Jordan JE, Zhao Z-Q, Vinten-Johansen J: The role of neutrophils in myocardial ischemia-reperfusion injury. *Cardiovascular Research*. 1999;43:860-878.

98. Kaminski KA, Bonda TA, Korecki J, Musial WJ: Oxidative stress and neutrophil activation - the two keystones of ischemia/reperfusion injury. *International Journal of Cardiology*. 2002;86:41-59.

99. Salter JW, Krieglstein CF, Issekutz AC, Granger N: Platelets modulate ischemia/reperfusion-induced leukocyte recruitment in the mesenteric circulation. *Am J Physiol Gastrointest Liver Physiol*. 2001;281:G1432-G1439.

100. Xu Y, Huo Y, Toufektsian M-C, Ramos SI, Ma Y, Tejani AD, French BA, Yang Z: Activated platelets contribute importantly to myocardial reperfusion injury. *Am J Physiol Heart Circ Physiol*. 2006;290:H692-H699.

101. Rabb H, Daniels F, O'Donnell M, Haq M, Saba SR, Keane W, Tang WW: Pathophysiological role of t lymphocytes in renal ischemia-reperfusion injury in mice. *Am J Physiol Heart Renal Physiol*. 2000;279:F525-F531.

102. Zwacka RM, Zhang Y, Halldorson J, Schlossberg H, Dudus L, Engelhardt JF: Cd4+ t-lymphocytes mediate ischemia/reperfusion-induced inflammatory responses in mouse liver. *J Clin Invest*. 1997;100:279-289.

103. Massberg S, Enders G, Matos FCdM, Tomic LID, Leiderer R, Eisenmenger S, Messmer K, Krombach F: Fibrinogen deposition at the postischemic vessel wall promotes platelet adhesion during ischemia-reperfusion in vivo. *Blood*. 1999;94:3829-3838.

104. Calkins H, Yong P, Miller JM, Olshansky B, Carlson M, Saul JP, Huang SKS, Liem LB, Klein LS, Moser SA, Bloch DA, Gillette P, Prystowsky E: Catheter ablaiton of accessory pathways, atrioventricular nodal reentrant tachycardia, and the atrioventricular junction. *Circulation*. 1999;99:262-270.

105. Keller MW, Geddes L, Spotnitz W, Kaul S, Duling BR: Microcirculatory dysfunction following perfusion with hyperkalemic, hypothermic, cardioplegic solutions and blood reperfusion. *Circulation*. 1991;84:2485-2494.

106. Guyton AC, Hall JE. Overview of the circulation: Medical physics of pressure, flow, and resistance. In: Guyton AC, ed. *Textbook of medical physiology*. Tenth ed. Philadelphia: W. B. Saunders Company; 2000:144-151.

107. Nikfarjam M, Muralidharan V, Malcontenti-Wilson C, Christophi C: Progressive microvascular injury in liver and colorectal liver metasteses following laser induced focal hyperthermia therapy. *Lasers in Surgery and Medicine*. 2005;37:64-73.

108. Hammill SC: Epicardial ablation: Reducing the risks. *J Cardiovasc Electrophysiol*. 2006;17:550-552.

109. Sosa E, Scanavacca M, d'Avila A: Transthoracic epicardial catheter ablation to treat recurrent ventricular tachycardia. *Current Cardiology Reports*. 2001;3:451-458.

110. d'Avila A, Gutierrez P, Scanavacca M, Reddy V, Lustgarten DL, Sosa E, Ramires JAF: Effects of radiofrequency pulses delivered in the vicinity of the coronary arteries: Implications for nonsurgical transthoracic epicardial catheter ablation to treat ventricular tachycardia. *PACE*. 2002;25:1488-1495.

111. Thyer IA, Kovoor P, Barry MA, Pouliopoulos J, Ross DL, Thiagalingam A: Protection of the coronary arteries during epicardial radiofrequency ablation with intracoronary chilled saline irrigation: Assessment in an in vitro model. *J Cardiovasc Electrophysiol*. 2006;17:544-549.

112. Flaherty JT, Schaff HV, Goldman RA, Gott VL: Metabolic and functional effects of progressive degrees of hypothermia during global ischemia. *Am J Physiol Heart Circ Physiol*. 1979;236:H839-H845.

113. Sosa E, Scanavacca M: Epicardial mapping and ablation techniques to control ventricular tachycardia. *J Cardiovasc Electrophysiol*. 2005;16:449-452.

114. Trim DW. Derivation of partial differential equations of mathematical physics. In: Trim DW, ed. *Applied partial differential equations*. First ed. Boston, MA: PWS Publishing Company; 1990:10-21.

115. Pennes HH: Analysis of tissue and arterial blood temperatures in the resting human forearm. *Journal of Applied Physiology*. 1948;1:93-122.

116. Chen MM: Microvascular contributions in tissue heat transfer. *Annals of the New York Academy of Sciences*. 1980;335:137-150.

117. Weinbaum S, Jiji LM, Lemons DE: Theory and experiment for the effect of vascular microstructure on surface tissue heat transfer--part i: Anatomical foundation and model conceptualization. *Journal of Biomechanical Engineering*. 1984;106:321-329.

118. Jiji LM, Weinbaum S, Lemons DE: Theory and experiment for the effect of vascular microstructure on surface tissue heat transfer--part ii: Model formulation and solution. *Journal of Biomechanical Engineering*. 1984;106:331-341.

119. Weinbaum S, Jiji LM: A new simplified bioheat equation for the effect of blood flow on local average tissue temperature. *Journal of Biomechanical Engineering*. 1985;107:131-139.

120. Wissler EH: Comments on the new bioheat equation proposed by weinbaum and jiji. *Journal of Biomechanical Engineering*. 1987;109:226-233.

121. Wissler EH: Comments on weinbaum and jiji's discussion of their proposed bioheat equation. *Journal of Biomechanical Engineering*. 1987;109:355-356.

122. Weinbaum S, Jiji LM: Discussion of papers by wissler and baish et al. Concerning the weinbaum-jiji bioheat equation. *Journal of Biomechanical Engineering*. 1987;109:234-237.

123. Panescu D, Whayne JG, Fleischman SD, Mirotznik MS, Swanson DK, Webster JG: Three-dimensional finite element analysis of current density and temperature distributions during radio-frequency ablation. *IEEE Transactions on Biomedical Engineering*. 1995;42:879-890.

124. Peterson HH, Chen X, Pietersen A, Svendsen JH, Haunso S: Tissue temperatures and lesion size during irrigated tip catheter radiofrequency ablation: An in vitro comparison of temperature-controlled irrigated tip ablation, power-controlled irrigated tip ablation, and standard temperature-controlled ablation. *PACE*. 2000;23:8-17.

125. Nikolski VP, Sambelashvilli AT, Krinsky VI, Efimov IR: Effects of electroporation on optically recorded transmembrane potential responses to high-intensity electrical shocks. *Am J Physiol Heart Circ Physiol*. 2004;286:H412-H418.

126. Cheek ER, Fast VG: Nonlinear changes of transmembrane potential during electrical shocks: Role of membrane electroporation. *Circ Res*. 2004;94:208-214.

127. Al-Khadra A, Nikolski V, Efimov I: The role of electroporation in defibrillation. *Circ Res*. 2000;87:797-804.

128. Gillis AM, Fast VG, Rohr S, Kleber AG: Spatial changes in transmembrane potential during extracellular electrical shocks in cultured monolayers of neonatal rat ventricular myocytes. *Circ Res*. 1996;79:676-690.

129. Knisley SB, Trayanova N, Aguel F: Roles of electric field and fiber structure in cardiac electric stimulation. *Biophysical Journal*. 1999;77:1404-1417.

130. Knisley SB, Hill BC: Effects of bipolar point and line stimulation in anisotropic rabbit epicardium: Assessment of the critical radius of curvature for longitudinal block. *IEEE Transactions on Biomedical Engineering*. 1995;42:957-966.

131. Zhou X, Ideker RE, Blitchington TF, Smith WM, Knisley SB: Optical transmembrane potential measurements during defibrillation-strength shocks in perfused rabbit hearts. *Circ Res*. 1995;77:593-602.

132. Girouard SD, Laurita KR, Rosenbaum DS: Unique properties of cardiac action potentials recorded with voltage-sensitive dyes. *J Cardiovasc Electrophysiol*. 1996;7:1024-1038.

133. Knisley SB, Justice RK, Kong W, Johnson PL: Ratiometry of transmembrane voltage-sensitve fluorescent dye emission in hearts. *Am J Physiol Heart Circ Physiol*. 2000;279:H1421-H1433.

134. Himel HD, Knisley SB: Imaging of cardiac movement using ratiometric and nonratiometric optical mapping: Effects of ischemia and 2, 3-butanedione monoxime. *IEEE Transactions on Medical Imaging*. 2006;25:122-127.

135. Plonsey R, Barr RC. *Bioelectricity: A quantitative approach*. Second Edition ed. New York: Kluwer Academic/Plenum Publishers; 2000.

136. deBakker JMT, Hauer RNW, Simmers TA. *Activation mapping: Unipolar versus bipolar recording*. Second Edition ed. Philadelphia: W. B. Saunders; 1995.

137. Blanchard SM, Ralph J. Damiano J, Asano T, Smith WM, Ideker RE, Lowe JE: The effects of distant cardiac electrical events in local activation in unipolar epicardial electrograms. *IEEE Transactions on Biomedical Engineering*. 1987;34:539-546.

138. Delacretaz E, Soejima K, Gottipaty VK, Brunckhorst CB, Friedman PL, Stevenson WG: Single catheter determination of local electrogram prematurity using simultaneous unipolar and bipolar recordings to replace the surface ecg as a timing reference. *PACE*. 2001;24:441-449.

139. Durrer D, Lier AAWV, Buller J: Epicardial and intramural excitation in chronic myocardial infarction. *Am Heart J*. 1964;68:765-776.

140. Scher AM, Young AC: Ventricular depolarization and the genesis of qrs. *Ann NY Acad Sci*. 1957;65:768-779.

141. Stevenson WG, Soejima K: Recording techniques for clinical electrophysiology. *J Cardiovasc Electrophysiol*. 2005;16:1017-1022.

142. Steinhaus BM: Estimating cardiac transmembrane activation and recovery times from unipolar and bipolar extracellular electrograms: A simulation study. *Circ Res*. 1989;64:449-462.

143. Neuman MR. Biopotential electrodes. In: Webster JG, ed. *Medical instrumentation: Application and design*. Third Edition ed. Danvers, MA: John Wiley & Sons, Inc.; 1998:691.

144. Geddes LA, Baker LE, Moore AG: Optimum electrolytic chloriding of silver electrodes. *Med Biol Eng*. 1969;7:49-56.

145. Josephson ME, Wit AL: Fractionated electrical activity and continuous electrical activity: Fact or artifact? *Circulation*. 1984;70:529-532.

146. Paul T, Moak JP, Morris C, Arthur Garson J: Epicardial mapping: How to measure local activation? *PACE*. 1990;13:285-292.

147. deBakker JMT, VanRijen HMV: Continuous and discontinuous propagation in heart muscle. *J Cardiovasc Electrophysiol*. 2006;17:567-573.

148. Ideker RE, Lofland GK, Bardy GH, Smith WM, Worley SJ, Wallace AG, Cox JL, Gallagher JJ: Late fractionated potentials and continuous electrical activity caused by electrode motion. *PACE*. 1983;6:908-914.

149. Waxman HL, Sung RJ: Significance of fragmented ventricular electrograms observed using intracardiac recording techniques in man. *Circulation*. 1980;6:1349-1356.

150. Man KC, Daoud EG, Knight BP, Bahu M, Weiss R, Zivin A, Souza SJ, Goyal R, Strickberger SA, Morady F: Accuracy of the unipolar electrogram for identification of the site of origin of ventricular activation. *J Cardiovasc Electrophysiol*. 1997;8:974-979.

151. Blanchard SM, Smith WM, Buhrman WC, Tedder M, Ideker RE, Lowe JE: Wavefront orientation effects on bipolar epicardial electrograms. *IEEE Transactions on Biomedical Engineering*. 1991:111-114.

152. Haissaguerre M, Dartigues J-F, Warin J-F, Metayer PL, Montserrat P, Salamon R: Electrogram patterns predictive of successful catheter ablation of accessory pathways: Value of unipolar recording mode. *Circulation*. 1991;84:188-202.

153. Stevenson WG, Khan H, Sager P, Saxon LA, Middlekauff HR, Natterson PD, Wiener I: Identification of reentry circuit sites during catheter mapping and radiofrequency ablation of ventricular tachycardia late after myocardial infarction. *Circulation*. 1993;88:1647-1670.

154. Ryu K, Shroff SC, Sahadevan J, Martovitz NL, Khrestian CM, Stambler BS: Mapping of atrial activation during sustained atrial fibrillation in dogs with rapid ventricular pacing induced heart failure: Evidence for a role of driver regions. *J Cardiovasc Electrophysiol*. 2005;16:1348-1358.

155. Kleber AG, Janse MJ, Wilms-Schopmann FJG, Wilde AAM, Coronel R: Changes in conduction velocity during acute ischemia in ventricular myocardium of the isolated porcine heart. *Circulation*. 1986;73:189-198.

156. Sano T, Takayama N, Shimamoto T: Directional difference of conduction velocity in the cardiac ventricular syncytium studied by microelectrodes. *Circ Res*. 1959;7:262-267.

157. Clerc L: Directional differences of impulse spread in trabecular muscle from mammalian heart. *J Physiol*. 1976;255:335-346.

158. Roberts DE, Hersh LT, Scher AM: Influence of cardiac fiber orientation on wavefront voltage, conduction velocity, and tissue resistivity in the dog. *Circ Res*. 1979;44:701-712.

159. Draper MH, Mya-Tu M: A comparison of the conduction velocity in cardiac tissues of various mammals. *Q J Exp Physiol Cogn Med Sci*. 1959;44:91-109.

160. Cabo C, Pertsov AM, Baxter WT, Davidenko JM, Gray RA, Jalife J: Wave-front curvature as a cause of slow conduction and block in isolated cardiac muscle. *Circ Res*. 1994;75:1014-1028.

161. Selvester RH, W. L. Kirk J, Pearson RB: Propagation velocities and voltage magnitudes in local segments of dog myocardium. *Circ Res*. 1970;27:619-629.

162. Rushton WAH: Initiation of the propagated disturbance. *Proceedings of the Royal Society of London, Series B, Biological Sciences*. 1937;124:210-243.

163. Cascio WE, Yang H, Muller-Borer BJ, Johnson TA: Ischemia-induced arrhythmia: The role of connexins, gap junctions, and attendant changes in impulse propagation. *Journal of Electrocardiology*. 2005;38:55-59.

164. Jongsma HJ, Wilders R: Gap junctions in cardiovascular disease. *Circ Res*. 2000;86:1193-1197.

165. Gutstein DE, Morley GE, Tamaddon H, Vaidya D, Schneider MD, Chen J, Chien KR, Stuhlmann H, Fishman GI: Conduction slowing and sudden arrhythmic death in mice with cardiac-restricted inactivation of connexin43. *Circ Res*. 2001;88:333-339.

166. Eloff BC, Lerner DL, Yamada KA, Schuessler RB, Saffitz JE, Rosenbaum DS: High resolution optical mapping reveals conduction slowing in connexin43 deficient mice. *Cardiovasc Res*. 2001;51:681-690.

167. Lerner DL, Yamada KA, Schuessler RB, Saffitz JE: Accelerated onset and increased incidence of ventricular arrhythmias induced by ischemia in cx43-deficient mice. *Circulation*. 2000;101:547-552.

168. Scheinman MM, Morady F, Hess DS, Gonzalez R: Catheter-induced ablation of the atrioventricular junction to control refractory supraventricular arrhythmias. *JAMA*. 1982;248:851-855.

169. Haissaguerre M, Jais P, Shah DC, Gencel L, Pradeau V, Garrigues S, Chouairi S, Hocini M, Metayer PL, Roudaut R, Clementy J: Right and left atrial radiofrequency catheter therapy of paroxysmal atrial fibrillation. *J Cardiovasc Electrophysiol*. 1996;7:1132-1144.

170. Cox JL, Schuessler RB, Boineau JP: The development of the maze procedure for the treatment of atrial fibrillation. *Seminars in Thoracic and Cardiovascular Surgery*. 2000;12:2-14.

171. Sueda T, Nagata H, Shikata H, Orihashi K, Morita S, Sueshiro M, Okada K, Matsuura Y: Simple left atrial procedure for chronic atrial fibrillation associated with mitral valve disease. *The Annals of thoracic surgery*. 1996;62:1796-1800.

172. Sueda T, Nagata H, Orihashi K, Morita S, Okada K, Sueshiro M, Hirai S, Matsuura Y: Efficacy of a simple left atrial procedure for chronic atrial fibrillation in mitral valve operations. *Annals of Thoracic Surgery*. 1997;63:1070-1075.

173. Spitzer SG, Richter P, Knaut M, Schuler S: Treatment of atrial fibrillation in open heart surgery - the potential role of microwave energy. *Thoracic and Cardiovascular Surgery*. 1999;47 (Supplement):374-378.

174. Knaut M, Spitzer SG, Karolyi L, Ebert HH, Richter P, Tugtekin SM, Schuler S: Intraoperative microwave ablation for curative treatment of atrial fibrillation in open heart surgery - the micro-staf and micro-pass pilot trial. *Thoracic and Cardiovascular Surgery*. 1999;47 (Supplement):379-384.

175. Keane D, Ruskin JN: Linear atrial ablation with a diode laser fiberoptic catheter. *Circulation*. 1999;100:e59-e60.

176. Kubota H, Furuse A, Takeshita M, Kotsuka Y, Takamoto S: Atrial ablation with an irk-151 infrared coagulator. *The Annals of thoracic surgery*. 1998;66:95-100.

177. Gaita F, Riccardi R, Calo L, Scaglione M, Garberoglio L, Antolini R, Kirchner M, Lamberti F, Richiardi E: Atrial mapping and radiofrequency catheter ablation in patients with idiopathic atrial fibrillation: Electrophysiological findings and ablation results. *Circulation*. 1998;97:2136-2145.

178. Deneke T, Khargi K, Grewe PH, Dryander Sv, Kuschkowitz F, Lawo T, Muller K-M, Laczkovics A: Left atrial versus bi-atrial maze operation using intraoperatively cooled-tip radiofrequency ablation in patients undergoing open-heart surgery: Safety and efficacy. *J Am Coll Cardiol*. 2002;39:1644-1650.

179. Sie HT, Beukema WP, Misier ARR, Elvan A, Ennema JJ, Haalebos MMP, Wellens HJJ: Radiofrequency modified maze in patients with atrial fibrillation undergoing concomitant cardiac surgery. *The Journal of thoracic and cardiovascular surgery*. 2001;122:249-256.

180. Gillinov AM, Blackstone EH, McCarthy PM: Atrial fibrillation: Current surgical options and their assessment. *The Annals of thoracic surgery*. 2002;74:2210-2217.

181. Song HK, Puskas JD. Recent advances in surgery for atrial fibrillation. In: The Cardiothoracic Surgery Network; 2005.

182. Zhou L, Keane D, Reed G, Ruskin J: Thromboembolic complications of cardiac radiofrequency catheter ablation: A review of the reported incidence, pathogenesis and current research directions. *J Cardiovasc Electrophysiol*. 1999;10:611-620.

183. Cox JL: The central contraversy surrounding the interventional-surgical treatment of atrial fibrillation. *The Journal of Thoracic and Cardiovascular Surgery*. 2005;129:1-4.

184. Sie HT, Beukema WP, Misier ARR, Elvan A, Ennema JJ, Wellens HJJ: The radiofrequency modified maze procedure. A less invasive surgical approach to atrial fibrillation during open-heart surgery. *European Journal of Cardio-thoracic Surgery*. 2001;19:443-447.

185. Benussi S, Pappone C, Nascimbene S, Oreto G, Caldarola A, Stefano PL, Casati V, Alfieri O: A simple way to treat chronic atrial fibrillation during mitral valve surgery: The epicardial radiofrequency approach. *European Journal of Cardio-thoracic Surgery*. 2000;17:524-529.

186. Gillinov AM, McCarthy PM: Atricure bipolar radiofrequency clamp for intraoperative ablation of atrial fibrillation. *Ann Thorac Surg*. 2002;74:2165-8; discussion 2168.

187. Salenger R, Lahey SJ, Saltman AE: The completely endoscopic treatment of atrial fibrillation: Report on the first 14 patients with early results. *The Heart Surgery Forum*. 2004;7:E554-558.

188. Shah DC, Takahashi A, Jais P, Hocini M, Peng JT, Clementy J, Haissaguerre M: Tracking dynamic conduction recovery across the cavotricuspid isthmus. *J Am Coll Cardiol*. 2000;35:1478-1484.

189. Bru P, Duplanter C, Bourrat M, Valy Y, Lorillard R: Resumption of right atrial isthmus conduction following atrial flutter radiofrequency ablation. *PACE*. 2000;23:1908-1910.

190. Haissaguerre M, Jais P, Shah DC, Arentz T, Kalusche D, Takahashi A, Garrigue S, Hocini M, Peng JT, Clementy J: Catheter ablation of chronic atrial fibrillation targeting the reinitiating triggers. *J Cardiovasc Electrophysiol*. 2000;11:2-10.

191. Sanchez JE, Kay GN, Benser ME, Hall JA, Walcott GP, Smith WM, Ideker RE: Identification of transmural necrosis along a linear catheter ablation lesion during atrial fibrillation and sinus rhythm. *Journal of Interventional Cardiac Electrophysiology*. 2003;8:9-17.

192. Shah DC, Takahashi A, Jais P, Hocini M, Clementy J, Haissaguerre M: Local electrogram-based criteria of cavotricuspid isthmus block. *J Cardiovasc Electrophysiol*. 1999;10:662-669.

193. Pappone C, Rosanio S: Evolution of non-pharmological curative therapy for atrial fibrillation: Where do we stand today? *International Journal of Cardiology*. 2003;88:135-142.

194. Delacretaz E: Exploring atrial macroreentrant circuits. *J Cardiovasc Electrophysiol*. 2005;16:688-689.

195. Hansson A, Holm M, Blomstrom P, Johansson R, Luhrs C, Brandt J, Olsson SB: Right atrial free wall conduction velocity and degree of anisotropy in patients with stable sinus rhythm studied during open heart surgery. *European Heart Journal*. 1998;19:293-300.

196. Wu CC, 2nd RWF, Calkins H, Tung L: Sequential change in action potential of rabbit epicardium during and following radiofrequency ablation. *J Cardiovasc Electrophysiol*. 1999;10:1252-1261.

197. Gerstenfeld EP, Dixit S, Callans D, Rho R, Rajawat Y, Zado E, Marchlinski FE: Utility of exit block for identifying electrical isolation of the pulmonary veins. *J Cardiovasc Electrophysiol*. 2002;13:971-979.

198. Bugge E, Nicholson IA, Thomas SP: Comparison of bipolar and unipolar radiofrequency ablation in an in vivo experimental model. *European Journal of Cardio-thoracic Surgery*. 2005;28:76-82.

199. Oral H, Ozaydin M, Tada H, Chugh A, Scharf C, Hassan S, Lai S, Greenstein R, Frank Pelosi J, Knight BP, Strickberger SA, Morady F: Mechanistic significance of intermittent pulmonary vein tachycardia in patients with atrial fibrillation. *J Cardiovasc Electrophysiol*. 2002;13:645-650.

200. Melby SJ, Lee AM, Zierer A, Boineau JP, Schuessler RB, Jr. RJD: Do surgical ablations have to be transmural to prevent the propagation of atrial fibrillation? *Cardiothoracic Surgery*. 2005;201:S23.

201. delaFuente D, Sasyniuk B, Moe GK: Conduction through a narrow isthmus in isolated canine atrial tissue: A model of the w-p-w syndrome. *Circulation*. 1971;44:803-809.

202. deBakker JMT, Capelle FJLv, Janse MJ, Tasseron S, Vermeulen JT, Jonge Nd, Lahpor JR: Slow conduction in the infarcted human heart: 'zigzag' course of activation. *Circulation*. 1993;88:915-926.

203. Merino JL: Slow conduction and flutter following atrial fibrillation ablation: Proarrhythmia or unmasking effect of radiofrequency application? *J Cardiovasc Electrophysiol*. 2006;17:516-519.

204. Simmers TA, deBakker JMT, Wittkampf FHM, Hauer RNW: Effects of heating on impulse propagation in superfused canine myocardium. *J Am Coll Cardiol*. 1995;25:1457-1464.

205. Simmers TA, deBakker JMT, Wittkampf FHM, Hauer RNW: Effects of heating with radiofrequency power on myocardial impulse conduction: Is radiofrequency ablation exclusively thermally mediated? *J Cardiovasc Electrophysiol*. 1996;7:243-247.

206. Weingart R: The actions of oubain on intercellular coupling and conduction velocity in mammalian ventricular muscle. *J Physiol*. 1977;264:341-365.

207. Moe GK, Rheinboldt WC, Abildskov JA: A computer model of atrial fibrillation. *Am Heart J*. 1964;67:200-220.

208. Gray RA, Jalife J: Ventricular fibrillation and atrial fibrillation are two different beasts. *Chaos*. 1998;8:65-78.

209. Perez FJ, Wood MA, Schubert CM: Effects of gap geometry on conduction through discontinuous radiofrequency lesions. *Circulation*. 2006;113:1723-1729.

210. Rosen AD: Nonlinear temperature modulation of sodium channel kinetics in $gh_3$ cells. *Biochemica et Biophysica Acta*. 2001;1511:391-396.

211. Deleze J: The recovery of resting potential and input resistance in sheep heart injured by knife or laser. *J Physiol*. 1970;208:547-562.

212. Sugiura H, Joyner RW: Action potential conduction between guinea pig ventricular cells can be modulated by calcium current. *Am J Physiol Heart Circ Physiol*. 1992;32:H1591-H1604.

213. Spitzer KW, Pollard AE, Yang L, Zaniboni M, Cordeiro JM, Huelsing DJ: Cell-to-cell electrical interactions during early and late repolarization. *J Cardiovasc Electrophysiol*. 2006;17:S8-S14.

214. Elvan A, Huang X-d, Pressler ML, Zipes DP: Radiofrequency catheter ablation of the atria eliminates pacing-induced sustained atrial fibrillation and reduces connexin 43 in dogs. *Circulation*. 1997;96:1675-1685.

215. Shaw RM, Rudy Y: Electrophysiologic effects of acute myocardial ischemia: A mechanistic investigation of action potential conduction and conduction failure. *Circ Res*. 1997;80:124-138.